

5-2004

# Quantitative Endothelial Cell Monolayer Impedance Sensing and Analysis

Benjamin David Cowan
*University of Tennessee - Knoxville*

To the Graduate Council:

I am submitting herewith a thesis written by Benjamin David Cowan entitled "Quantitative Endothelial Cell Monolayer Impedance Sensing and Analysis." I have examined the final electronic copy of this thesis for form and content and recommend that it be accepted in partial fulfillment of the requirements for the degree of Master of Science, with a major in Engineering Science.

Anthony English, Major Professor

We have read this thesis and recommend its acceptance:

Mehran Kasra, Jack Wasserman

Accepted for the Council:
Dixie L. Thompson

Vice Provost and Dean of the Graduate School

(Original signatures are on file with official student records.)

To the Graduate Council:

I am submitting herewith a thesis written by Benjamin David Cowan entitled "Quantitative Endothelial Cell Monolayer Impedance Sensing and Analysis." I have examined the final electronic copy of this thesis for form and content and recommend that it be accepted in partial fulfillment of the requirements for the degree of Master of Science, with a major in Engineering Science.

Anthony English
Major Professor

We have read this thesis
and recommended its acceptance:

Mehran Kasra

Jack Wasserman

Acceptance for the Council:

Anne Mayhew
Vice Provost and Dean of Graduate Studies

(Original signatures are on file with official student records.)

# QUANTITATIVE ENDOTHELIAL CELL MONOLAYER IMPEDANCE SENSING AND ANALYSIS

A Thesis
Presented for the
Master of Science
Degree
The University of Tennessee, Knoxville

Benjamin David Cowan
May 2004

## DEDICATION

I dedicate this thesis to my fiancée, Amelia, my parents, Lynn and Cynthia, and all of the people around me who helped me so much in what seemed more than I could bear. They say you never appreciate what you have till it's gone, but through all of this I have a new appreciation for the kindness and generosity of others.

## ACKNOWLEDGMENTS

I would like to thank everyone who helped me complete my Master of Science degree in Engineering Science. I thank Dr. Anthony English first and foremost, for his guidance and effort, and his resolve to push me towards my goal. His expertise in hydrogels and cellular electrical measurements were an endless resource as I began a thesis that seemed totally foreign to my education. I would also like to thank Dr. Mehran Kasra for his flexibility, support, and willingness to help. And finally, I thank Dr. Jack Wasserman, for his expertise in vibratory biomechanics, a next step in the application of this project.

# ABSTRACT

The electrical analysis of the biological material has been in existence since the turn of last century. A novel application of this technology to cellular monolayers was implemented by Giaever and Keese 20 years ago with their Electrical Cell-Substrate Impedance Sensing (ECIS) system. The capabilities of a real-time system for endothelial impedance measurement are of immense importance. The endothelium is typically the body's first contact with stimuli and its reaction to medical conditions of inflammation, disease, and body response are of great significance to understanding the physiology of numerous conditions ranging from heart, lung, and renal disease, to intestinal diseases. It is the purpose of this Master's thesis to analyze and optimize the ECIS system for making quantitative measurements of endothelial monolayer impedance, and accurately applying the results to a thoroughly reviewed analysis package in order to produce accurate cellular resistance parameters. The optimization of data acquisition (DAQ) is accomplished by systematic noise recognition, examination, and minimization; a task that has previously been unexplored in any studies using the ECIS system. Harmonic, 60 Hz, and Gaussian noise sources were well documented in unfiltered data and successfully minimized in the DAQ. Analog to digital (A/D) noise was found to be the lower limit of reducible noise and was properly documented and considered in analysis. Contamination of the electrode arrays from manufacturing processes and proper electrical connection were also found to be of concern to the proper functioning of the system. Analysis of the optimized acquired data was performed in the LabVIEW programming environment, as it offered a more flexible software package than that provided by the current commercially

available ECIS system. The optimized system was applied to a further look into hand arm-vibration syndrome (HAVS) and it was concluded that the acceleration exposure dose, incorrectly calculated from the international standards, did not elicit an acute endothelial inflammation response by our measurements. The cumulative result of this study is that the ECIS system has been optimized and various unresolved sources of error were corrected for a more accurate real-time measurement of the endothelial monolayer barrier function in response to stimuli.

# TABLE OF CONTENTS

# LIST OF TABLES

# LIST OF FIGURES

# NOMENCLATURE

| | |
|---|---|
| Ω | Ohm (unit of electric resistance) |
| μ- | micro- (prefix meaning $10^{-6}$ units) |
| A | Ampere (unit of electric current) |
| c- | centi- (prefix meaning $10^{-2}$ units) |
| $Ca^{++}$ | Calcium ion |
| dB | Decibel (unit of logarithmic ratio of power magnitude) |
| F | Farad (unit of capacitance) |
| g | gram (unit of mass) |
| G | acceleration of gravity (9.81 $m/s^2$) |
| Hz | Hertz (unit of Frequency, 1/s) |
| K | kilo- (prefix meaning $10^3$ units) |
| L | liter (unit of volume) |
| M- | mega- (prefix meaning $10^6$ units) |
| m | meter (unit of length) |
| m- | milli- (prefix meaning $10^{-3}$ units) |
| n- | nano- (prefix meaning $10^{-9}$ units) |
| p- | pico- (prefix meaning $10^{-12}$ units) |
| $Mg^{++}$ | Magnesium ion |
| V | Volt (unit of electric potential) |

**Abbreviations**

| | |
|---|---|
| AC | Alternating Current |
| A/D | Analog to Digital |
| AP | Action Potential |
| BSA | Bovine Serum Albumin |
| DAQ | Data Acquisition |
| DC | Direct Current |
| DMSO | Dimethylsulfoxide |
| ECIS | Electrical Cell-Substrate Impedance Sensing |
| et al. | et alii (Latin for "and others") |
| FBS | Fetal Bovine Serum |
| FFT | Fast Fourier Transform |
| HAVS | Hand-Arm Vibration Syndrome |
| LDL | Low-density Lipoprotein |
| M199 | Cell media solution |
| NIOSH | National Institute for Occupational Safety and Health |
| PBS | Phosphate Buffered Saline |
| PPAEC | Porcine Pulmonary Artery Endothelial Cells |
| PSD | Phase Sensitive Detection |
| SR830 | Stanford Research Lock-in Amplifier Model # 830 |
| SYNC | Synchronization (Filter on the SR830) |
| VI | Virtual Instrument (programmable LabVIEW application) |

# PART 1: INTRODUCTION

# I. Introduction

## *A. THE CELL AND ITS POTENTIAL*

The cell is often thought of as the basic building block upon which living organisms are made. For a medical researcher, the cell is an important area of interest. Behavior at the tissue or cellular level is one of the lowest levels at which physical phenomenon can be inferred to the greater organism as a whole, specifically the health of an individual. There are over 200 different types of cells alone in the human body and much about those cells that remains unknown. Disease, infection, trauma, and other health related phenomenon have all been traced down to the cellular level to better understand their cause and impact on a cell. There is much to be learned from the mysterious cell.

What was known about the properties of living cells until the application of electrical measurement to biological materials was based on traditional objective research. The entire field of cell biology was based upon the microscope viewing of particular cells and a further chemical decomposition of certain parts of those cells. The behavior and reaction of cells in culture was limited to a visual account of the behavior and by the limited objective magnification of a light diffraction/reflection microscope. The invention of technology that allowed for the electrical measurement of cells would in turn allow for another dimension - another facet of cell existence to be uncovered - besides their visual appearance and chemical composition: their electrical nature.

Much of the intricate behavior of organisms is made possible by the electrical activity of the living cells that comprise the organism. [1] The control and regulation of organism sensory perception, circulatory function, muscle control, assessment, etc. is

viable though the electrical activity and response of different cells in the body. The fundamental mechanisms for the electrical activity of different cells in general are quite similar. The membrane of a eukaryotic mammalian cell is composed of a lipid bilayer that serves the purpose of separating the intracellular ionic solution of the cytoplasm from the extracellular environment. This membrane includes various proteins, receptors, ionic channels, and ionic pumps that are responsible for maintaining the intracellular ionic concentrations and electric potential relative to the extracellular environment. [2]

### *B. A BRIEF HISTORY OF CELLULAR ELECTRICAL MEASUREMENTS*

Since the turn of last century, the electrical activity of cultured cells has been studied. In 1902, Bernstein first hypothesized that there was a resting potential to a cell. [3] Experimental studies into the electrical properties of cell membranes began in 1923, with Cole and Curtis. Using a Wheatstone bridge the two were able to measure membrane resistance and capacitance. [4] Their studies demonstrated that a cell has high-conductance in its cytoplasm (nearly 30-60% of that of the bath environment) surrounded by a membrane of low conductance with a capacitance of approximately 1 $mF/cm^2$. In 1939, Cole and Curtis were able to measure the change in conductance of a giant squid axon during the firing of an action potential (AP) using a Wheatstone bridge. [5] Around the same time, Hodgkin and Huxley, using microelectrodes, were able to measure the AP of a squid axon cell. [6]

Traditionally, cell potential has been measured in three ways: an intracellular recording, a cell patch, and a close proximity extracellular electrode placement. [1] (**Figure A-1**) In all three techniques, the ground lead is a distant reference electrode in

the extracellular bath. Because the system has such a large impedance, the leads are connected to a high input impedance amplifier to be able to measure the small cellular potential. For the intracellular measurement, the lead is placed intracellularly by the difficult process of inserting a micropipette with an internal electrode through the cell membrane. This process forms a seal between the cytoplasm and the electrode, but suffers from a fragile connection that makes long-term recordings very difficult to take, because the cell is in constant motion. As is often is the case, the damage caused by the impalement of the cell membrane compromises the intracellular ionic composition, that in turn can affect the intrinsic properties of the cell. [7] In the second method, a whole cell patch is formed when the micropipette electrode is brought into contact with the cell membrane, but does not pierce it. A seal with the membrane is formed by applying light suction in the pipette. This allows for measurement of the transmembrane potential and is done without damaging the cell membrane and thus compromising the interior ionic composition of the cell. Additionally, it allows for the observation of current flow and impedance through the small patch of membrane encompassed by the tip of the micropipette. Similar to the intracellular electrode placement, this method suffers from a weak connection to the cell that inhibits the long-term recording of cell potential. In a third method, the micropipette can be removed from any contact with the cell altogether and positioned in close proximity to the cell membrane. This potential measurement is on a much smaller order of magnitude to the other reference electrode than the other two methods. While this technique does not harm the cell in any way, the measurement is limited by a much smaller signal amplitude, as well as a signal shape that is very different from the transmembrane potential readings of the first two methods.

Longer time period measurement of the electrical properties of cultured cells in-vitro were made possible by rethinking the positioning of the electrodes, from placing them on or near a cellular surface to bringing the cells themselves to the electrode surface. [1] Thus the invention of the planar microelectrode in the beginning of the 1970s. The planar microelectrode has since been used as a substrate for culturing and observing cell APs, and additionally, measuring the impedance of the cell/substrate system. The later being the focus of this study.

Planar microelectrode arrays for cellular impedance studies are comprised of substrate of glass, plastic, or silicon in which the circuitry of the array may be imprinted. [1] (**Figure A-2**) On top of the substrate layer, a conductor (gold, platinum, indium-tin-oxide, iridium, etc.) is put down to form the circuit. A non-conductive layer (photoresist, polyamide, silicon dioxide, silicon nitride, etc.) is deposited over the entire surface and then removed in the areas where the electrodes are located so that the sites where recording takes place are more accurately defined. Cells are then cultured directly on this surface in a contained volume, making direct contact with the electrode at the exposed conductor site. The number of cells, from a single cell to a population of cells, that can be recorded is both directly and indirectly dependent upon the size of the electrode. The larger the electrode, the more cells that can be cultured on its surface, but the less resolution for individual cell impedance measurement. [8] This is actually encompassed into the design of the planar microelectrode, because the electrode where the cellular measurements are made is a very small area, designed to sufficiently restrict the impedance enough to allow measurement of cellular impedance. The other much larger electrode on the culture surface serves as the ground for the return current. Since the

larger electrode can be considered to be in series with the small but much larger impedance electrode, its larger size does not sufficiently increase the impedance. Therefore, the large ground electrode only serves the purpose of connecting the circuit. As with the traditional cell potential measurement methods, each electrode must be connected to a high input impedance, low noise amplification voltage recorder to amplify the extremely small extracellular potential.

In 1972, C A. Thomas et al. were the first to use a microelectrode array to record electrically active cells cultured in vitro. [9] They used a gold plated nickel electrode on glass and finished with a patterned photoresist. A glass ring was glued to the glass with beeswax to form the containment volume chamber over the patterned microelectrodes. Thomas used this system to simultaneously record the extracellular electrical activity of contracting embryonic chick heart cells in different electrodes. Following the success of Thomas, the planar microelectrode array has been used to study many differing cell types in many differing conditions.

With the advent of the technology, the means for testing the electrical properties of biological material became possible. Impedance measurements have been made on everything from whole blood and erythrocytes [10], [11], to algae [12], neural tissue [5], [6], cultured cell suspensions [13], bacterial growth [14], anchorage dependent cell cultures [15], human body water volume [16], and even organs in the body [17]. Much regarding the behavior of biological material has been found through these studies, and perhaps most importantly, that the electrical properties of biological materials are frequency dependent; that allows the researcher to study a more focused range of frequencies in order to observe cellular response. However, in only the study of

anchorage dependent cells (Giaever and Keese) was the planar microelectrode used with an applied external current to measure cellular impedance. Giaever and Keese named their technique Electrical Cell-Substrate Impedance Sensing or ECIS.

### *C. THE GIAEVER/KEESE ELECTRICAL IMPEDANCE MEASUREMENT SYSTEM*

Electrical Cell-Substrate Impedance Sensing allows for real-time data of cellular impedance to be acquired, specifically allowing for a biosensory system that is capable of detecting the effect of whatever stimuli are put into the cells' environment. The importance of a technology such as ECIS is not only evident in the scientific community, where factors such as cell micromotion [8], growth and toxicity [18], and cell adhesion [19],[20] have been studied, but also in the medical field, researching breast cancer [21], the blood/brain barrier effect [22],[23], dose-response effects [24],[25], and angiogenesis [26], just to name a few of the areas in which ECIS plays a large role.

Giaever and Keese published their first paper on the ECIS system in 1984. In this work, the ECIS system is defined and applied to a culture of fibroblasts. Giaever and Keese were the first to apply an external electric field from planar microelectrodes to cell culture, whereas in previous studies involving the Ussing chamber [27] or planar microelectrodes [9], only the innate bioelectric field of tissue was measured. From this study, Giaever and Keese determined that the resistance measurements they were making were dependent on the morphology and density of the attached cells. Furthermore, the fluctuations of those resistances represented the micromotion of the cells, as evidenced by the application of cytochalasin B, a known microtubule inhibiting drug. [28]. Once the

cytochalasin was added to the culture, implying that the micromotion of the cells was stopped, the fluctuation in the resistance "disappeared," meaning that the micromotion of the cells was causing the fluctuating resistance. Giaever and Keese also determined that the system they had originated had no effect on the normal attachment and growth of cultured cells. However, this was only done with a microscope analysis of the cells at different time periods to check for excessive cell death at the electrode site. The implications of this study would revolutionize the way that cells could be viewed. The implementation of the ECIS system in cell studies would provide another glimpse into the window of cell behavior, a real-time quantitative observation of electrical behavior, and a much-needed tool for scientists researching biological material.

Giaever and Keese did a follow-up analysis of their micromotion studies in 1991. In this study Giaever and Keese were able to quantify some of the measurements they were making and give a more detailed account of the ECIS system. The amount of resolution their system was able to detect was down to 1 nm of movement of the cell layer on the electrode, much better resolution than a traditional light microscope. In the 1984 study, the two believed that the micromotion of the cell occurred only from the initial attachment to confluence of the cells, and a result of the movements of cell during division and subsequent covering of the electrode. However, with further analysis, the micromotion behavior was found not to end upon the cells reaching confluence. The hypothesis then was that the cell motion was between the cell surface and the electrode surface. This required them to take the cell/electrode geometry into account in their model; the extent to which will be further discussed in Part 3. Giaever and Keese concluded that while the spatial values for quantifying micromotion were very much

dependent on the shape used to model the cell, the resistance was only dependent on two values: the resistance between the cells, and the resistance beneath the cells and the electrode. The quantification of cell impedance into these two values becomes integral to the way in which the ECIS system is used in all further scientific studies.

## II. Motivation/Problem Definition

Electrical Cell-Substrate Impedance Sensing was pioneered by Giaever and Keese in 1984 as a way of applying an electric field to cultured cells and reading back the information. Little about the system has changed in the almost 20 years it has been around. In 1991, Giaever and Keese formed the Applied BioPhysics Company in order to market a totally contained ECIS system to researchers. The system has been used since then in dozens of peer referenced journal articles without much question as to the validity of the measurements this system is making. Several studies have emphasized an optimization [20] or redefining [29] of the ECIS system, but this refers only to the analysis of the data, not the analysis of the data acquisition.

A system such as ECIS, since it involves the application of electricity, will have some definite sources of noise to contend with in an electrically wired environment. To date, there have been few studies involving ECIS that have also involved a look at the noise that the electrodes are recording. The gold plated surface that cultured cells adhere to must first be coated with a substrate that binds the cells to it. It is a very non-physiologic surface for the cells, that does not have elastic properties or permeate substances as many tissues surrounding the cells would in a non-cultured environment. Furthermore, ECIS is touted as a non-invasive method for observing cells[15],[20], but

repeatedly shocking cells with a non-physiologic external electrical field is bound to cause some effect. Even in one of the studies involving ECIS, a direct current (a thousand times larger than that used to record data) is applied to endothelial cells, effectively shocking them off the electrode. [26]

Another one of the limitations of ECIS is the scale of the observable area of the individual culture wells. The aperture of the photoresist covering the electrode is only 250 μm. The well holds 50 μL of fluid and only about 50 cells actually cover the electrode. This small volume of cells will attach and reach confluence within a manner of hours. This makes any study on long-term cell response, longer than 1 to 3 days, very difficult to perform with ECIS, because the cells die off so quickly. The window of time that cellular effects are visible to ECIS is only enough for the acute response of cells to stimulus to be measured.

This look at the shortcomings of ECIS is meant in no way to overshadow the importance of the information ECIS has to offer. It still provides an extra dimension to cellular research. However, a scientific research tool cannot and should not be used in peer referenced scientific journal articles without a careful examination of its faults. It is the purpose of this project to research the ECIS system itself and analyze the accuracy and credibility of its results. Improvements in noise reduction, data acquisition, data analysis, and an overall improvement in the qualitative accuracy of Giaever and Keese's original ECIS system are all objectives of this Master's thesis.

## III. Thesis Outline

This thesis presents a definitive study of the ECIS system and the optimization of its assessment of the endothelial monolayer barrier function. This is accomplished through the identification of errors in measurement of electrical voltage data, caused by noise, and corrections to the analytical model used to formulate the quantitative impedance terms. The remainder of this thesis is organized into parts outlining cellular impedance system noise, experimental cellular impedance measurements, and the overall conclusions of the thesis. There is an abstract, introduction, body, and conclusion to each part, so that each may be mostly inclusive.

Part 2, on cellular impedance system noise, deals with the process of defining, determining, and minimizing noise sources from the system. A discussion of common noise sources is given in order to define them in the system. The general electrical model of the ECIS system and recording system are introduced. Examples of specific noise sources documented in the ECIS system are shown and methods are applied to minimize the noise prevalent in our system. Part 3, on experimental cell measurement, deals with the process of preparing cell culture and electrodes for ECIS and the subsequent data obtained from cell attachment, micromotion, and further experimentation concerning drug reaction and other stimuli. A data analysis section is included in this part as a demonstration of the application of the theoretical model to the formulation of the quantitative resistance variables. Part 4 discusses the application of the optimized system to vibration induced cell response, included as a study on the effectiveness of the new system to an area of study that has not previously been focused on with ECIS. Finally, an entire part is dedicated to the summary of all of the conclusions of the previous parts and

a subsequent integration of those conclusions into a concise conclusion for the entire thesis. A definitive conclusion is formed that addresses the improvements made to the original ECIS system and the overall optimization of ECIS for further scientific studies.

# PART 2: CELLULAR IMPEDANCE SYSTEM NOISE CHARACTERIZATION AND REDUCTION

## Abstract

This part focuses on the analysis and optimization of the Electrical Cell-Substrate Impedance Sensing (ECIS) system, with respect to noise, in order to produce accurate cellular resistance parameters that represent the endothelial monolayer barrier function. The optimization of data acquisition (DAQ) is accomplished by careful noise recognition, examination, and cancellation on the naked or non-cell seeded electrode measurements. This has not been explored in any previous studies based on the ECIS system. Harmonic noise was observed and removed with the synchronization (SYNC) filter of the SR830 lock-in amplifier. Sixty Hz noise from voltage induced by environmental electrical devices was of concern and minimized with a filtering regime time constant of 300 ms. Gaussian noise, characterized by a random spread of noise around a frequency, was also documented and removed using the same filtering time constant and the maximum rolloff, 24 dB/octave. Analog to digital (A/D) noise was demonstrated in unfiltered data at each scanning frequency and marked the lowermost limit of noise. Since it could not be removed from the data, it was documented for each scanning frequency level and considered in the data analysis performed in Part 3.

## I. Introduction

This part focuses on the analysis and optimization of the ECIS system, with respect to noise found in the environment and subsequently observed in data. In order to produce accurate cellular resistance parameters that represent the endothelial monolayer barrier function, all sources of noise must be minimized first on the uncovered or naked electrode measurements. This ensures that no additional error is introduced to the system

by the addition of a dynamic biological material. The optimization of data acquisition (DAQ) is accomplished by careful recognition, examination, and minimization of noise sources. This has not been explored in any previous studies based on the ECIS system.

Noise is defined by the Concise Oxford Dictionary as "irregular fluctuations accompanying a transmitted signal but not relevant to it." [30] A system such as ECIS, that involves the application of electricity, will have some definite sources of noise to contend with in an electrically wired environment. To date, there have not been any studies involving ECIS that have also involved a look at the noise that the electrodes are recording. The system was created in 1984 and has been used since then in dozens of peer referenced journal articles without much question as to the validity of the measurements this system is making.

Giaever and Keese believed that there was not any "problem" with noise in their system merely from the observation over time of formalin frozen cells. [8] The constant behavior to their plot, the smoothness of the data, suggested to them that there were no sources of noise in the ECIS system. This is in no way a scientific categorizing or defining of system noise. Since there were in fact saturation artifacts in some of this data, the opposite is true. Some sort of noise created those artifacts. Therefore, the ECIS system must be analyzed for noise sources that in the data and possibly affect the stability of the cellular impedance parameters that are being solved for.

The remainder of this part deals with an introduction to the theory and methods that define the measurement system for ECIS. A discussion of common noise sources is given so that they may be identified in the data. The electrical model of the ECIS system and recording system are introduced. Examples of specific noise sources documented in

the ECIS system are shown and methods are applied to minimize the noise prevalent in our system. Filtering must be used to minimize any remaining noise sources. Examples from raw data and analyzed data are used to demonstrate the minimization process. Conclusions about the minimization of DAQ noise and therefore DAQ error are drawn from experimental results and demonstrate the optimization of the ECIS DAQ system.

# II. Theory

## *A. DIGITAL SIGNAL PROCESSING*

Digital Signal Processing, or DSP, is the process of transferring analog data information to digital information. Digital Signal Processing involves the "representation of signals by sequences of numbers or symbols," thus enabling one to process the sequence. [31] This allows an experimenter to make a better assemblance of the data towards the determination of some desired data characteristic (in our case, specific parameters of endothelial monolayer impedance). This process is integral to the implementation of DAQ and subsequent computer processing of this project's experimental data. It is therefore very important for all sources of noise in the experimental system to be found, characterized, and reduced as much as possible through the use of filtering in order that the DAQ process be optimized.

Optimization of a system is not a singularly defined point to be reached. There is a trade-off in the amount of analog data that is lost to the amount of noise that can be filtered out. A sampling of data is performed by an acquisition system at specific time intervals. The subsequent data values are then compiled into a signal. The sampling rate of the system defines the response time and the resolution of the data signal. If the

sampling is performed too slowly, the data lacks resolution. There is not enough data in the signal to accurately represent the analog signal.

Effects such as aliasing can occur if the sampling rate is too slow. In this case, a periodic digital signal will appear to have a period other than that of its analog counterpart, because the sampling will only detect part of the signal and represent it at intervals that do not correctly recreate the signal. Therefore, not only does a low sampling rate distort the data, it can completely misrepresent it in an aliasing case. To prevent this from happening, the Nyquist frequency [32] is defined as the sampling rate and only signals with a frequency of half the Nyquist frequency can be correctly sampled.

If the sampling rate is too high, too much of the true data is stored. The essential information of the signal is not compromised, but the amount of data can cause problems with large file sizes and cumbersome digital signal processing. In the hypothetical case of an infinitesimal sampling interval, the digital signal is exactly the analog signal, however it is infinite in size and therefore impossible to analyze.

### *B. COMMON SOURCES OF NOISE*

An important consideration in the distortion of a data signal is noise. One of the most common is harmonic distortion. [33] The appearance of signals at multiples of a reference frequency characterizes harmonic noise. These multiple frequencies are caused by the current source passing through non-linear circuitry or ground loops between a source and detector. A 60 Hz noise source is caused by the electric fields from the alternating current (AC) sources in the surrounding environment. These AC sources induce voltage into the loops of the voltage recording device, causing distortion.

A noise source can often be caused by a combination of many different "processes," giving it a Gaussian distribution of frequency around a source signal. [34] Gaussian noise is the noise characterized by a random scatter of noise around a signal. White noise is a form of Gaussian noise and is defined as the culmination of noise of all frequencies, where components are made up of all frequencies in equal amounts and random phases. [34] It draws its name from a parallel to the way in which white light works, since white light is the presence of all the colors of the spectrum. Shot noise, another form of Gaussian noise, results from statistical fluctuations in current due to charge quantization. The noise is caused by the non-uniform flow of electrons as they arrive and are emitted and at random times from a current source. [35]

Analog to digital (A/D) noise is characterized by a block-like structure in the profile of a signal. This is due to the discretization of the analog signal into a digital signal. The digital signal contains A/D noise when the digital amplification is too large and forces the information to skip from one discrete level to another too quickly, creating a block-like appearance. By defining common sources of noise in the system, these noise sources can be minimized and effectively eliminated from the signal, providing an optimized signal that better represents the true data signal being recorded.

### *C. REMOVING NOISE THROUGH DATA FILTERING*

The filtering of a data signal is performed to remove unwanted and erroneous data in that signal. Since noise is often at frequencies other than that of the desired signal, its removal can be accomplished by applying algorithms to the data that attenuate frequencies in the signal that are some "distance" away from a desired frequency. This

algorithm is called a filter. The filter succeeds in the minimization of noise by applying a function that maintains the magnitude of a desired frequency and increasingly minimizes those with increasingly different frequencies. A low pass filter passes the lower frequency components of a signal and attenuates the higher frequencies. A high pass filter passes the high frequencies and minimizes the lower frequencies around the desired frequency. Since the data we will be recording is induced by a known signal, we will want to keep the signal and minimize the noise around it. We will need to use a low pass filter.

There are two components to a filter, the time constant and the slope. The notion of time constant arises from the fact that the actual output is supposed to be a constant value over the interval it is sampled. [33] When noise is present, this is definitely not the case. By increasing the time over which a filter is applied, the output becomes steadier with a more accurate representation of the signal. The frequency attenuation varies inversely with the time constant; the longer the time constant, the closer the frequency of noise attenuated. The drawback and why we do not always use infinitely long time constants is a result of changes in the input signal that takes many time constants to be reflected at the output. Too long a time constant will delay the effect of a DSP signal, because it takes approximately 4 to 5 time constants for a filter to settle to its final value (i.e. maximum filtering). Therefore, filtering time constants must generally be of a small enough time scale to be effective in measuring real-time changes in a measured signal.

The slope, or roll off, of a filter refers to the amount of attenuation in signal with respect to distance away from a specified frequency. The larger the roll off, the quicker it minimizes the noise around a frequency. The smaller the roll off, the longer it takes for

full filtering to occur and the less it attenuates the frequencies that are closest to a specified frequency. The largest possible roll off can lead to filter instability and oscillation, but can be carefully selected by knowing the frequencies and the corresponding amplitudes of the interfering signals around it.

## III. Experimental Methods and Procedure

### *A. THE ECIS CIRCUIT*

Cellular monolayer impedance values are calculated from voltage measurements, $V_c$, obtained from the PSD of an SR830 lock-in amplifier. **Figure A-3** shows a general circuit diagram for the ECIS instrumentation. The voltage source resistance, $R_s$, is 50 Ω and the input resistance, $R_v$, and capacitance, $C_v$, of the phase sensitive detector are 10 MΩ and 25 pF respectively. Parasitic lead resistances and capacitances are associated with the source, $R_{ps}$ & $C_{ps}$, and phase sensitive detector, $R_{pv}$ & $C_{pv}$. Typical values for the parasitic resistance and capacitance are 1 kΩ and 0.19 nF, respectively. A 1 MΩ resistor, $R_{cc}$, is connected in series with the AC voltage source to stabilize the current through the electrode, creating a current clamp. The electrode resistance, $R_c$, and capacitance, $C_c$, are functions of frequency.

For calculation purposes, the resistors and capacitors may be more easily approximated as impedances, containing the real and imaginary terms of resistance. The voltage source impedance is $Z_s$ and the input impedance of the phase sensitive detector is $Z_v$. Parasitic lead impedances are associated with the source, $Z_{ps}$, and phase sensitive detector, $Z_{pv}$. A resistor with impedance, $Z_{cc}$, is connected in series with the AC voltage source to stabilize the current through the electrode. If in the circuit, the source

impedance, $Z_s$, is very small, the voltmeter impedance, $Z_v$, is very large, and the parasitic capacitance of the voltage leads, $Z_{pv}$, is very large then the electrical impedance of the electrode is

$$Z_c = \frac{V_c Z_{cc}}{V_s - V_c}. \quad \textbf{( 2.1)}$$

When $Z_{cc}$ is much smaller than $Z_c$, then $V_c << V_s$, and we get

$$Z_c = \frac{V_c Z_{cc}}{V_s} \quad \textbf{( 2.2)}$$

for the electrode impedance. This simplifies the circuit diagram to the case in Figure A-4. Therefore, given a voltage measurement, the electrode impedance can be estimated as

$$Z_c = \frac{V_c Z_{cc}}{V_s} = V_c \times 1{,}000{,}000 \quad \textbf{( 2.3)}$$

under the constant current clamp assumption, a 1 V source, $V_s$, and a 1 MΩ resistor, $Z_{cc}$, and as

$$Z_c = \frac{V_c Z_{cc}}{V_s - V_c} = \frac{V_c \times 1{,}000{,}000}{1 - V_c} \quad \textbf{( 2.4)}$$

under the voltage divider assumption. Assuming a 1 V source, there will be a 1 μA current through the electrode. We will use the later method for the analysis of our voltage readings, because it better calculates the impedance when it is at the level of magnitude of that of the 1 MΩ resistor.

### *B. LOCK-IN AMPLIFIER & PHASE SENSITIVE DETECTION*

The SR830 uses a process known as lock-in amplification, wherein a very small voltage signal can be singled out from noise signals that are many times larger. As described by Stanford Research Systems [33], this is accomplished by "locking-in" the frequency and phase of the generated reference to the detection of the resulting signal by a phase sensitive detection process. The SR830 multiplies the detected signal, $V_{sig}$, by the lock-in reference signal, $V_L$, producing two sign waves, one at the sum, $(\omega_R + \omega_L)$, and one at the difference frequency, $(\omega_R - \omega_L)$,

$$V_{psd} = \tfrac{1}{2} V_{sig} V_L \cos\left[(\omega_R - \omega_L)t + \theta_{sig} - \theta_{ref}\right] - \tfrac{1}{2} V_{sig} V_L \cos\left[(\omega_R + \omega_L)t + \theta_{sig} + \theta_{ref}\right]. \quad \textbf{(2.5)}$$

Since the frequencies of the two waves are the same, $(\omega_R = \omega_L)$ only the phase shift will remain in the first wave. After filtering out the harmonic produced in the second signal with a low pass filter, only a direct current (DC) signal, independent of time, from the PSD

$$V_{psd} = \tfrac{1}{2} V_{sig} V_L \cos\left[\theta_{sig} - \theta_{ref}\right] \quad \textbf{(2.6)}$$

remains. Because of the nature of PSD, noise sources at differing frequencies are removed by filtering and only noise at the lock-in frequency remain in the signal. This noise is assumed to be much smaller than that of the original noise signal, and the careful choice of sampling frequency will allow the experimenter to avoid frequencies known to contain the greatest noise signals (i.e. 60 and 120 Hz).

The explanation above demonstrates the PSD for the real component of the signal. This will give us the voltage data that we can transform into the real component of impedance, resistance. As for the imaginary component of the signal detected by PSD,

the signal is multiplied by another lock-in signal that is 90° out of phase of the real signal. The trigonometric simplification results in a quadrature reading and the imaginary component of the voltage,

$$V_{psd} = \frac{1}{2} V_{sig} V_L \sin[\theta_{sig} - \theta_{ref}], \quad \textbf{( 2.7)}$$

that will be transformed into the reactive component of the impedance.

### *C. FOURIER TRANSFORMS AND SPECTRAL ANALYSIS*

For a better understanding and observation of the noise sources that occur in our system, the digital signal of the voltage may be transferred into the frequency domain. The voltage signal sampled from the SR830 is in the time domain. [36] The voltage is a "representation" of the amplitudes of the true voltage signal at the discrete intervals of time from which it had been sampled. An algorithm known as the fast Fourier transform (FFT) is utilized by a computer to transform the sampled signal from the time domain into the frequency domain. The FFT is an algorithm based on the Fourier transform but numerically faster with the processing power of a computer, due to the lack of having to calculate intermediate results.

A plot showing the square of the magnitude obtained for each frequency from the FFT is called a power spectrum. Since the power is the square of the magnitude, it is always a real and positive number. Any phase information in the signal is lost in the power spectrum, which converts the 90° out of phase complex signal to a real power spectrum. Thankfully, the PSD has already sorted out real and imaginary voltage signals for us so that spectral analysis can be done individually.

> *You can use the power spectrum in applications where phase information is not necessary (for example, to calculate the harmonic power in a signal). You can apply a sinusoidal input to a nonlinear system and see the power in the harmonics at the system output.* [36]

This is exactly what we are going to use our spectral analysis for, to see the power in the harmonics (and additionally the various other noise sources) at the output.

# IV. Results and Discussion

## *A. FREQUENCY DEPENDANT MINIMALLY FILTERED INSTRUMENTAL NOISE*

Now that we have the tools to be able to identify and minimize the noise, we need to find it in our system. The voltage signal for the naked electrodes (i.e. those that do not contain cell culture, only cell media and a fibronectin coating that will be described in Part 4) was recorded at four logarithmically evenly spaced lock-in frequency levels per decade, ranging from 10 Hz to 100 kHz, which is in excess of the typical frequency range of cellular effect. In all, 17 frequencies were recorded per scan in order to span a large spectrum of possible frequency related cellular impedance behavior, which is something that the commercially available system does not do. The lowest filtering time constant (10 μsec), the lowest roll off (6 dB/octave), and the fastest sampling rate (512 Hz) of the SR830 were chosen as sampling parameters for the baseline "raw" voltage signal. This protocol allows for the maximum amount of noise to be acquired with the highest time resolution to the data.

**Figure A-5** shows the resistive (real impedance component) and reactive (imaginary impedance component) signals, calculated from the measured voltage, as a function of frequency. The point for each frequency level represents the average of 1024 data points taken over a time period of 2 seconds with the 512 Hz sampling rate. **Figure A-6** shows the square root determinate of the covariance matrix of the resistive and reactive measurements as a function of frequency using the above DAQ protocol. The square root of the determinant of the covariance matrix will be a good approximation of the correlated error between the real and imaginary signals in the system. It is in units of $\Omega^2$, meaning that it can be thought of as the area of the correlated data spread of the two signals. The larger the square root determinate, the less correlation there is between the real and imaginary data and the more error in the measurements. The smaller the square root determinate, the more correlation there is between the data and the less error in the system.

The data point time sequence and power spectrum at individual frequency levels reveal several sources of instrument noise. Only frequencies from 1 to 256 Hz can be detected without aliasing when a sampling rate of 512 Hz is used over a time period of 1 second. This is due to the limitation of the Nyquist frequency. We will initially use the resistance time sequence and power spectrum as an example. The average resistance has been subtracted from the resistance values over the 1 second time period before spectral analysis in order to better observe the spectra. Following PSD with the lowest amount of filtering, several forms of noise are present in the power spectrum. In **Figure A-7**, the resistance data point time sequence and power spectrum are given for a naked electrode at the 10 Hz frequency level. At 10 Hz, several frequency components in multiples of 10

Hz are present with a predominant peak at 20 Hz, representing harmonic distortion. This is also surrounded by what appears to be random Gaussian noise, characterized by random peaks throughout the spectrum.

**Figure A-8** illustrates the time and the frequency sequences at the 1 kHz frequency level. The interference seen in the power spectrum is harder to discern at reference frequencies higher than the sampling rate, because it gets folded back to lower frequencies in range of the Nyquist frequency. A strong 50 Hz component is caused by the 1 kHz reference frequency. This is actually a 48 Hz peak due to a difference signal from the PSD sampling fourth harmonic (2048 Hz) and the lock-in frequency second harmonic (2 kHz). There is also a gradual roll-off from the aliasing and spectral folding of higher frequency harmonics.

At 100 kHz, (**Figure A-9**) the interference appears to consist of random Gaussian noise. The PSD process of the SR830 eliminates most of the "white" power spectrum noise sources, since they are far away from the lock-in frequency. However, harmonic, 60 Hz, and Gaussian noise sources presumably still remain in the output. More aggressive filtering regimes must be implemented that attack each of these noise sources that are closer to the reference frequency.

### *B. HARMONIC DISTORTION FOLLOWING PHASE SENSITIVE DETECTION*

The range in which harmonic distortion is prevalent is exacerbated by the sum and difference behavior of PSD. Even if the input signal were to be free of noise, the PSD output always contains a component at twice the measuring frequency corresponding to the sum or difference of the signal frequency and reference. The amplitude of this signal

equals or exceeds the desired DC output depending upon the phase. **Figure A-10** shows the power spectra for a 100 Hz measurement. The 100 Hz level is a good place to begin more aggressive filtering, because it contains a large amount of harmonic and 60 Hz noise. Its proximity to 60 Hz and its harmonic distortion at multiples of 100 will allow for a better separation of the two sources than an analysis at the 56.6 Hz level, which will have too much interference due to its extreme proximity to 60 Hz, and at higher frequency levels where the effects are folded back into the Nyquist frequency range. Without synchronization filtering (SYNC filtering by the SR830), spectral peaks show up at 100 and 200 Hz, the reference frequency and its second harmonic. **Figure A-11** shows the result of adding SYNC filtering. The spectral peaks present at 40 and 160 Hz are produced by the sum and difference of a 60 Hz noise component following phase sensitive detection and SYNC filtering. The harmonic components of the 100 Hz reference signal have been removed from the spectrum.

The SYNC filter was used in all subsequent measurements to avoid having to use long filter time constants at low frequencies to remove the harmonic noise. When the SYNC filter is on, the PSD is followed by 2 stages of low pass filtering, the SYNC filter, then 2 more stages of low pass filtering (the same low pass filters that are used throughout the rest of the frequency scan). [33] Similarly, the results of the SYNC filter greatly decreased the determinate square root of the impedance covariance below 200 Hz. (**Figure A-12**)

### *C. FILTERING SIXTY HERTZ NOISE AND ALIASING*

Two possible interfering inputs are from stray magnetic fields and capacitively coupled noise. Interfering 60 Hz and 120 Hz inputs are common sources of experimental noise induced in the loops by environmental AC magnetic fields. The desired and the interfering voltages are in series, so both components appear at the input to the lock in amplifier. Also, the difference between the capacitively coupled displacement currents flowing through each lead and the electrode to ground causes an interfering voltage to appear across the electrode. Following PSD and SYNC filtering the 60 Hz and 120 Hz interfering signal components appear as sum and difference frequencies with respect to the measuring frequency. The power spectrum peaks for the sum and difference of the 60 Hz noise from a reference signal of 100 Hz can be observed in **Figure A-11**. As increasingly more aggressive time constants were used in the DAQ, the 60 Hz noise began to be minimized. With a 300 ms time constant, the 60 Hz noise was minimized and aliased into the level of random fluctuations in the power spectrum. The aliasing and spectral folding of 60 Hz and higher frequency harmonic noise are what cause the power spectrum to slope asymptotically over the power spectrum.

### *D. FILTERING GAUSSIAN NOISE*

The random fluctuations in the power spectrum represent Gaussian noise. They are spread over the entire spectrum, but do not pose as much interference to the signal as other noise sources with larger power spectra (i.e. Harmonic and 60 Hz noise). With more aggressive filtering (SYNC, 300 ms, and 24 dB/octave) an aliasing of the 60 Hz and Gaussian noise appears in the spectral analysis of the data and the random fluctuations

caused by Gaussian noise are minimized substantially from **Figure A-13** to **Figure A-14.**

### *E. A/D NOISE*

A/D noise can be seen when we return to the time sequence of the signal in **Figure A-15**. After SYNC, 300 ms, and 24 dB/octave filtering, A/D noise serves as the lower limit of possible error in the sampled data, because the DSP process creates it in the first place. The A/D noise level is directly dependent on the discretization size set by the SR830. The SR830 has 16 bit resolution or $2^{16}$ discretized intervals of recording resolution per sensitivity setting. The size of those discrete intervals and correspondingly the size of the A/D error depends on the sensitivity setting of the SR830 and not the reference frequency of the measurement. (**Table 1**) The sensitivity ranges used in a full frequency scan range from 500 mV at the largest down to 5 mV at the smallest end, with A/D errors of approximately 30 Ω at the largest down to .2 Ω at the smallest end. To further limit the A/D noise, the dynamic reserve (the ratio of the largest tolerable noise signal to the full scale signal) [33] of the SR830 can be left at a low reserve. From the power spectrum of our data, which has all been sampled at a low noise reserve, the noise sources that are not initially removed by the PSD can successfully be filtered out. There is no need to use a larger reserve on the SR830 to prevent the overload of the system from noise.

In fact, when the DAQ system is not in danger of overloading the sensitivity range, a high dynamic reserve, coupled with a large front-end amplification of a signal will actually increase the output noise in the A/D converter. The noise in the lock-in

**Table 1. A/D error estimates from sensitivity settings**

Naked Electrode Frequency Sweep (Scale by 1,000,000)

| Frequency (Hz) | Sensitivity (mV) | Time Constant (ms) | Roll Off (dB) | Reserve | A/D Interval Error (Ω) |
|---|---|---|---|---|---|
| 10 | 1000 | 300 | 12 | Low Noise | 61.0300 |
| 10 | 500 | 300 | 12 | Low Noise | 30.5170 |
| 10 | 200 | 300 | 12 | Low Noise | 7.6290 |
| 10 | 100 | 300 | 12 | Low Noise | 3.8147 |
| 10 | 50 | 300 | 12 | Low Noise | 1.9073 |
| 10 | 20 | 300 | 12 | Low Noise | 0.9536 |
| 10 | 10 | 300 | 12 | Low Noise | 0.4768 |
| 10 | 5 | 300 | 12 | Low Noise | 0.2384 |
| 10 | 2 | 300 | 12 | Low Noise | 0.1192 |
| 10 | 1 | 300 | 12 | Low Noise | 0.0596 |
| 316 | 200 | 300 | 12 | Low Noise | 7.6291 |
| 1,000 | 100 | 300 | 12 | Low Noise | 3.8147 |

amplification of the SR830 may become detectable at high reserve. [33] To prevent this, a low dynamic reserve, especially at small sensitivity ranges which translate to large gain, will decrease the output noise, which becomes detectable as A/D noise.

## V. Conclusions

The DAQ of impedance signals from the ECIS electrode will inherently have some noise input. The PSD process initially removes most of this noise, since the noise is relegated to the same frequency at which lock-in frequency has been set, or at least very close to that frequency. The outlying frequency noise signals are removed with a low-pass filter. However, the noise that remains after this process is the most difficult to remove, because it has not been removed in the first place. It is close enough to the signal

that a broad sweeping filter did not reduce it in magnitude, and because it is so close to the reference frequency it interferes more with the detection of the signal at the recorder. The solution: more filtering.

Harmonic and Gaussian noise sources were demonstrated in unfiltered data following PSD. (**Figure A-7**, **Figure A-8**, **Figure A-9**, and **Figure A-10**) Using a power spectral analysis to isolate and identify noise, increased filtering could be systematically applied to the system to sequentially minimize or very nearly eliminate the noise. Synchronous filtering was found to remove harmonic noise below 200 Hz in lieu of applying a long time constant to the low pass filter (**Figure A-11**), which would in effect decrease the time resolution of the DAQ system to sudden signal changes. The result of SYNC filter was to greatly decrease the error of impedance averages below 200 Hz. (**Figure A-12**) The results of the SYNC filter can also be illustrated in **Figure A-16**, where the determinant square root for increasing time constants (LEFT) and increasing roll off (RIGHT) is greatly minimized in the operating range of the SYNC filter. Following SYNC filtering, 60 Hz noise was revealed in the system. (**Figure A-11**) Increasing the time constant of filtering decreased the 60 Hz noise to the level of random Gaussian noise in the signal. (**Figure A-13**) After minimizing random Gaussian noise by as much as possible with the largest filter roll off (24 dB/octave) (**Figure A-14**) A/D noise was concluded to be the lowermost limit to the level of system noise remaining. (**Figure A-15**) It could not be removed from the system, just minimized by limiting dynamic reserve. It was therefore documented for each scanning frequency level. (**Table 1**)

From a careful analysis of noise sources and a quantification of the amplitude of noise that is introduced into the ECIS system, it was found that the optimal sampling parameters were a SYNC filter for removing low frequency harmonic noise, a 300 ms time constant for 60 Hz noise, and the maximum 24 dB/octave roll off for filtering Gaussian noise around the signal information. A low noise reserve, considering that the signal was actually very low noise, further insured the minimization of overall system noise, most specifically A/D.

This filtering regime resulted in an overall smooth power spectrum for the impedance signal. (**Figure A-14**) Aliasing of higher frequency harmonics and 60 Hz noise creates the sloping arc to the power spectrum. For the time domain, this translates to a slight drift in the lower reference frequency recordings. (**Figure A-15**) **Figure A-17** represents the frequency scans before (in white) and after (in orange) filtering. The optimally filtered data has dropped resistance and added impedance in the lower frequencies, due to drift, and gained some resistance in the mid-range frequencies, an effect of minimizing the noise. The square root determinate was also greatly reduced by filtering. (**Figure A-18**) Additionally, an interim of 2.2 seconds between each frequency scan allowed for equilibration of the filter, considering that 5 time constants would require 1.5 seconds, between reference frequency shifts.

In conclusion, the ECIS DAQ system protocol for system noise minimization samples 1024 points of a real and imaginary voltage signal resulting from a lock-in reference frequency for 2 seconds with a SYNC, 300 ms, and 24 dB/octave low-pass filter with a low noise reserve. The SR830 then waits 2.2 seconds to step up the

frequency a quarter of a decade and begin sampling again. In all, 17 different frequencies are sampled from 10 Hz to 100 kHz for a full frequency scan of a single electrode.

# PART 3: EXPERIMENTAL CELLULAR IMPEDANCE MEASUREMENTS

## Abstract

This part deals with the process of preparing cell culture and electrodes for ECIS and the subsequent data obtained from cell attachment, micromotion, and further experimentation concerning drug reaction and other stimuli. Since the formulation of ECIS was intended for the measurement of cellular impedance, the cell and nuances associated with applying it to a non-physiologic environment, namely the ECIS electrode, are of interest to a thesis that is aimed at optimizing the ECIS system. Further system errors applying to the preparation and fabrication of the electrodes, as well as those related to the seeding of the cells, are documented and minimized. The protocol for inoculating the ECIS electrode array is explained in the methods section. A section on the analysis of the endothelial monolayer impedance data is included in this part as a demonstration of the application of the theoretical model to the formulation of the quantitative resistance variables, $\alpha$, resistance per unit area underneath the cells and between the electrode surface, and $R_b$, the resistance between the cells. It has been concluded that the cellular impedance data has been minimized of erroneous noise sources and that the greatest cellular effect to normalized resistance data is at the 3.16 - 5.62 kHz frequency levels. Time dependent frequency scans also reveal that the peak of cellular impedance occurs within a matter of hours to the initial cell attachment, restricting the use of ECIS to acute response studies of endothelial monolayer function.

## I. Introduction

Electrical analysis of biological materials has been around since the turn of last century. A novel application of adapting some of this technology to cellular monolayers

was implemented by Giaever and Keese nearly 20 years ago with their Electrical Cell-Substrate Impedance Sensing (ECIS) system. Further adapting this system to endothelial monolayers is of great importance because of their direct link to physiologic stimuli in biotransport. Electrical Cell-Substrate Impedance Sensing allows for real-time data of cellular impedance to be acquired, specifically allowing for a biosensory system that is capable of detecting the effect of whatever stimuli are placed into the cells' environment. In the case of endothelial cells, the stimuli that affects them and their response to the stimuli is physiologically very important to overall body response.

Endothelium forms the lining of blood vessels, the kidneys, intestines, and anywhere else where physiologic diffusion or filtration occurs. [37] It is made up of simple squamous epithelium, that is a single layer of thin flat cells. It has a free surface, meaning that one side of the layer is not in direct contact with other cells. The cells are tightly bound to each other, creating what is known as a tight junction. This allows for the epithelia to protect underlying tissues, act as a barrier preventing movement of substances through the layer (the endothelial barrier function), permit the passage of some substances allowing food and nutrient exchange at its interface, secrete substances oftentimes eliciting an inflammatory or immune response, and finally absorb substances, as in the case of the kidneys and intestine where vitamins and ions are absorbed through the epithelia. The epithelium that is classified as endothelium is typically the body's first contact with stimuli [38] and its reaction to medical conditions of inflammation [19],[39], disease [40], and body response are of immense importance to understanding the physiology of numerous conditions, ranging from heart, lung, and renal disease, to intestinal disease and more. Furthermore, the resistance of the endothelial monolayer is

composed of tight junction resistance and lateral intercellular resistance (to be discussed later) [41], meaning that the resistance is partly a function of tight junction, and therefore permeability or barrier function of the endothelium. It is for this reason that ECIS of the endothelial monolayer is important to the better understanding of its barrier function in response to stimuli.

In the remainder of this part, the Giaever/Keese ECIS model for cell impedance is defined and discussed. The discussion provides insight into the workings of ECIS and an examination of the assumptions made for the model. The culmination of the model is the formulation of the two resistance variables, $\alpha$ and $R_b$, which serve as the summation of the physical impedance quantities of the endothelial monolayer. There is actually a third constant, $C_m$, the capacitance of the cell membrane that Giaever and Keese chose to arbitrarily set to a constant.

Porcine pulmonary artery endothelial cells (PPAEC) were chosen to serve as the parallel physiologic model for human endothelium in the ECIS studies. Their isolation and preparation was performed internally by the laboratory. This was done to insure that the cell culture used in the ECIS experiments was viable and directly applicable to the ECIS experiments. The protocol for cell culture involved the use of commercially available cell media solution to which vitamins and antibiotics were added to ensure the sterility and continuity of the cell tissue for multiple passaging and experimentation.

Attachment and confluence scans were initially performed using ECIS to validate the proper protocol for obtaining cell impedance data. Once the attachment was confirmed, further time dependent studies were performed in order to obtain the

longevity of ECIS measurements. Finally, monolayer barrier function's relationship to stimuli was determined using chemical agents.

Analysis of the optimized acquired data was performed in the LabVIEW programming environment, as it offered a more flexible software package than that provided by the current commercially available ECIS setup. The Levenberg-Marquardt Method, an iterative nonlinear least-squares minimization of the chi-square function for fitting the real and imaginary average impedance values calculated from the data acquisition, allows for the quantitative resistance values, $\alpha$ and $R_b$, and the membrance capacitance, $C_m$, to be calculated using a computer.

A summary of the experimental results of PPAEC seeded electrode scans using ECIS and subsequent variations of stimuli added to the culture environment is given in the results section. In addition, quantitative resistance values from the Giaever and Keese model are calculated in tabular form for comparison to the various studies. Conclusions are drawn as to the efficacy of the optimized DAQ and analysis system for observing the endothelial monolayer barrier function impedances.

## II. ECIS Theory

Giaever and Keese realized that cell/electrode geometry was integral to the formulation of their circuit model.[8] This can be seen in **Figure A-19**. $V_n$ is the voltage of the electrode and $V_m$ is the voltage of the media just outside the cell layer. h is the height of the space between the bottom of the cell and the electrode. The variable r represents the variable to be differentiated for the spatial voltage and current equations and $r_c$, the radius of the assumed circular disk shaped cell. The resistivity of the cell

media is ρ, $Z_n(v)$ the specific impedance of the electrode/electrolyte interface and can be measured directly from a cell free electrode (as in Part 2), and $Z_m(v)$ is the specific membrane impedance of the cells, which is set by an assumed capacitance, $C_m$=1 μF by Giaever and Keese. We will actually solve for $C_m$, in contrast to assuming an arbitrary value, by iterative solution in our analysis package.

The resistance of the cell media, referred to as the electrolyte, is in series with the impedance of the electrode. However, it is limited by the aperture or the size of the electrode. The constrictive resistance is then ρ/2d that of a circular disk, [42] where d is the diameter of the electrode. The resistance for the electrode/electrolyte interface is proportional to inverse area, $4/\pi d^2$. This resistance can be made sufficiently large by decreasing the size of the electrode aperture to dominate the resistance of the cell media since media resistance is only proportional to 1/d. Therefore the resistance of the electrode/electrolyte is dominant and the cell fluctuations can be observed in the data. Giaver and Keese then introduce voltages,

$$-dV = \frac{\rho dr}{h 2\pi r} I \quad , \qquad \textbf{( 3.1)}$$

$$V_n - V = \frac{Z_n(v)}{2\pi r dr} dI_n \quad , \qquad \textbf{( 3.2)}$$

and,

$$V - V_m = \frac{Z_m(v)}{2\pi r dr} dI_m \quad , \qquad \textbf{( 3.3)}$$

and a current equation,

$$dI = dI_n - dI_m \quad , \qquad \textbf{( 3.4)}$$

incorporating the electrical flow and potential of the geometry of the system into the model, as well as a relationship for the specific membrane impedance,

$$Z_m = -i / 2\pi(C_m / 2), \quad \textbf{(3.5)}$$

where $C_m$ is the arbitrary 1 μF capacitance of a single cell membrane.

These are then combined into the solution,

$$\frac{d^2V}{dr^2} + \frac{1}{r}\frac{dV}{dr} - \gamma^2 V + \beta = 0, \quad \textbf{(3.6)}$$

where $\gamma^2 = \frac{\rho}{h}\left(\frac{1}{Z_n} + \frac{1}{Z_m}\right)$ and $\beta = \frac{\rho}{h}\left(\frac{V_n}{Z_n} + \frac{V_m}{Z_m}\right)$. **(3.7)**

These equations can be solved using Bessel functions. Then solving for the inverse of the cell covered electrode's specific impedance, $Z_c$,

$$\frac{1}{Z_c} = \frac{1}{Z_n}\left(\frac{Z_n}{Z_n + Z_m} + \frac{\frac{Z_m}{Z_n + Z_m}}{\frac{\gamma r_c}{2}\frac{I_0(\gamma r_c)}{I_1(\gamma r_c)} + R_b\left(\frac{1}{Z_n} + \frac{1}{Z_m}\right)}\right), \quad \textbf{(3.8)}$$

where $I_0$ and $I_1$ are modified Bessel functions of the first kind, order 0 and 1, Giaever and Keese have defined the much sought after $R_b$ and α, the only two independent parameters of the model and therefore the values that define the impedance function of the cell layer. Where α, the resistance per unit area between the cell and the electrode, is found in the relationship

$$\gamma r_c = r_c\sqrt{\frac{\rho}{h}\left(\frac{1}{Z_n} + \frac{1}{Z_m}\right)} = \alpha\sqrt{\frac{1}{Z_n} + \frac{1}{Z_m}} \quad \textbf{(3.9)}$$

and $R_b$ is the resistance between the cells. Additionally, Cm may be solved from these equations, when not assuming it is 1 μF.

So, in order to obtain these two values, the specific impedance of the cell covered electrode, $Z_c$, is found by recording the electrode with an applied voltage current over a range of frequencies. The system has been previously scanned at different frequencies with only fibronectin on the electrode and cell media in the culture dish. This will give the value for the constrictive impedance on the media/electrode impedance, $Z_{n,}$ the naked electrode impedance that is to be subtracted from the value of the cell-laden electrode, $Z_c$, in order to obtain the true cellular impedance of the cells. In our case, we will normalize the two, to demonstrate the relative impedance effect of the monolayer.

## III. Experimental Methods and Procedure

### *A. ENDOTHELIAL CELL ISOLATION AND PREPARATION*

Pulmonary endothelial cells were isolated from porcine pulmonary arteries, obtained from a local slaughterhouse, to serve as the actualization of the cellular component for the Giaever/Keese model. After resecting a couple of inches of a pulmonary artery, each end was clamped using a hemostat, the artery was quickly dipped in 70% ethanol, and then rinsed thoroughly with M199, a cell media solution from GibcoBRL. The arteries were then transferred back to our laboratory in M199 containing penicillin (100 U/mL) and streptomycin (100 μg/mL) (GibcoBRL). Each artery was longitudinally dissected with sterile scissors and the intimal layer of endothelial cells carefully scraped from the luminal surface using a sterile scalpel, then transferred to a 35 mm Petri dish by gently tapping the scalpel blade on the dish surface. The 35 mm tissue culture dish contained 2 mL of conditioned M199. All cells were cultured using a conditioned M199 solution containing penicillin and streptomycin, supplemented with L-

glutamine (GibcoBRL), BME amino acids (Sigma), BME vitamins (Sigma) and fetal bovine serum, commonly known as FBS (Hyclone). After 4 hours in a water jacketed incubator at physiologic conditions (37°C and a 5% $CO_2$ medical air mixture), the media from the 35 mm culture dishes was removed and replaced with 2 mL of fresh conditioned media. The culture was maintained in the incubator until the endothelial cells neared confluence after approximately 7 to 10 days. They were then passaged into 60 mm tissue culture dishes when near confluence.

Passaging was performed using 0.05% trypsin to remove the PPAEC monolayer from the 35 mm dish. The trypsin/cell suspension was transferred to a 10 mL centrifuge tube and spun down to pellet the PPAEC. The trypsin was then drawn off and replaced with conditioned M199 and the cells were ready to be added to the 60 mm dish. They were immediately returned to the incubator. Approximately 1 week later, when the endothelial cells in the 60 mm dishes had reached confluence, each dish was passaged into one 100 mm tissue culture dish, using the aforementioned technique. The endothelial cells were then passaged once a week at a ratio of 1:3, 1:4, or 1:5, depending on the time necessary for culture to reach confluence. Cell lines were not passaged beyond passage 12, to limit the contamination of the culture with slower growing smooth muscle cells and to maintain a young, healthy endothelial tissue culture. Porcine pulmonary artery endothelial cells between passages four and eight were used for this study. Cultures were identified as endothelial cells by their characteristic uniform morphology, uptake of acetylated LDL, and by indirect immunofluorescent staining for Factor VIII. All procedures in the lab that involved removing the cells from the incubator were performed

under a sterile fume hood and using sterile lab techniques to prevent infection of the culture.

### *B. ECIS ELECTRODE ARRAY PREPARATION AND IMPEDANCE MEASUREMENT PROTOCOL*

The DAQ of PPAEC was performed using the system noise minimization protocol determined in Part 2. The ECIS DAQ system protocol for system noise minimization samples 1024 points of a real and imaginary voltage signal resulting from a lock-in reference frequency for 2 seconds with a SYNC, 300 ms, and 24 dB/octave low-pass filter with a low noise reserve. The SR830 then waits 2.2 seconds to step up the frequency a quarter of a decade and begin sampling again. In all, 17 different frequencies are sampled for a single frequency scan, ranging from 10 Hz to 100 kHz.

Several five well arrays of ECIS electrodes, model 5W1E, were obtained from Applied BioPhysics. (**Figure A-20**) The array consists of gold film electrodes insulated by a photoresist film and mounted on a .025 mm thick clear Lexan polycarbonate substrate. [43] The gold layer and photoresist are clear enough to allow for the observation of cells using an inverted microscope. Each electrode has a 250 μm diameter exposed area, on which about 50 PPAEC can attach. On top of the 5 electrodes, 5 circular rings appeared to have been glued with cyanoacrylate to seal the volume well for cell culture. Each well holds approximately 500 μL.

An initial naked electrode measurement is taken of each electrode array, without cells, to serve as the control or reference for cellular impedance. The gold electrode surfaces were coated with fibronectin (BD Biosciences), a protein used to anchor the

PPAEC to the gold, using a 100 μg/mL solution that was prepared by thawing a frozen 50 μl aliquot of fibronectin. A volume of 450 μL of sterilized phosphate buffered saline, or PBS, containing $Ca^{++}$ and $Mg^{++}$, was then added and gently mixed with the fibronectin. This was added to each of the 5 wells to allow the fibronectin to adsorb to the surface for 30 minutes. The remaining PBS was pipetted from each of the wells and replaced with 450 μL of conditioned M199. Each of the 5 electrodes on the array was then sampled with the SR830 and recorded on a computer to serve as the naked electrode scan. The array was now ready to be inoculated with cells.

The PPAEC were trypsinized using 0.05% trypsin and counted using a hemocytometer at which cells counts of 30, 34, 41, and 35 were obtained in each of four quadrants, yielding an average of 3.5 million cells in the entire 100 mm dish. The cells were then spun down and the trypsin was drawn off, after which 10 mL of conditioned M199 was added to the centrifuge tube. From this cell solution, 500 μL were added to each of the 5 wells, maintaining a seeding density of approximately $10^5$ cells/$cm^2$ in each well. The inoculated electrode array was then placed back into the incubator for DAQ to begin. The DAQ system performed continuous frequency scans of the array for a 24 hour period while the PPAEC attached and spread over the seeded surfaces. Pictures of each well were taken at the time of cell seeding (**Figure A-21**) as well as the following morning after the endothelial cells had formed a confluent layer (**Figure A-22**). The entire surface of the wells was examined carefully for endothelial cell confluence and cobblestone morphology.

Once the PPAEC had successfully attached to the electrode/fibronectin substrate and reached confluence, impedance testing of the PPAEC with various added stimuli

could be justifiably performed to provide accurate barrier function estimates. When cellular impedance effect had dropped, signaling the death of the culture, or the application of stimuli ceased, the array was discarded. New electrode arrays were used for each experiment, necessitating the requirement for individual naked electrode scans of each electrode, due to the variability in manufacturing and quality of the electrodes.

### *C. NUMERICAL METHODS AND PROCEDURES*

The data obtained from cellular measurements was analyzed to solve for α and $R_{b.}$. This was handled by LabVIEW virtual instrument (VI) programs that have been programmed to perform the following analysis. The model, defined by Giaever and Keese and discussed previously in the part, that is to be fitted in this study is of the form,

$$Z_c = Z_c(\mathbf{x};\mathbf{a}), \tag{3.10}$$

where the measured electrode impedance value, $Z_c$, has both real ($\Re$) and imaginary ($\Im$) components, and the terms x and a are the frequency and parameters α, $R_b$, and $C_m$, respectively, that define the impedance for a frequency scan. [44] In our experimental system we assume that the noise at different data sampling frequencies is independent but that the real and imaginary noise components at a given frequency can have different amplitudes and can be correlated; through a covariance matrix. The chi square, $\chi^2$, merit function in this case is

$$\chi^2(\alpha, R_b, C_m) = \sum_{j=1}^{N} \left[\Re(Z_{cj} - Z_c) \quad \Im(Z_{cj} - Z_c)\right] \Xi_j^{-1} \begin{bmatrix} \Re(Z_{cj} - Z_c) \\ \Im(Z_{cj} - Z_c) \end{bmatrix} \tag{3.11}$$

where $\Xi_j$ is the covariance matrix of the *j*th data point. The matrix $\Xi_j$ for the *j*th data point is obtained by repeatedly sampling the data at the *j*th frequency and using the real and imaginary values to calculate the sample covariance matrix. That is,

$$\Xi_j = \begin{bmatrix} S_{rr}^j & S_{ii}^j \\ S_{ir}^j & S_{ii}^j \end{bmatrix}, \tag{3.12}$$

where,

$$S_{rr}^j = \sum_{j=1}^{N} \frac{\Re\left(Z_{cj} - \bar{Z}\right)\Re\left(Z_{cj} - \bar{Z}\right)}{(N-1)}, \qquad S_{ri}^j = \sum_{j=1}^{N} \frac{\Re\left(Z_c - \bar{Z}\right)\Im\left(Z_c - \bar{Z}\right)}{(N-1)}, \tag{3.13}$$

$$S_{ir}^j = \sum_{j=1}^{N} \frac{\Im\left(Z_c - \bar{Z}\right)\Re\left(Z_c - \bar{Z}\right)}{(N-1)}, \qquad S_{ii}^j = \sum_{j=1}^{N} \frac{\Im\left(Z_c - \bar{Z}\right)\Im\left(Z_c - \bar{Z}\right)}{(N-1)},$$

and where the averages are calculated from the sample data averages,

$$\bar{Z} = \frac{1}{N}\sum_{j=1}^{N} Z_{cj}. \tag{3.14}$$

If we write the real and imaginary disturbance terms as

$$\Delta Z^j = \begin{bmatrix} \Delta Z_1^j \\ \Delta Z_2^j \end{bmatrix} = \begin{bmatrix} \Re\left(Z_{cj} - Z_c\right) \\ \Im\left(Z_{cj} - Z_c\right) \end{bmatrix}. \tag{3.15}$$

The $\chi^2$ function becomes

$$\chi^2(\mathbf{a}) = \sum_{j=1}^{N} Z_j^T \Xi_j^{-1} Z_j. \tag{3.16}$$

The gradient of $\chi^2$ with respect to the set of parameters, a = {α, $R_b$, $C_m$}, which will be zero at the $\chi^2$ minimum, gives the best estimation of the parameters and has components

$$\frac{\partial \chi^2(\mathbf{a})}{\partial a_k} = \sum_{j=1}^{N} \left\{ \frac{\partial Z_j^T}{\partial a_k} \Xi_j^{-1} Z_j + Z_j^T \Xi_j^{-1} \frac{\partial Z_j}{\partial a_k} \right\}. \tag{3.17}$$

or

$$\frac{\partial \chi^2(\mathbf{a})}{\partial a_k} = -2\sum_{j=1}^{N} \frac{\partial Z_c^T}{\partial a_k} \Xi_j^{-1} Z_j \quad . \qquad \textbf{( 3.18)}$$

Taking an addition partial derivative gives

$$\frac{\partial^2 \chi^2(\mathbf{a})}{\partial a_l \partial a_k} = \sum_{j=1}^{N} \left( \frac{\partial^2 Z_j^T}{\partial a_l \partial a_k} \Xi_j^{-1} Z_j + \frac{\partial Z_j^T}{\partial a_k} \Xi_j^{-1} \frac{\partial Z_j}{\partial a_l} + \frac{\partial Z_j^T}{\partial a_l} \Xi_j^{-1} \frac{\partial Z_j}{\partial a_k} + Z_j^T \Xi_j^{-1} \frac{\partial^2 Z_j}{\partial a_l \partial a_k} \right) . \qquad \textbf{( 3.19)}$$

If the second order partial derivatives are ignored, considering they will be small or approximately zero compared to the first order derivatives, the Hessian matrix of the $\chi^2$ function reduces to

$$\frac{\partial^2 \chi^2(\mathbf{a})}{\partial a_l \partial a_k} = \sum_{j=1}^{N} \left( \frac{\partial Z_j^T}{\partial a_k} \Xi_j^{-1} \frac{\partial Z_j}{\partial a_l} + \frac{\partial Z_j^T}{\partial a_l} \Xi_j^{-1} \frac{\partial Z_j}{\partial a_k} \right) , \qquad \textbf{( 3.20)}$$

or

$$\frac{\partial^2 \chi^2(\mathbf{a})}{\partial a_l \partial a_k} = 2\sum_{j=1}^{N} \left( \frac{\partial Z_{cj}^T}{\partial a_l} \Xi_j^{-1} \frac{\partial Z_{cj}}{\partial a_k} \right) . \qquad \textbf{( 3.21)}$$

For numerical computation, it is convenient to remove the factors of 2 by defining

$$\beta_k = -\frac{1}{2} \frac{\partial \chi^2(\mathbf{a})}{\partial a_k} \quad \text{and} \quad \alpha_{kl} = \frac{1}{2} \frac{\partial^2 \chi^2(\mathbf{a})}{\partial a_l \partial a_k} \quad . \qquad \textbf{( 3.22)}$$

In the case of nonlinear dependence on the set of unknown parameters, the minimization of the merit function cannot be done directly and iterations are needed. The Levenberg-Marquardt method, the standard routine for nonlinear least-squares minimization, must be used to analyze the gradient and Hessian. This is performed in a separate LabVIEW VI for output into the analysis VI and an interpolated curve from the calculated α, $R_b$, $C_m$ that will closely resemble the original normalized impedance vs. frequency curve.

## IV. Results and Discussion

### *A. IMPEDANCE DATA*

The impedance vs. frequency curves for a typical electrode can be seen in **Figure A-23.** The curves for the naked (shown in white) and cell covered (red) real and imaginary impedances observed over a frequency are on the top, and on the bottom, the normalized versions. The normalized curves (covered impedance to naked impedance) demonstrate the magnitude that the PPAEC monolayer impedance has on top of the impedance of the naked electrode alone. The largest cellular effect can be seen at the 5.62 kHz frequency level, although it has also been seen at the 3.16 kHz level, and is approximately 6 times the effective resistance of the naked electrode at that level. Even with the difference of cell type (Giaever and Keese used WI-38 fibroblasts) and equipment, the general shape of the curves found in our study matches that of the results found by Giaever and Keese in their 1991 study [8]; a good thing, since we have to fit their model to our data. The square root determinate for the covariance matrix of the real and imaginary variances can be seen in **Figure A-24**. The A/D noise level is the base level for all noise in the system. Its inclusion in the plot demonstrates the frequency range where actual noise in the signal is overcome by the limiting A/D noise generated by the SR830, above 10 kHz. Thankfully, this is above the level were the greatest cellular effect takes place.

In order to complete the ECIS model, the calculated parameters, $\alpha$, $R_b$, and $C_m$, were used to fit a curve (in green) to the recorded frequency scans of a single electrode. (**Figure A-25**) In the normalized curves, the curve calculated from the arbitrary starting parameters for $\alpha$, $R_b$, and $C_m$ input into the Marquardt analysis for both the real and

imaginary channel is also given (in yellow), showing the improvement of the interpolation with iteration. These starting values may be any arbitrary value and will not affect the result of the fit, only the amount of time it takes to reach a suitable fit. This is in contrast to the Giaever/Keese analysis where $C_m$ was arbitrarily set to 1 μF as previously stated. The parameters for this electrode and the rest of its neighbors on the array are as follows. (**Table 2**) The reduced chi square, the normalized "goodness of fit," is quite low for all of the fits, excluding that of wells 1 and 2. However, the fit for the curve well 1, the well with the largest reduced chi square, is still quite acceptable. (**Figure A-26**) The stability of the model depends on many different factors in impedance curves (shape, magnitude, time, etc.). Even with wells on the same array, the parameters for the fit vary; α, from .9 to 5.4, $R_b$, from 3.3 to 9. Only $C_m$ remains relatively constant, from 1.6 to 1.9.

Time dependent scans at a single frequency level could also be compiled from the analysis program to better observe the attach (**Figure A-27**) and micromotion (**Figure A-28**) of the PPAEC monolayer. The frequency level chosen for this study was 5.62 kHz, as it represented the largest cellular effect in the frequency scans of all 5 wells. The attachment of the PPAEC to the fibronectin results in the increase in impedance,

**Table 2. α, $R_b$, and $C_m$ parameters with the reduced $\chi^2$ of the fit for a 5 well array.**

| Well | α ($\Omega^{1/2}\cdot cm^2$) | $R_b$ ($\Omega\cdot cm^2$) | $C_m$ ($\mu F/cm^2$) | Reduced $\chi^2$ (unitless) |
|---|---|---|---|---|
| 1 | 0.991160 | 9.035666 | 1.667611 | 6.183709677 |
| 2 | 3.913890 | 7.483377 | 1.684545 | 5.059806452 |
| 3 | 5.391472 | 3.808105 | 1.628483 | 1.585580645 |
| 4 | 1.700680 | 6.625979 | 1.906022 | 1.052032258 |
| 5 | 3.775439 | 3.343787 | 1.767128 | 0.137032258 |

demonstrated in the plot. The variation in the data for both the attach and micromotion plots cannot be caused by noise (since steps were taken to minimize it well below the level of these changes), but by the changing morphology of the PPAEC in the monolayer. [8] This is supported by the time study involving the use of cytochalasin. (**Figure A-29**) Cytochalasin D (Sigma), a known actin and contractile microfilament inhibiting agent, was administered to each well. [45] From the 30 mL stock, 40 μL of cytochalasin was added to 360 μL of M199 containing 10 mg/mL bovine serum albumin, or BSA, and served to bring the experimental run to an end, whereby the micromotion of the PPAEC monolayer was halted. The fluctuations in impedance over time at the 5.62 kHz level disappear altogether, because the cells have been "frozen" in place. This is a curve of normalized impedance vs. time, meaning that when it moves towards unity there is no difference between the naked and cytochalasinated cell covered measurements.

In addition to a single frequency time plot, a 3 dimensional surface plot of an entire frequency scan over the entire time period of a study can be compiled. (**Figure A-30**) While not as effective for observing micromotion, this analysis allows for a better understanding of the effective time period for studying the PPAEC by the relative cellular effect, because it is relative to the maximum ridge of the normalized resistance vs. frequency vs. time surface.

In addition to data for the PPAEC monolayer under normal conditions, various stimuli were added to the culture. Cytochalasin (discussed previously), nocodozole (a microtubule disrupter) [46],[47], and acrylamide (also a microtubule disrupter) [48],[49] were three chemicals added to stimulate cellular response. For the nocodazole (Sigma) treatment, a 2 mM dimethylsulfoxide (DMSO) stock solution was prepared by adding

16.595 mL DMSO to 10 mg nocodozole; to be stored as 100 μL aliquots in a freezer. At the time of testing, a 20 μM stock solution was prepared by adding 100 μL of the 2 mM DMSO stock solution to 9.9 mL of M199. A final concentration of 2 μM in the ECIS well was obtained by adding 40 μL to 360 μL M199 in the well. Acrylamide (Sigma) was prepared in an initial 400 mM stock solution by adding 4 mM acrylamide to 10 mL conditioned M199. One mL of 400 mM stock was diluted out to a 40 mM stock by adding 1 mL of 400 mM stock to 9 mL of conditioned M199. A final concentration of 4 mM was obtained by diluting the solution another 10 fold by adding 40 mL to 360 mL conditioned M199 in the well.

As in the case of cytochalasin, the result of adding these two chemicals was very much the same. (**Figure A-31**) The normalized impedance went to one some time after administering the drugs to the cell culture. However, the effect of the nocodozole was only temporary, and the cells returned to normal within a matter of hours. The acrylamide seemingly has a more permanent effect. The response rate for acrylamide was also much faster than that of the cytochalasin.

The cellular resistance parameters $\alpha$, $R_b$, and $C_m$ were calculated for each electrode before and after treatment. Their values are presented below in **Table 3**. There appears to be no clear relationship between the parameters and the ceasing of micromotion. There is no linear trend in any of the 3 parameters to define the cellular response. With the nocodozole treatment, the parameters should have remained relatively unchanged, since the drug's effect to the culture was transient and impedance levels returned to normal. The reduced chi square values for the parameter fits may explain some of the problem. They are rather erratic from one row to the next. The nocodozole

**Table 3. α, $R_b$, and $C_m$ before and after drug studies.**

| Chemical Stimuli | Time | α ($\Omega^{1/2}\cdot cm^2$) | $R_b$ ($\Omega\cdot cm^2$) | $C_m$ ($\mu F/cm^2$) | Reduced $\chi^2$ (unitless) |
|---|---|---|---|---|---|
| Cytochalasin | Before | 0.991160 | 9.035666 | 1.667611 | 6.183709677 |
| | After | 4.970295 | 0.828805 | 3.027519 | 3.568032258 |
| Nocodozole | Before | 0.378575 | 2.711654 | 1.162044 | 43.70967742 |
| | After | 0.412652 | 0.990456 | 1.237872 | 4.061741935 |
| Acrylamide | Before | 6.643628 | 2.104086 | 1.388202 | 0.062354839 |
| | After | 4.325187 | 4.837655 | 1.697501 | 10.99245161 |

before reduced chi square is 43 and the acrylamide before only .06, an excellent fit. Such a low chi square for the acrylamide is probably just a chance occurrence of the data to fit the model. Again, the failure of the fit is dependent on many different factors. Unfortunately, the altering of the cell culture by chemical means does not explain the large reduced chi square for the well before treatment with nocodozole.

### *B. ELECTRODE PROBLEMS*

During the process of preparing and running these experiments, various problems with the system occurred that affected the quality of data we were taking. Besides the obvious complications of setting up a DAQ system from the ground up, problems with electrical contacts and connections were the most common. Contamination of the delicate gold leaf circuitry of the electrode arrays was one of the first problems we encountered. Fingerprints on the gold leaf introduced noise to the lower frequency scans and distorted the overall shape of impedance plots. To avoid this type of contamination, gloves were worn at all times during the handling of the electrode arrays and all of the procedures involving the arrays in which it was feasible to do so were performed under the sterile

fume hood. Although electrode arrays were supposed to be shipped sterile from the manufacturer, contamination of the electrode arrays from manufacturing processes was found to be of concern to the proper functioning of the system. (**Figure A-32**) The impedance vs. frequency curves would have an atypical shape that could only be attributed to contamination. A careful visual examination of "faulty" electrodes proved to be all that was necessary to prevent their inclusion in experimental runs. The contamination introduced into the "faulty" arrays could not be removed from the electrode surfaces. Any attempt to do so resulted in further damage to the gold surface of the contacts.

Further manufacturing defects resulted in a propensity for the wells to leak during experiments. The process by which the wells are secured to the plate containing the contacts appears to be merely a hand glued joint. The inconsistency in the seal of the wells to liquid results in the leaking of most of the contents of one or more of the wells of an electrode array onto the contacts of adjacent properly functioning electrodes. The array must be removed from the incubator and wiped of the cell media spill with a Kimwipe. This results in further damage to intact electrodes because of the roughening of the gold contact by the cleaning process.

Another problem developed with the leads being used to connect the electrode array to the SR830. The data acquired with these leads also resulted in the distortion of data, with an extreme negative outlier in the frequency scan data signal for the reactance, occurring around 3 kHz. This was of great concern to the validity of the results, as the greatest cellular impedance effect occurs in the resistance curve around this frequency level. Upon removal of the faulty leads and replacement with different leads that had

different alligator clips, the erroneous dip in the reactance was removed as well. One explanation for the error induced by the faulty leads is a junction potential created by the connection between dissimilar metals.

## V. Conclusions

The quantification of PPAEC monolayer impedance involves a complex system of DAQ and an even more complicated system of analysis. From the formulation of ECIS by Giaever and Keese, the curve of cellular impedance vs. frequency was found to have a best fit interpolation dependent on two constants innate to the monolayer, $\alpha$ and $R_b$. Where $\alpha$ is the resistance per unit area underneath the cells and between the substrate. $R_b$ is the resistance between the individual cells. With an improvement upon the ECIS analysis, a third innate cellular constant was also solved for, $C_m$, the capacitance per unit area of the monolayer. (**Table 2**) The solution of these parameters was accomplished by a non-linear least squares minimization called the Levenburg-Marquardt Method. Unfortunately, the parameters are so dependent on the stability of the model of a very robust cell culture that it is difficult to make qualitative observations about cellular response with them. The best indicator for the response of the PPAEC to stimuli remains the general impedance of the system.

The software package for analysis of raw voltage data, in addition to solving for the quantitative resistance values $\alpha$ and $R_b$ and the membrane capacitance $C_m$, was quite flexible for the further analysis. The LabVIEW programming environment allowed us to characterize our 1024 sampled impedance values for each frequency level in virtually every way imaginable. The best quantitative indicator for the success of the minimization

of noise in the solution involves the square root of the determinant of the covariance matrix for the real and imaginary impedance averages over an entire frequency scan. (**Figure A-24**)

For a time dependent study of the barrier function/impedance/micromotion of the monolayer, the frequency scans iterated over the course of several hours could be repositioned onto the time axis. Although not included in the results, the 3.16 kHz frequency level was also a normalized resistance maximum for some of the results, indicating a drift in the system most likely caused by the dynamic cellular environment. The frequency level that demonstrated the highest cellular impedance response in these results was 5.62 kHz, the peak of the normalized impedance curve for all wells (**Figure A-23**) and was the most often used frequency level for time study. (**Figure A-28**, **Figure A-29**, **Figure A-31**) However, depending on the time and time resolution (because a full frequency scan takes more time than a single frequency scan) needed for a study, other surrounding frequencies, if not all, are of importance to the impedance measurements of the monolayer. All the full frequency scans for a study can be stacked side-by-side to form an impedance/frequency/time surface. (**Figure A-30**) This gives the observer a better general sense of the behavior of the monolayer in the frequency and time domain simultaneously.

In summation, the noise minimized, DAQ optimized ECIS system that we compiled was successful in correctly recording and extensively analyzing the impedance of a PPAEC monolayer subjected to various experimental conditions, of great importance to the responsible utilization of ECIS for scientific research.

# PART 4: APPLICATION OF ECIS TO VIBRATION INDUCED ENDOTHELIAL RESPONSE

## Abstract

A condition known as “white-finger” or hand-arm vibration syndrome (HAVS) is prevalent in workers who use vibrating work tools for extended periods of time and is a result of restricted blood flow to the tissues undergoing vibration. It is believed that HAVS is an effect of an acute inflammatory response to vibration that has become a permanent factor in the affected tissue. It is the purpose of this part to determine the acute cellular response, if any, of a modified regiment of vibration on the porcine pulmonary artery endothelial cell (PPAEC) monolayer. This is a new area of study that has not previously been an area of focus for the Electrical Cell-Substrate Impedance Sensing (ECIS) system, which will be used for monitoring the PPAEC. The protocol for vibration was developed for this study through the use of international standards for measuring long-term induced vibration and its damage to tissue. Although the results of the study were indeterminate as to the endothelial monolayer barrier function when induced to vibration, it was concluded that the acceleration exposure dose, which was incorrectly calculated from the international standards, was not enough to induce an acute inflammatory response from our endothelial monolayer. The study also provides insights into the implementation of parallel multiple-array data acquisition and the time resolution tradeoff.

## I. Introduction

Vibration can create disturbances in circulation, neurological conduction, and musculoskeletal control in the hands and arms of workers who use vibrating tools everyday for several years. Studies also suggest that there is a “linear relationship”

between level and time of exposure to the time of onset and severity of HAVS. [50] Standards such as BS6842 [51], BS7482 [52], ISO5349 [53], ISO8041 [54], and ISO10819 [55] to name a few, are dedicated solely to measuring, characterizing, and limiting hand-transmitted vibration in the workplace. While the procedures for measuring the transmitted vibration are well documented, little is known about the physiological cause of resulting degenerative diseases.

A condition known as hand-arm vibration syndrome (HAVS) is prevalent in workers who use vibrating work tools for extended periods of time and is a result of restricted blood flow to the tissues undergoing vibration. It is believed that HAVS is an effect of a progressive peripheral neural and vascular change in the affected tissue. [50] Vibration directly affects the nerves, creating a tingling, numbing sensation in the fingers and hands. Over time, these effects lead to a permanent reduction in sensation. Carpal-tunnel, the compression of the median nerve in the hand, which is often caused by a repetitive pinching of the nerve from improper hand posture, is also attributed to vibration damage in addition to the pressure applied to a hand tool. [53]

The vascular change (vasoconstriction, the natural body response to cold) occurs when the smooth muscle sheaths around blood vessels contract to limit the blood volume in the outer extremities. One hypothesis for the development of HAVS is that this reaction becomes exaggerated when exacerbated by vibration, resulting in the loss of blood flow to tissue, further damaging the tissue. [53] Over time, more serious conditions arise such as ulcers and gangrene. The loss of blood flow also results in a loss of sensation and ultimately control of the hand tool that is causing the detrimental vibration, further increasing the danger of the situation. Since the ECIS system has been optimized

for the study of endothelial barrier function, the vascular component of HAVS can be directly measured; assuming a response can be initiated.

In addition to neural and vascular changes, musculoskeletal damage occurs from detrimental vibration exposure. [50] Cysts, vacuoles, and ossification have an increased occurrence in the hands and arms of workers who operate low-frequency vibrating tools (< 50 Hz). [53] Tendonitis and a weakness and loss of grip also suggest an effect on the muscle tissue in hands and arms that is not necessarily a complication caused by neurological inflammation, but of the ergonomic stress of the vibration.

In many of these situations, the physiologic stimuli behind these effects are unknown. [56] The cellular response of affected tissue to induced vibration is a mystery. There are three pathological changes in the affected tissue: a thickening of the muscular layers of artery walls, a demyelinating of peripheral neural pathways with increased number of fibroblasts, and increased amounts of connective tissue, causing peripheral vascular neural fibrosis. [57] Additional factors, such as poor circulation resulting from tobacco use or other vasoconstricting substances contribute to the prevalence of HAVS. [53] Hand-arm vibration syndrome can take years to reveal symptoms and even then, its prevalence in workers varies (from 0 to 100%).

Little or no scientific studies have been able to bring this unpredictable degenerative behavior to light. Standards have been set to limit the exposure to vibration. Epidemiologic studies of the extent of HAVS in workers have been performed using cold water immersion to elicit the blanching effect [58],[59], but few studies have been made into the physiologic origin of the white finger effect. In a handful of papers on HAVS, damaged endothelium has been found to release chemicals, but the true cause of the

response has merely been to assume that shearing and mechanical stress cause damage to the tissue. [60], [61] A better understanding of the pathophysiologic response to HAVS holds the possibility of further reducing the occurrence of this complex syndrome. [62] It is the purpose of this part to better determine the acute cellular response, if any, of vibration on the PPAEC through the use of the ECIS system.

## II. Theory & Methods

There are three components to acceleration exposure dose: acceleration, frequency, and time. The magnitude of acceleration is often given in terms of gravity (G), where G is the acceleration due to gravity: 9.81 $m/s^2$. Acceleration of a mass induces a force upon that mass. The frequency represents the number of oscillations in the orientation of that force per second, since the acceleration can be assumed to be an oscillating wave (sine, square, or otherwise). The amount of time of vibration exposure completes the set of parameters that defines acceleration exposure dose.

Many differing and complex methods for measuring the acceleration exposure dose have been used in studies of HAVS. [63],[64],[65] However, applying the ECIS system to a vibration source drastically limits the complexity of the spatial variables. Instead of the triaxial basicentric coordinate system commonly used for HAVS grip measurements, the coordinate system can be simplified to a simple single axis linear measurement. This is accomplished by placing the 5 well ECIS array directly on top of a vibratory "shaker." (**Figure A-33**) Then the vibration is transferred directly normal to the plane of the ECIS array electrodes and hence, the endothelial monolayer cultured on their surface.

In order to submit the cell culture to an acceleration exposure dose that is equivalent to the dose seen in longer time period studies, a transformation from the typical 8 hour daily vibration exposure must be made to a time period better suited to the PPAEC culture which must be removed from the incubator for the duration of the vibration. The time period for vibration exposure to the PPAEC will be limited to approximately 30 minutes, so that the PPAEC will not also be affected by the temperature drop and air mixture change while external to the incubator. The relationship between the 8 hour vibration exposure, A(8), and the 30 minute vibration exposure, a(.5), is,

$$A(8) = a(.5)\sqrt{\frac{T_i}{T_o}}\,, \qquad \textbf{( 4.1)}$$

where $T_i$ is the time of the vibration exposure (.5 hours) and $T_o$ is the typical 8 hour time period. The ISO 5349 frequency-weighting curve (**Figure A-34**) will be used to determine the frequency that will deliver the highest weighting factor, and therefore the greatest amount of detrimental vibration to the tissue. The frequency-weighted acceleration can be calculated as,

$$a_w = \sqrt{(W \cdot a)^2}\,, \qquad \textbf{( 4.2)}$$

where $W$ is the weighting factor and $a$ is the unweighted acceleration. The greatest weighting factor, 1, will be around the 15 Hz level. In the studies organized in the National Institute for Occupational Safety and Health (NIOSH) epidemiologic survey from 1997, the acceleration levels for workers were typically 5 to 36 m/s$^2$. [66] A good midrange acceleration from these values is approximately 15 m/s$^2$ or about 1.5 G.

Therefore, the acceleration exposure dose given to the PPAEC will be 1.5 G at 15 Hz for 30 mins a day, to approximate a typical dose for vibration tool workers.

## III. Experimental Results and Discussion

### *A. INITIAL ACCELERATION EXPOSURE DOSE STUDY*

A run of two experiments was done to determine the effects, if any, of applied vibration on the PPAEC culture monolayer in a 5 well ECIS array. For the first run, the cells were passaged with the method discussed in Part 3 into the two 5 well ECIS arrays; the first array to serve as the acceleration dosed PPAEC and the second as the unvibrated control. The arrays were connected to a SCXI switching mechanism to allow for successive iterative DAQ of all 10 wells. The switching mechanism was added to the DAQ system to discretize the interim between the successive frequency scans of individual wells and allow for a wider parallel DAQ. The first array was intact with 5 fully functioning wells. The control array, due in part to a wiring problem with the SCXI switching mechanism, has data on only 1 of its wells, well 7. However, all of the control wells were seeded with cells. The arrays stood in the incubator for a period of 18 hours to measure cell attachment.

The second array stood untouched outside of the incubator in the fume hood for the 30 minute time period in which the other array was shaken. The first array was shaken for 30 minutes under 1.5 G's at 15 Hz. This was done with the attachment of the array to the shaker with three screws through a modified 100 mm Petri dish to prevent rotation in any direction. Parafilm was applied to the tops of all five wells to create a seal between the top of the well and the top of the modified Petri dish; thus preventing

spillage of the contents of the wells. Once vibration was complete, both arrays were fed with fresh conditioned M199 and returned to the incubator for another scan. The second round of scanning was stopped after 18 hours. The first array was then shaken again for a period of 30 minutes and the control array left in the fume hood. Both arrays were returned to the incubator for more scanning. The third round of scanning began on the arrays was stopped the next day. All noticeable cell impedance was gone and the arrays were discarded.

A typical result of the preliminary experiment can be seen in **Figure A-35** where the naked and covered resistance and normalized resistance are compared from initial scan, after the first session of vibration, and after the second and final session of vibration. The results of the shaken well can further be compared to the control well in **Figure A-36**. From the resistance data seen between the two wells, there is no apparent difference between the well that was shaken and the control. The slight drop in normalized resistance over the three scans is caused by the diminishing health of the PPAEC monolayer of time. This is typical of monolayer impedances over a period of a few days. However, the control in this experiment appears to be faulty and not representative of a normally functioning electrode (the large normalized resistance hump in the lower frequencies).

A further time study of the shaken well (**Figure A-37**) reveals plateaus between the three scans that are more likely caused by the refreshing of cell media than by a vibration induced response. Additionally, a 3 dimensional surface from the full frequency range scans over time reveal that the plateau effect is actually a slight jump up in resistance. (**Figure A-38**) Perhaps this is caused by the addition of cell media to the

culture before returning the arrays to the incubator. The α, $R_b$, and $C_m$ parameters were also calculated for comparison of the shaken and control wells at simultaneous scans. (**Table 4**) As evidenced by the parameters, the control well is faulty. The capacitance of the monolayer becomes increasingly large over time and there is a spike in $R_b$ at the end of the run. The model was unable to fit the odd shape of the normalized resistance curve. The parameters for the shaken well appear to be much better. Unfortunately, the Marquardt analysis did not iterate for the third scan, giving an incorrect set of parameters. For the first two scans though, it appears that the acceleration dose has left the culture unaffected. Furthermore, since normalized resistance did not drastically change in the time study between the shakes, it can be assumed that the acceleration exposure dose did not significantly affect the PPAEC, which would most likely cause a drop in the normalized resistance. Due to the failure in the control array, the results of the initial experiment cannot be assumed as conclusive and another attempt to elicit a HAVS response in the PPAEC will be attempted.

**Table 4. α, $R_b$, and $C_m$ parameters for the initial acceleration exposure dose study**

| Well | Scan | α ($\Omega^{1/2}\cdot cm^2$) | $R_b$ ($\Omega\cdot cm^2$) | $C_m$ ($\mu F/cm^2$) | Reduced $\chi^2$ (unitless) |
|---|---|---|---|---|---|
| Shaken | Covered (14) | 6.370240 | 1.198577 | 1.890094 | 3.436580645 |
| | Shake 1 (0) | 7.561077 | 0.136316 | 2.039865 | 2.598806452 |
| | Shake 2 (0) | 4.000000 | 2.000000 | 1.000000 | 9.959806452 |
| Control | 14 | 12.571775 | 0.000189 | 3.781357 | 7.097451613 |
| | 0 | 13.474427 | 0.023806 | 15.149149 | 5.963677419 |
| | 0 | 0.473666 | 53.742328 | 31.984908 | 69 |

### *B. SECOND ACCELERATION EXPOSURE DOSE STUDY*

Frequency scans were initiated on two more 5 well ECIS arrays. The first array served as a variable for vibration study on cell-coated electrodes (wells 1-4), the second (containing only one working electrode due to the SCXI) as a control (well 5). The arrays were seeded with PPAEC and allowed to reach confluence overnight. The first array was then shaken for a period of 30 minutes the following morning, while the second array remained unshaken, though in the fume hood. The arrays were then filled with fresh media and returned to the incubator for more scans.

A typical result of the second acceleration exposure dose experiment can be seen in **Figure A-39** where normalized data of the resistance for the well 1 confluent scan (Cell Covered) is compared to the scan after the acceleration exposure dose (Shaken). The results of well 1 compared to those of the control well, well 5 in **Figure A-40** show very little difference between the PPAEC that were shaken and those that were not. Again, the slow drop in normalized resistance is likely caused by the length of time between the scans and not a drastic change in the PPAEC as would likely be evidenced if the acceleration exposure dose had affected the culture. The time dependent relationship for normalized resistance can be illustrated in **Figure A-41**. The time study is given for the shaken well (TOP) and unshaken control well (BOTTOM). There is no plateau effect between the two scans as in the initial experiment, indicating that there was no effect from the acceleration exposure dose to the shaken well. Additionally, a 3-D plot of the entire frequency scan over time is given in **Figure A-42**; further demonstrating the continuity between confluent and shaken data. The $\alpha$, $R_b$, and $C_m$ parameters were also calculated for this study to compare the shaken and control wells at simultaneous scans.

(**Table 5**) The results of the parameter fits are again inconclusive as to a vibration induced cellular response. Both wells show an increase in α, a decrease in $R_b$, and an increase in $C_m$, but the magnitudes for these changes are all different. All of the fits are extremely good, excluding the final fit for the control well, but again, no clear cellular effect can be seen from the parameters, deleterious or otherwise. However, it can be concluded from the time studies that there was no adverse effect resulting from the vibration on the shaken well. A second time, the acceleration exposure dose has not elicited a cellular response.

## V. Conclusions

HAVS is a debilitating condition known to affect many workers who continually use vibrating power tools. Many studies on the epidemiologic factors of HAVS have been made, and there are many methods for measuring and numerous standards limiting the acceleration exposure dose. However, little of the pathophysiologic origins of HAVS is known. It was the purpose of these studies to induce HAVS in the PPAEC monolayer seeded on ECIS electrodes to better understand the pathophysiologic response of endothelial tissue to vibration.

**Table 5. α, $R_b$, and $C_m$ parameters for the second acceleration exposure dose study**

| Well | Scan | α ($\Omega^{1/2}\cdot cm^2$) | $R_b$ ($\Omega\cdot cm^2$) | $C_m$ ($\mu F/cm^2$) | Reduced $\chi^2$ (unitless) |
|---|---|---|---|---|---|
| Shaken | Covered (5) | 9.578743 | 0.494185 | 1.759107 | 2.711516129 |
| | Shaken (0) | 11.005859 | 0.001692 | 17.041833 | 1.180064516 |
| Control | 5 | 10.640809 | 0.018096 | 2.600414 | 0.60916129 |
| | 0 | 10.993167 | 0.000045 | 8.815284 | 12.46770968 |

A typical result of the preliminary experiment can be seen in **Figure A-35** where the naked and covered resistance and normalized resistance are compared from initial scan, after the first session of vibration, and after the second and final session of vibration. The results the shaken well can further be compared to the control well in **Figure A-36**. From the resistance data seen between the two wells, there is no apparent difference between the well that was shaken and the control. The slight drop in normalized resistance over the three scans is caused by the diminishing health of the PPAEC monolayer of time. However, the control in this experiment appears to be faulty and not representative of a normally functioning electrode (the large normalized resistance hump in the lower frequencies). A further time study of the shaken well (**Figure A-37**, **Figure A-38**) reveals jumps between the three scans. Perhaps this is caused by the addition of cell media to the culture before returning the arrays to the incubator. The $\alpha$, $R_b$, and $C_m$ parameters were also calculated for comparison of the shaken and control wells at simultaneous scans. (**Table 4**) As evidenced by the parameters, the control well is faulty. The capacitance of the monolayer is obviously not accurate. It is much too large. The parameters cannot be considered as indicative of the PPAEC. However, since normalized resistance has not drastically changed between the shakes, it can be assumed that the acceleration exposure dose did not significantly affect the PPAEC. Additionally, due to the failure in the control array, the results of the initial experiment cannot be assumed as conclusive.

A typical result of the second acceleration exposure dose experiment can be seen in **Figure A-39** where normalized data of the resistance for the shaken well confluent scan is compared to the scan after the acceleration exposure dose. The results of the

shaken well (**Figure A-39**) compared to those of the control well in **Figure A-40** show very little difference between the PPAEC that were shaken and those that were not. Again, the slow drop in normalized resistance is likely caused by the length of time between the scans and not a drastic change in the PPAEC as would likely be evidenced if the acceleration exposure dose had affected the culture. The time dependent relationship for normalized resistance can be illustrated in **Figure A-41** and **Figure A-42**. In **Figure A-41** the time study is given for the shaken well (TOP) and unshaken control well (BOTTOM). There is no plateau effect between the two scans as in the initial experiment, indicating that there was no effect from the acceleration exposure dose to the shaken well. **Figure A-42** further demonstrates the continuity between confluent and shaken data. The $\alpha$, $R_b$, and $C_m$ parameters were also calculated for this study to compare the shaken and control wells at simultaneous scans. (**Table 5**) As evidenced by the parameters, the control well is faulty. The capacitance of the monolayer becomes increasingly larger over time and there is a spike in $R_b$ at the end of the run. The model was unable to fit the odd shape of the normalized resistance curve. The parameters for the shaken well appear to be much better. Unfortunately, the Marquardt analysis did not iterate for the third scan, giving an incorrect set of parameters. For the first two scans though, it appears that the acceleration dose has left the culture unaffected. Furthermore, since normalized resistance did not drastically change in the time study between the shakes, it can be assumed that the acceleration exposure dose did not significantly affect the PPAEC, which would most likely cause a drop in the normalized resistance.

Although the results of the study were indeterminate as to the endothelial monolayer barrier function when induced to vibration, it was concluded that the protocols

for inducing long-term tissue damage with vibration were not enough to induce an acute inflammatory response in our endothelial monolayer; most likely because of a mistake made in the transformation of the acceleration values given in the NIOSH review [66] to an equivalent acceleration exposure dose for this experiment. These accelerations were probably acceleration exposure doses for an 8 hour period and not general magnitude values. Since a 30 minute time period was used for these experiments, the 8 hour acceleration exposure dose would have transferred to a much larger magnitude acceleration over the 30 minutes. Using Eq. **4.1**, the acceleration exposure dose that should have been applied to the PPAEC monolayer would be 60 $m/s^2$ or approximately 6 G for 30 minutes a day. Further experimentation into vibration response with an accurately calculated acceleration exposure dose or even a higher acceleration dose may prove to induce the acute inflammatory response desired for inducing HAVS. Additionally, equipment failure in the electrical switching mechanism controlled by LabVIEW limited the number of control electrodes in both studies to one. In the first study, the control electrode appeared to be faulty, due the to inconsistent normalized resistance curve at the completion of the experiment. (**Figure A-36**)

These studies also provide some insight into the implementation of parallel multiple-array data acquisition and the time resolution tradeoff. With software controlled switching of the SR830 current clamp to each of the electrodes on an ECIS array, the number of electrodes that can feasibly be scanned is greatly increased. Similarly, the time between frequency scans on an electrode is an interval equal to the magnitude of the time it takes to scan the total number of other electrodes in the experiment. In cellular attach studies, the initial attachment occurs within a period of 4 to 5 hours, and the time to reach

confluence is approximately 18 hours. This means that the culture will be the most robust about 18 hours after seeding and will begin to lose normalized resistance slowly over the course of the next few days. The observation of time dependent interactions with ECIS requires that the number of parallel electrode arrays be minimized for maximum time resolution in each electrode frequency scan.

# PART 5: CONCLUSIONS

# I. Introduction

The purpose of this master's thesis was to present a definitive study of the ECIS system and make improvements to its application to the assessment of the endothelial monolayer barrier function. This was accomplished through the identification of errors in measurement of electrical voltage data such as noise sources and corrections to the circuit model theory used to formulate the analysis of the electrical impedance data. Parts were organized into inclusive subjects that might serve as a stand-alone entity focused on a specific area of the ECIS system. The introduction part served as a general survey into the history of electrical cell measurement and a further look into the application of that technology to the endothelial monolayer barrier function. The pioneering work by Giaever and Keese as well as the numerous scientific studies involving ECIS was briefly discussed. Cellular impedance system noise was identified in the discussion of the second part and filtering regimes to minimize that noise were implemented into the DAQ of the ECIS system. Cellular impedance experimental data was taken for the third part and the process of cell culture and electrode preparation for the process were included in the methods section of that part as an example of the many areas for improvement to the protocols and setup of the ECIS system. The analysis model and software package for the cellular impedance data was also included and improvements made to the system. In Part 4, the optimized DAQ system for ECIS was applied to the study of HAVS, a syndrome affecting many workers who use vibrating tools. A pathological study of induced HAVS was attempted using the ECIS system. In summation, a systematic approach was made to improve the problems of ECIS, necessitated by the lack of any such optimization of the

system by its originators and contributors over the years and further applied to a new area of research.

## II. Part Conclusions

In Part 2, it was found that harmonic, 60 Hz, Gaussian, and A/D noise sources all appeared in the unfiltered data of a naked ECIS electrode following PSD. (**Figure A-7**, **Figure A-8**, **Figure A-9**, and **Figure A-10**) Using a power spectral analysis to isolate and identify noise, increased filtering could be systematically applied to the system to sequentially minimize or very nearly eliminate the noise. Synchronous filtering was found to remove harmonic noise below 200 Hz in lieu of applying a long time constant to the low pass filter (**Figure A-11**), which would in effect decrease the time resolution of the DAQ system to sudden signal changes. The result of SYNC filter was to greatly decrease the error of impedance averages below 200 Hz. (**Figure A-12**) The results of the SYNC filter can also be illustrated in **Figure A-16**, where the determinant square root for increasing time constants (LEFT) and increasing roll off (RIGHT) is greatly minimized in the operating range of the SYNC filter. Following SYNC filtering, 60 Hz noise was revealed in the system. (**Figure A-11**) Increasing the time constant of filtering decreased the 60 Hz noise to the level of random Gaussian noise in the signal.(**Figure A-13**) After minimizing random Gaussian noise by as much as possible with the largest filter roll off (24 dB/octave) (**Figure A-14**) A/D noise was concluded to be the lowermost limit to the level of system noise remaining. (**Figure A-15**) It could not be removed from the system, just minimized by limiting dynamic reserve. It was therefore documented for each scanning frequency level. (Table 1)

From a careful analysis of noise sources and a quantification of the amplitude of noise that is introduced into the ECIS system, it was found that the optimal sampling parameters were a SYNC filter for removing low frequency harmonic noise, a 300 ms time constant for 60 Hz noise, and the maximum 24 dB/octave roll off for filtering Gaussian noise around the signal information. A low noise reserve, considering that the signal was actually very low noise, further insured the minimization of overall system noise, most specifically A/D. This filtering regime resulted in an overall smooth power spectrum for the impedance signal. (**Figure A-14**) Aliasing of higher frequency harmonics and 60 Hz noise creates the sloping arc to the power spectrum. For the time domain, this translates to a slight drift in the lower reference frequency recordings. (**Figure A-15**) **Figure A-17** represents the frequency scans before (in white) and after (in orange) filtering. The optimally filtered data has dropped resistance and added impedance in the lower frequencies, due to drift, and gained some resistance in the mid-range frequencies, an effect of minimizing the noise. The square root determinate was also greatly reduced by filtering. (**Figure A-18**) Additionally, an interim of 2.2 seconds between each frequency scan allowed for equilibration of the filter, considering that 5 time constants would require 1.5 seconds, between reference frequency shifts.

In Part 3, the cell was added to the optimized DAQ system. The quantification of PPAEC monolayer impedance involves a complex system of DAQ and an even more complicated system of analysis. From the formulation of ECIS by Giaever and Keese, the curve of cellular impedance vs. frequency was found to have a best fit interpolation dependent on two constants innate to the monolayer, $\alpha$ and $R_b$. Where $\alpha$ is the resistance per unit area underneath the cells and between the substrate. $R_b$ is the resistance between

the individual cells. With an improvement upon the ECIS analysis, a third innate cellular constant was also solved for, $C_m$, the capacitance per unit area of the monolayer. (**Table 2**) The solution of these parameters was accomplished by a non-linear least squares minimization called the Levenburg-Marquardt Method.

The software package for analysis of raw voltage data, in addition to solving for the quantitative resistance values $\alpha$ and $R_b$ and the membrane capacitance $C_m$, was quite flexible for the further analysis. The LabVIEW programming environment allowed us to characterize our 1024 sampled impedance values for each frequency level in virtually every way imaginable. For a time dependent study of the barrier function/impedance/micromotion of the monolayer, the frequency scans iterated over the course of several hours could be repositioned onto the time axis. Although not included in the results, the 3.16 kHz frequency level was also a normalized resistance maximum for some of the results, indicating a drift in the system most likely caused by the dynamic cellular environment. The frequency level that demonstrated the highest cellular impedance response in these results was 5.62 kHz, the peak of the normalized impedance curve for all wells (**Figure A-23**) and was the most often used frequency level for time study. (**Figure A-28**, **Figure A-29**, **Figure A-31**) However, depending on the time and time resolution (because a full frequency scan takes more time than a single frequency scan) needed for a study, other surrounding frequencies, if not all, are of importance to the impedance measurements of the monolayer. All the full frequency scans for a study can be stacked side-by-side to form an impedance/frequency/time surface. (**Figure A-30**) This gives the observer a better general sense of the behavior of the monolayer in the frequency and time domain simultaneously.

In Part 4, HAVS, a debilitating condition known to affect many workers who continually use vibrating power tools, is studied with ECIS. It was the purpose of these studies to induce HAVS in the PPAEC monolayer seeded on ECIS electrodes to better understand the pathophysiologic response of endothelial tissue to vibration.

Two studies were made into the acceleration exposure dose and laboratory induced HAVS. A typical result of the preliminary experiment can be seen in **Figure A-35** where the naked and covered resistance and normalized resistance are compared from initial scan, after the first session of vibration, and after the second and final session of vibration. The results of the shaken well can further be compared to the control well in **Figure A-36**. From the resistance data seen between the two wells, there is no apparent difference between the well that was shaken and the control. The slight drop in normalized resistance over the three scans is caused by the diminishing health of the PPAEC monolayer of time. However, the control in this experiment appears to be faulty and not representative of a normally functioning electrode (the large normalized resistance hump in the lower frequencies). A further time study of the shaken well (**Figure A-37**, **Figure A-38**) reveals jumps between the three scans. Perhaps this is caused by the addition of cell media to the culture before returning the arrays to the incubator. The $\alpha$, $R_b$, and $C_m$ parameters were also calculated for comparison of the shaken and control wells at simultaneous scans. (**Table 4**) As evidenced by the parameters, the control well is faulty. The capacitance of the monolayer becomes increasingly larger over time and there is a spike in $R_b$ at the end of the run. The model was unable to fit the odd shape of the normalized resistance curve. The parameters for the shaken well appear to be much better. Unfortunately, the Marquardt analysis did not

iterate for the third scan, giving an incorrect set of parameters. For the first two scans though, it appears that the acceleration dose has left the culture unaffected. Furthermore, since normalized resistance did not drastically change in the time study between the shakes, it can be assumed that the acceleration exposure dose did not significantly affect the PPAEC, which would most likely cause a drop in the normalized resistance. Due to the failure in the control array, the results of the initial experiment were inconclusive and another attempt to elicit a HAVS response in the PPAEC was attempted.

A typical result of the second acceleration exposure dose experiment can be seen in **Figure A-39** where normalized data of the resistance for the shaken well confluent scan is compared to the scan after the acceleration exposure dose. The results of the shaken well (**Figure A-39**) compared to those of the control well in **Figure A-40** show very little difference between the PPAEC that were shaken and those that were not. Again, the slow drop in normalized resistance is likely caused by the length of time between the scans and not a drastic change in the PPAEC as would likely be evidenced if the acceleration exposure dose had affected the culture. The time dependent relationship for normalized resistance can be illustrated in **Figure A-41** and **Figure A-42**. In **Figure A-41**, the time study is given for the shaken well (TOP) and unshaken control well (BOTTOM). There is no plateau effect between the two scans as in the initial experiment, indicating that there was no effect from the acceleration exposure dose to the shaken well. **Figure A-42** further demonstrates the continuity between confluent and shaken data. The $\alpha$, $R_b$, and $C_m$ parameters were also calculated for this study to compare the shaken and control wells at simultaneous scans. (**Table 5**) The results of the parameter fits are again inconclusive as to a vibration induced cellular response. However, it can be

concluded from the time studies that there was no adverse effect to the vibration on the shaken well. The acceleration exposure dose has not elicited a cellular response.

Although the results of the study were indeterminate as to the endothelial monolayer barrier function when induced to vibration, it was concluded that the protocols for inducing long-term tissue damage with vibration were not enough to induce an acute inflammatory response in our endothelial monolayer. There was a mistake made in the transformation of the acceleration values given in the NIOSH review [66], presumably for the 8 hour period, to the 30 minute time period used in these experiments. Using equation **4.1**, the acceleration exposure dose that should have been applied to the PPAEC monolayer would be 60 $m/s^2$ or approximately 6 G for 30 minutes a day. Further experimentation into vibration response with an accurately calculated acceleration exposure dose or even a higher acceleration dose may prove to induce the acute inflammatory response desired for inducing HAVS. Additionally, equipment failure in the electrical switching mechanism controlled by LabVIEW limited the number of control electrodes in both studies to one. In the first study, the control electrode appeared to be faulty, due the to inconsistent normalized resistance curve at the completion of the experiment. (**Figure A-36**)

The acceleration exposure dose studies also provided some insight into the implementation of parallel multiple-array data acquisition and the time resolution tradeoff. With software controlled switching of the SR830 current clamp to each of the electrodes on an ECIS array, the number of electrodes that can feasibly be scanned is greatly increased. Similarly, the time between frequency scans on an electrode is an interval equal to the magnitude of the time it takes to scan the total number of other

electrodes in the experiment. In cellular attach studies, the initial attachment occurs within a period of 4 to 5 hours, and the time to reach confluence is approximately 18 hours. This means that the culture will be the most robust about 18 hours after seeding and will begin to lose normalized resistance slowly over the course of the next few days. The observation of time dependent interactions with ECIS requires that the number of parallel electrode arrays be minimized for maximum time resolution in each electrode frequency scan.

## III. Thesis Conclusions

The purpose of this Masters thesis was to present a definitive study of the ECIS system and make improvements to its assessment of the endothelial monolayer barrier function. This was accomplished through the identification of errors in measurement of electrical voltage data such as noise sources and an improvement to the theoretical model used to formulate the analysis of the electrical impedance data. Environmental and random noise sources were minimized through a systematic observation of spectral peaks of individual frequency scans and the application of filtering to the DAQ. The software package for analysis of raw voltage data was successful in solving for the quantitative resistance values, $\alpha$ and $R_b$ and the membrane capacitance $C_{m,}$ instead of assuming a fixed membrane capacitance for all of the wells as Giaever and Keese had. The software package is also more flexible than that provided commercially, and allows for a researcher to set every recording variable ranging from settings on the lock-in amplifier to the GPIB card. The optimized system was then used on a study of acute inflammation and the endothelial monolayer barrier function response to vibration. Although the results

of the study were indeterminate as to the endothelial monolayer barrier function when induced to vibration, it was concluded that the acceleration exposure dose, incorrectly calculated from the international standards, was not enough to induce an acute inflammatory response from our endothelial monolayer. The study also provides incites into the implementation of parallel multiple-array data acquisition and the time resolution tradeoff. In summation, the noise minimized, DAQ optimized ECIS system that we compiled was successful in correctly recording and extensively analyzing the impedance of a PPAEC monolayer subjected to various experimental conditions, of great importance to the responsible utilization of ECIS for scientific research.

# REFERENCES

1. Borkholder, D.A., *Cell Based Biosensors Using Microelectrodes*, in *Department of Electrical Engineering*. 1998, Stanford. p. 253.

2. Weiss, T.F., *Transport*. Cellular Biophysics. Vol. 1. 1996. 693.

3. Bernstein, J., *Untersuchugen zu Thermodynamik der bioelektrischen Ströme.* Erster Theil Pfluegers Arch, 1902. **92**: p. 521-562.

4. Teisseyre, A., *The "Patch-Clamp" Technique and its application in investigations of the properties of human T lymphocyte potassium channels.* Cellular & Molecular Biology Letters, 2001. **6**: p. 93-105.

5. Cole, K.S. and H.J. Curtis, *Electrical impedance of the squid giant axon during activity.* Journal of General Physiology, 1939. **22**(5): p. 649-670.

6. Hodgkin, A.L. and A.F. Huxley, *A quantitative description of membrane current and its application to conduction and excitation in nerve.* Journal of Physiology, 1952. **117**: p. 500-544.

7. Breckenridge, L.J., et al., *Advantages of using microfabricated extracellular electrodes for in vitro neuronal recording.* Journal of Neuroscience Research, 1995. **42**: p. 266-276.

8. Giaever, I. and C.R. Keese. *Micromotion of mammalian cells measured electrically*. in *Proceedings of the National Academy of Sciences of the United States of America*. 1991.

9. Thomas, C.A., Jr., et al., *Miniature Microelectrode Array To Monitor Bioelectric Activity Of Cultured Cells.* Experimental Cell Research, 1972. **74**(1): p. 61-66.

10. Fricke, H. and S. Morse, *The electric resistance and capacity of blood for frequencies between 800 and 4.5 million cycles.* Journal of General Physiology, 1926. **9**: p. 153-167.

11. Fricke, H. and H.J. Curtis, *The electric impedance of hemolyzed suspensions of mammalian erythrocytes.* Journal of General Physiology, 1935. **18**: p. 821-836.

12. Cole, K.S. and H.J. Curtis, *Electrical impedance of Nitella during activity.* Journal of General Physiology, 1939. **22**(1): p. 37-64.

13. Schwan, H.P., *Electrical properties of tissue and cell suspensions*, in *Advances in Biological and Medical Physics*. 1957: New York. p. 147-209.

14. Hause, L.L., R.A. Komorowski, and F. Gayon, *Electrode and electrolyte impedance in the detection of bacterial growth.* IEEE Transactions on Biomedical Engineering, 1981. **BME-28**(5): p. 403-410.

15. Giaever, I. and C.R. Keese. *Monitoring Fibroblast Behavior in Tissue Culture with an Applied Electric Field*. in *Proceedings of the National Academy of Sciences of the United States of America*. 1984.

16. Johnson, H.L., et al., *Predicting total-body water and extracellular fluid volumes from bioelectrical measurements of the human-body.* Journal Of The American College of Nutrition, 1992. **11**(5): p. 539-547.

17. Dijkstra, A.M., et al., *Clinical applications of electrical impedance tomography.* Journal of Medical Engineering and Technology, 1993. **17**(3): p. 89-98.

18. Xiao, C. and J.H.T. Luong, *On-Line Monitoring of Cell Growth and Cytotoxicity Using Electric Cell-Substrate Impedance Sensing (ECIS).* Biotechnology Progress, 2003. **19**(3): p. 1000-1005.

19. Moy, A.B., et al., *Histamine and Thrombin Modulate Endothelial Focal Adhesion Through Centripetal and Centrifugal Forces.* The Journal of Clinical Investigation, 1996. **97**(4): p. 1020-1027.

20. Wegener, J., C.R. Keese, and I. Giaever, *Electric Cell-Substrate Impedance Sensing (ECIS) as a Noninvasive Means to Monitor the Kinetics of Cell Spreading to Artificial Surfaces.* Experimental Cell Research, 2000. **259**(1): p. 158-166.

21. Charboneau, A.L., et al., *Supression Of Growth And Increased Cellular Attachement After Expression Of DAL-1 In MCF-7 Breast Cancer Cells.* International Journal of Cancer, 2002. **100**: p. 181-188.

22. Burns, A.R., et al., *Analysis of tight junctions during neutrophil transendothelial migration.* Journal of Cell Science, 2000. **113**: p. 45-57.

23. Lo, C.-M., C.R. Keese, and I. Giaever, *Cell–Substrate Contact: Another Factor May Influence Transepithelial Electrical Resistance of Cell Layers Cultured on Permeable Filters.* Experimental Cell Research, 1999. **250**: p. 576-580.

24. Smith, T.J., et al. *Prostaglandin $E_2$ elicits a morphological change in cultured orbital fibroblasts from patients with Graves opthalmopathy*. in *Proceedings of the National Academy of Sciences of the United States of America*. 1994.

25. Tiruppathi, C., et al. *G protein-coupled receptor kinase-5 regulates thrombin-activated signaling in endothelial cells*. in *Proceedings of the National Academy of Sciences of the United States of America*. 2000.

26. Noiri, E., et al., *Podokinesis in endothelial cell migration: role of nitric oxide.* The American Journal of Physiology, 1998. **274**(Cell Physiology 43): p. C236-C244.

27. Misfledt, D., S. Hamamoto, and D. Pitelka. *Transepithelial Transport in Cell Culture*. in *Proceedings of the National Academy of Sciences of the United States of America*. 1976.

28. Fredriksen, O. and P.P. Leyssac, *Effects of cytochalasin B and dimethysulphoxide on isosmotic fluid transport by rabbit gall-bladder in vitro.* The Journal of Physiology, 1977. **265**(1): p. 103-118.

29. Lo, C.-M., C.R. Keese, and I. Giaever, *Cell-Substrate Contact: Another Factor May Influence Transepithelial Electrical Resistance of Cell Layers Cultured on Permeable Filters.* Experimental Cell Research, 1999. **250**: p. 576-580.

30. Thompson, D., ed. *The Concise Oxford Dictionary of Current English*. 9th ed., ed. H.W. Fowler and F.G. Fowler. 1995, Clarendon Press: Oxford. 1673.

31. Oppenheim, A.V. and R.W. Schafer, *Digital Signal Processing*. 1975, Englewood Cliffs: Prentice-Hall. 585.

32. Nyquist, H., *Regeneration theory.* Bell Systems Technology Journal, 1932. **11**: p. 126-147.

33. *Model SR830 DSP Lock-In Amplifier*. 2001, Sunnyvale: SRS, Inc. 174.

34. Bennett, W.R., *Electrical Noise*. 1960, York, PA: The Maple Press Company. 280.

35. Bell, D.A., *Electrical Noise Fundamentals and Physical Mechanism*. 1960, Glasgow: D. Van Nostrand Company. 342.

36. *National Instruments LabVIEW Analysis Concepts*. July 2000 ed. 2000, Austin: National Instruments Corporation. 82.

37. Seeley, R.R., T.D. Stephens, and P. Tate, *Essentials of Anatomy and Physiology*. 4th ed. 2002, New York: McGraw-Hill. 644.

38. DePaola, N., et al., *Electrical Impedance of Cultured Endothelium Under Fluid Flow.* Annals of Biomedical Engineering, 2001. **29**: p. 648-656.

39. Minnear, F.L., et al., *Platelet lipid(s) bound to albumin increases endothelial electrical resistance: mimicked by LPA.* American Journal of Physiology. Lung Cell Molecular Physiology, 2001. **281**: p. L1337-L1344.

40. Phelps, J.E. and N. DePaola, *Spatial variations in endothelial barrier function in disturbed flows in vitro.* American Journal of Physiology. Heart Circulatory Physiology, 2000. **278**: p. H469-H476.

41. Gonzalez-Mariscal, L., *The relationship between structure and function of tight junctions*. Tight Junctions, ed. M. Cereijido. 2001, Boca Raton, FL: CRC Press. 772.

42. Slade, P.G., ed. *Electrical contacts: principles and applications*. Electrical engineering and electronics. 1999, Marcel Dekker: New York. 1073.

43. Applied-BioPhysics, *www.biophysics.com*. 2003.

44. Press, W.H., et al., *Numerical Recipes, The Art of Scientific Computing, (FORTAN Version)*. 1989, Cambridge: Cambridge University Press. 702.

45. Stevenson, B.R. and D.A. Begg, *Concentration-dependent effects of cytochalasin D on tight junctions and actin filaments in MDCK epithelial cells.* Journal of Cell Science, 1994. **107**(3): p. 367-375.

46. Hunziker, W., P. Male, and I. Mellman, *Differential microtubule requirements for transcytosis in MDCK cells.* European Molecular Biology Organization Journal, 1990. **9**: p. 3515-3525.

47. Kobayashi, M., et al., *Protein kinase C activation by 12–0-tetradecanoylphorbol 13-acetate in CG-4 line oligodendrocytes stimulates turnover of choline and ethanolamine phospholipids by phospholipase D and induces rapid process contraction.* Journal of Neurochemistry, 2001. **76**(2): p. 361-371.

48. Park, J., et al., *Acrylamide-Induced Cellular Transformation.* TOXICOLOGICAL SCIENCES, 2002. **65**: p. 177-183.

49. Sickles, D.W., et al., *Direct effect of the neurotoxicant acrylamide on kinesin-based microtubule motility.* Journal of Neuroscience Research, 1996. **46**(1): p. 7-17.

50. *Criteria for a Recommended Standard: Occupational Exposure to Hand-Arm Vibration*. 1989, NIOSH: Cincinnati, Ohio. p. 127.

51. *BS 6842 Guide to Measurement and Evaluation of Human Exposure to Vibration Transmitted to the Hand*. 1987, BSI: London. p. 20.

52. *BS 7482 Instrumentation for the Measurement of Vibration Exposure of Human Beings - Specification for General Requirements for Instrumentation for Measuring the Vibration Applied to Human Beings*. 1991, GME/21: London. p. 8.

53. *ISO 5349 Mechanical vibration - Measurement and evaluation of human exposure to hand-transmitted vibration*. 2002, CEN: Brussels. p. 139.

54. *ISO 8041 Human Response to Vibration - Measuring Instrumentation*. 1990, ISO: Geneve. p. 24.

55. *ISO 10819 Mechanical Vibration and Shock - Hand-Arm Vibration - Method for the Measurement and Evaluation of the Vibration Transmissibility of Gloves at the Palm of the Hand*. 1996, ISO: Geneve. p. 17.

56. Chetter, I.C., P.J. Kent, and R.C. Kester, *The hand arm vibration syndrome: a review.* Cardiovascular Surgery, 1997. **6**(1): p. 1-9.

57. Takeuchi, T., et al., *Pathological changes observed in the finger biopsy of patients with vibration induced white finger.* Scandinavian Journal of Work, Environment and Health, 1986. **12**: p. 280-283.

58. Welsh, C.L., *Digital rewarming time in the measurement of vibration-induced white finger.* Scandinavian Journal of Work, Environment and Health, 1986. **12**(4): p. 259-250.

59. Chetter, I.C., et al., *The Utilization of Cold Provocation Thermography in Upper Limb Vasospastic Conditions.* Cardiovascular Surgery, 1997. **5**(Supplement 1): p. 45.

60. Stoyneva, Z., et al., *Current pathophysiological views on vibration-induced Raynaud's phenomenon.* Cardiovascular Research, 2003. **57**(3): p. 615-624.

61. Kanazuka, M., et al., *Increase in plasma thrombomodulin level in patients with vibration syndrome.* Thrombosis Research, 1996. **82**(1): p. 51-56.

62. Gemne, G. *Where is the research frontier for hand arm vibration?* in *8th International Conference on Hand-Arm Vibration*. 1998. Umea, Sweden.

63. Gurram, R., S. Rakheja, and G.J. Gouw, *Mechanical impedance of the human hand-arm system subject to sinusoidal and stochastic excitations.* International Journal of Industrial Ergonomics, 1995. **16**: p. 135-145.

64. Wasserman, D., J. Wasserman, and J.I. Ahn, *Instrumentation for Measuring Coupling Forces of Hand-Held Tools.* Sound and Vibration, 2001(Materials Reference): p. 2-5.

65. Wu, J.Z., et al., *Simulation of mechanical responses of fingertip to dynamic loading.* Medical Engineering & Physics, 2002. **24**: p. 253-264.

66. *Musculoskeletal Disorders and Workplace Factors; A Critical Review of Epidemiologic Evidence for Work-Related Musculoskeletal Disorders of the Neck, Upper Extremity, and Low Back; 5c Hand-Arm Vibration Syndrome*. 1997, NIOSH: Cincinatti. p. 31.

# APPENDIX: FIGURES

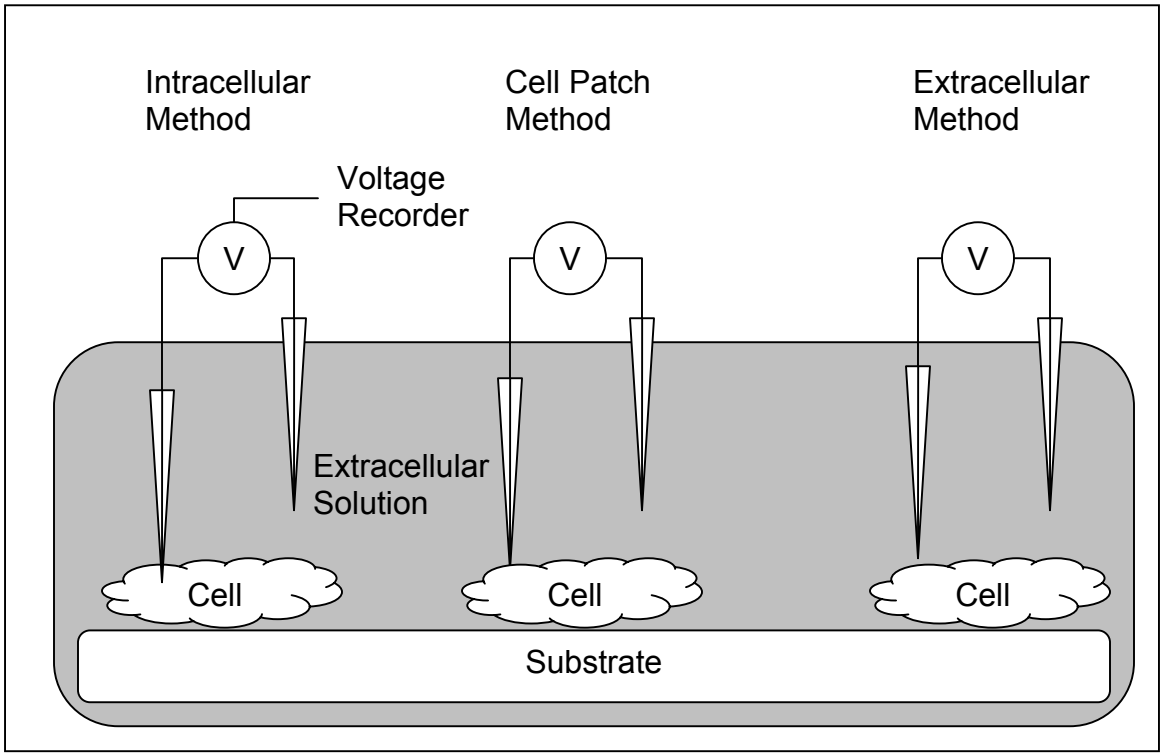


**Figure A-1. Three traditional methods for measuring cellular electrical activity. For intracellular recordings the micropipette can be inserted through the membrane to directly measure the intracellular potential. Secondly, for the whole cell patch the micropipette can be brought into contact with the cell and a light suction applied, forming a tight seal and adding the ability to monitor membrane impedance. For extracellular recordings a micropipette or microwire is positioned in close proximity to the cell. Adapted from [1].**

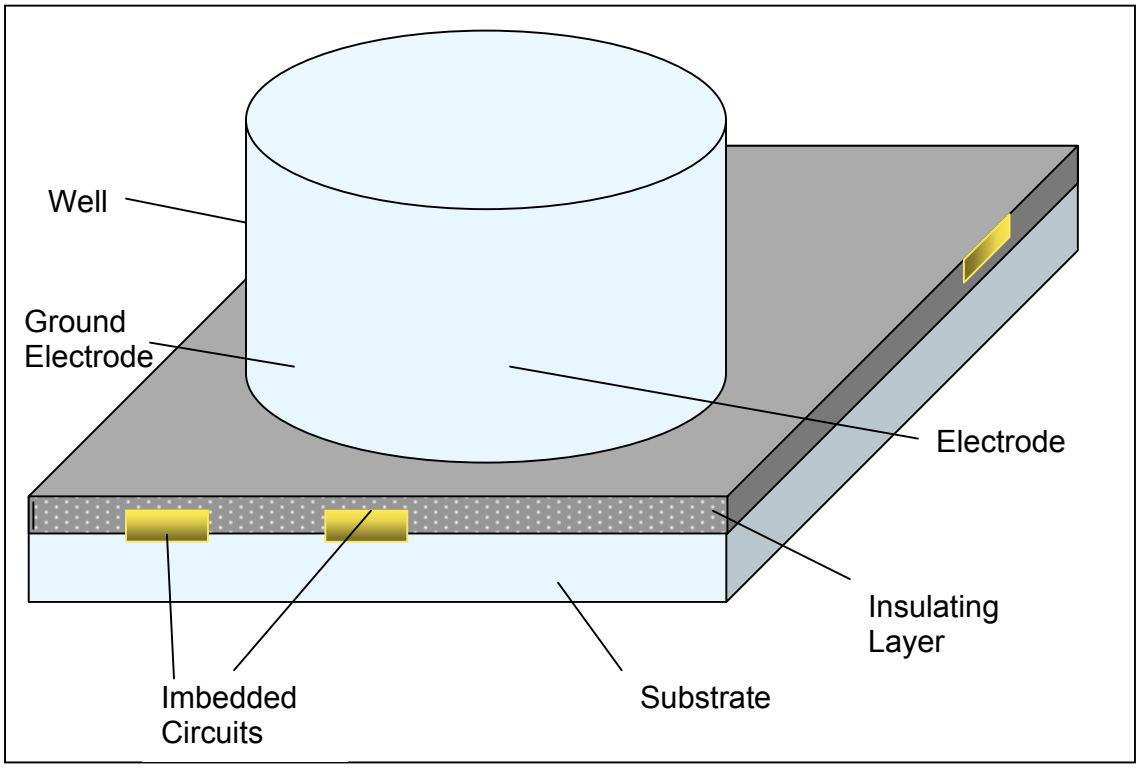


**Figure A-2. Cross-section of a planar microelectrode, comprised of a substrate, a conductor to form the circuit, and an insulating layer, removed in the areas to define the electrode. Cells are cultured directly on the electrode surface in a contained volume well.**

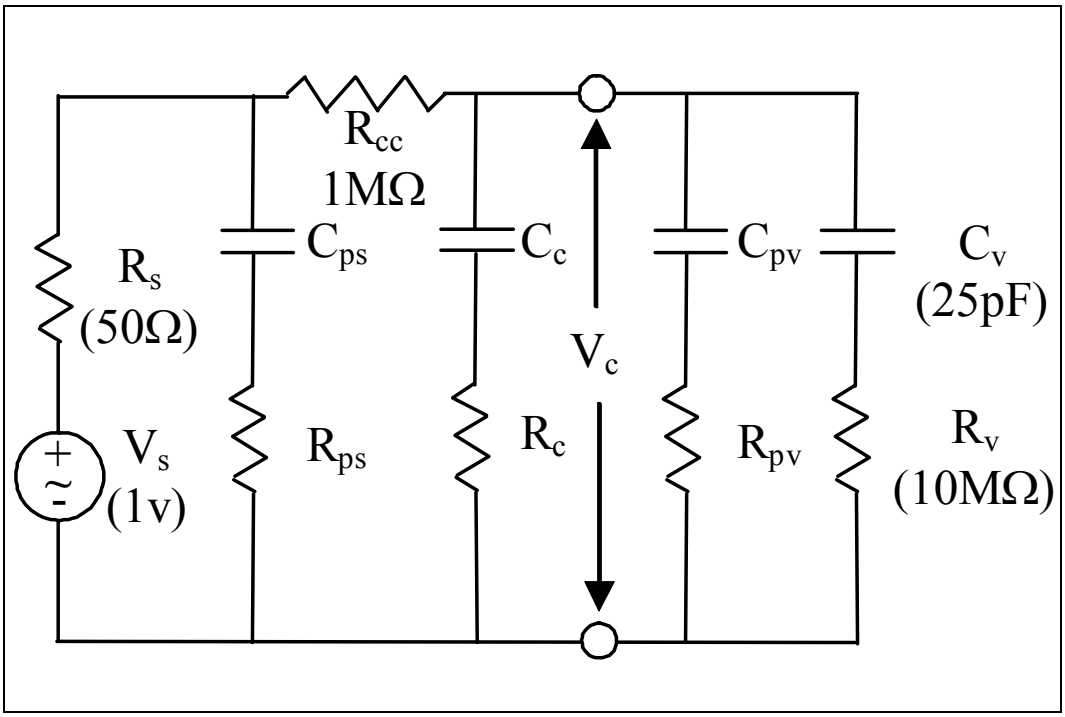


**Figure A-3. A general circuit diagram for the ECIS instrumentation. The voltage source resistance, Rs, is 50 Ω and the input resistance, Rv, and capacitance, Cv, of the phase sensitive detector are 10 MΩ and 25 pF respectively. Parasitic lead resistances and capacitances are associated with the source, Rps & Cps, and phase sensitive detector, Rpv & Cpv. Typical values for the parasitic resistance and capacitance are 1 kΩ and 0.19 nF Respectively. A 1 MΩ resistor, Rcc, is connected in series with the AC voltage source to stabilize the current through the electrode. The electrode resistance, Rc, and capacitance, Cc, are functions of frequency.**

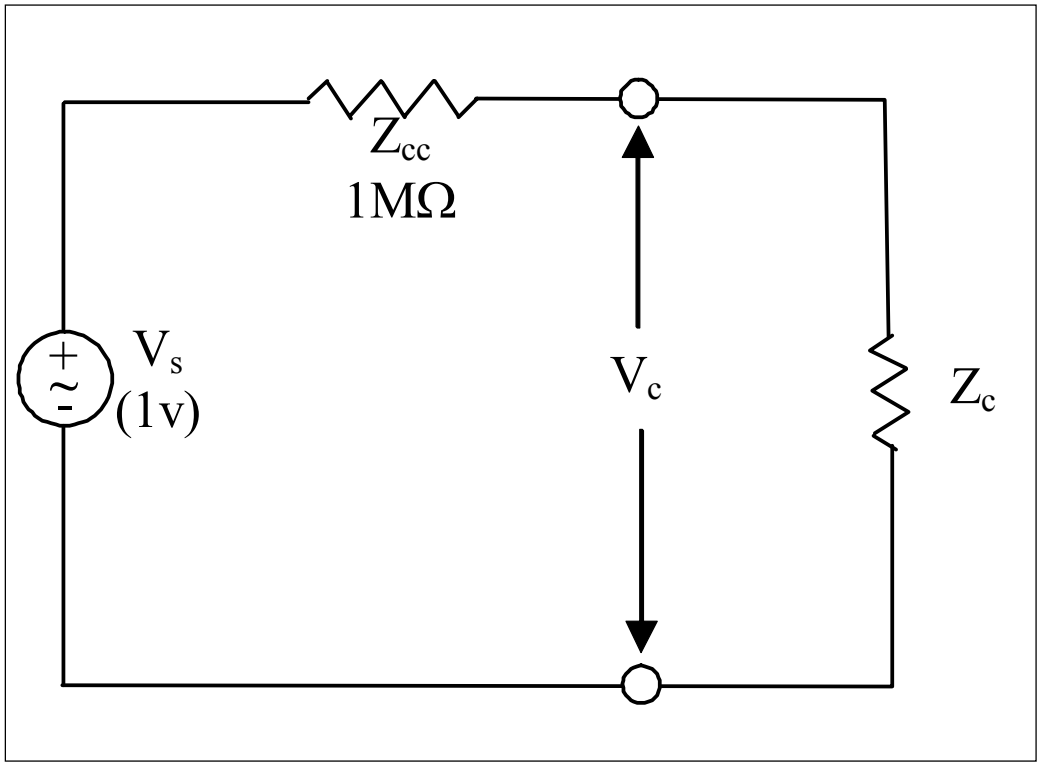


**Figure A-4. Simplified circuit diagram for cellular impedance measurements. A 1MΩ resistor, Zcc, in series with a 1 V voltage source, Vs, provides a 1 μA current clamp on the electrode, with impedance Zc, to be measured.**

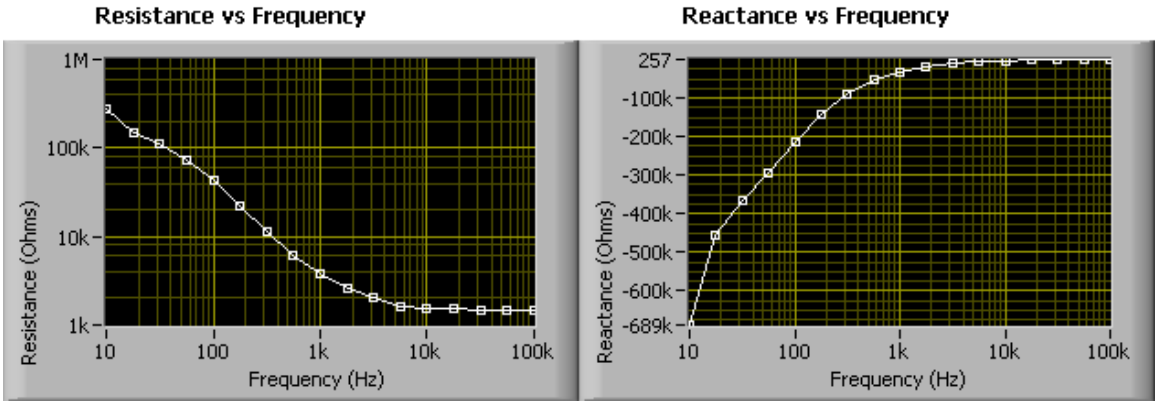


**Figure A-5. Minimally filtered (10 µsec, 6 dB/octave) resistive and reactive average measurements of a naked gold electrode containing only cell culture media as a function of frequency.**

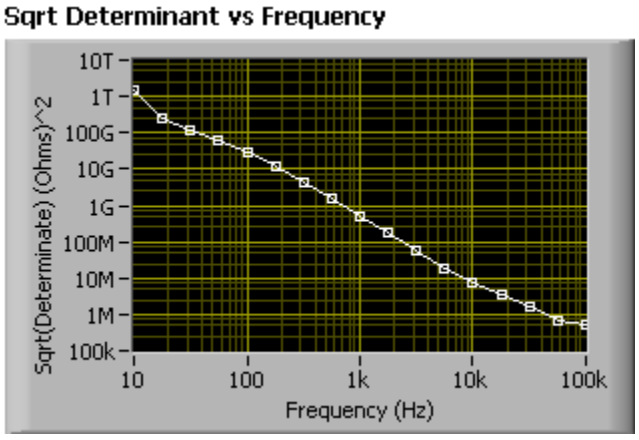


**Figure A-6. Square root determinate of the covariance matrix of resistive and reactive measurements, minimally filtered (10 µsec, 6 dB/octave), of a naked electrode as a function of frequency. Demonstrating that the relative error to averaged measurements tends to decrease as a function of frequency.**

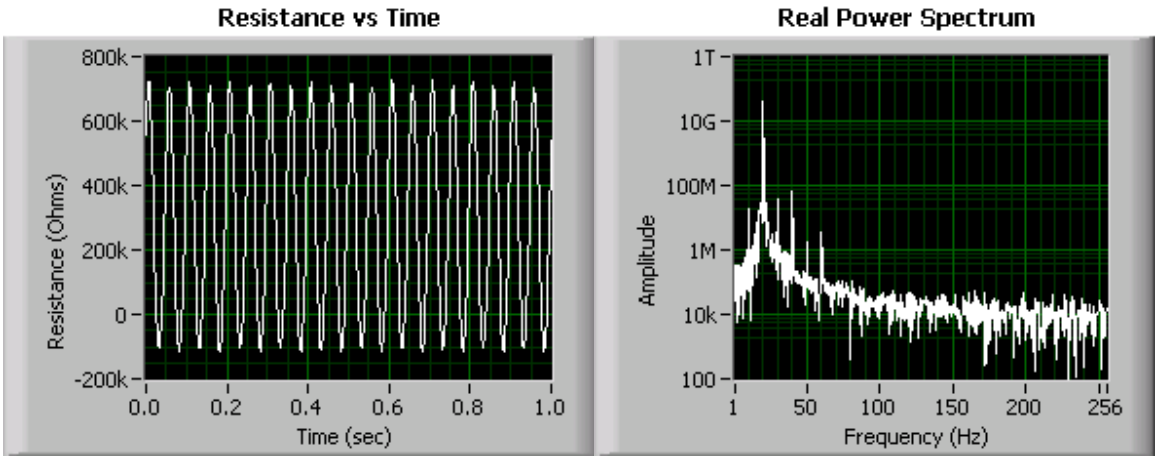


**Figure A-7. 10 Hz resistance data point time sequence and power spectrum, minimally filtered (10 µsec, 6 dB/octave), of a naked electrode. The interference can be seen in the spectral analysis and consists of harmonic noise at 20 Hz and other multiples of 10, surrounded by random Gaussian noise.**

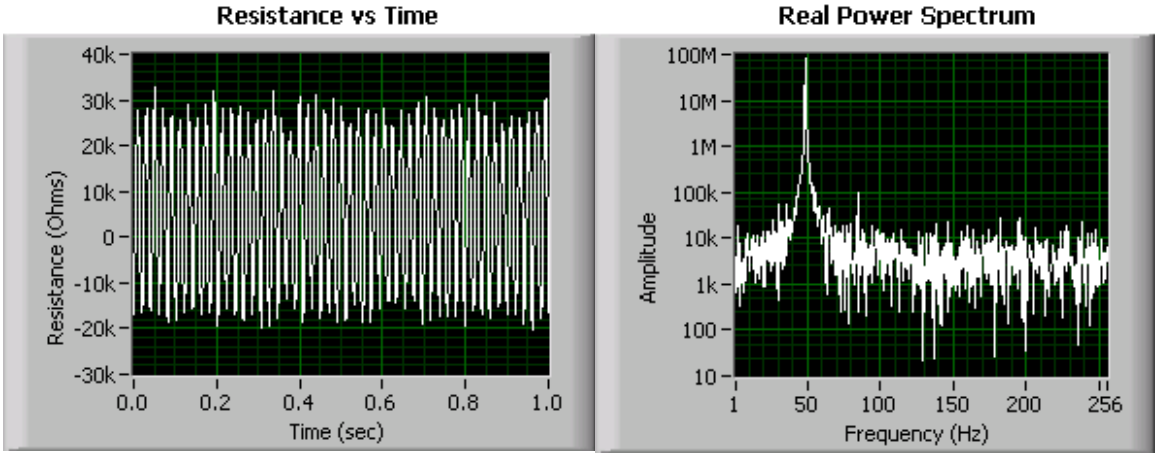


**Figure A-8. 1 kHz resistance data point time sequence and power spectrum, minimally filtered (10 µsec, 6 dB/octave), of a naked electrode. The interference can be seen in the spectral analysis and consists of harmonic noise following phase sensitive detection. A strong 48 Hz component is caused by the 1 kHz reference frequency, due to difference signal from the PSD sampling fourth harmonic and the lock-in frequency second harmonic. There is also a gradual roll-off from the aliasing and spectral folding of higher frequency harmonics.**

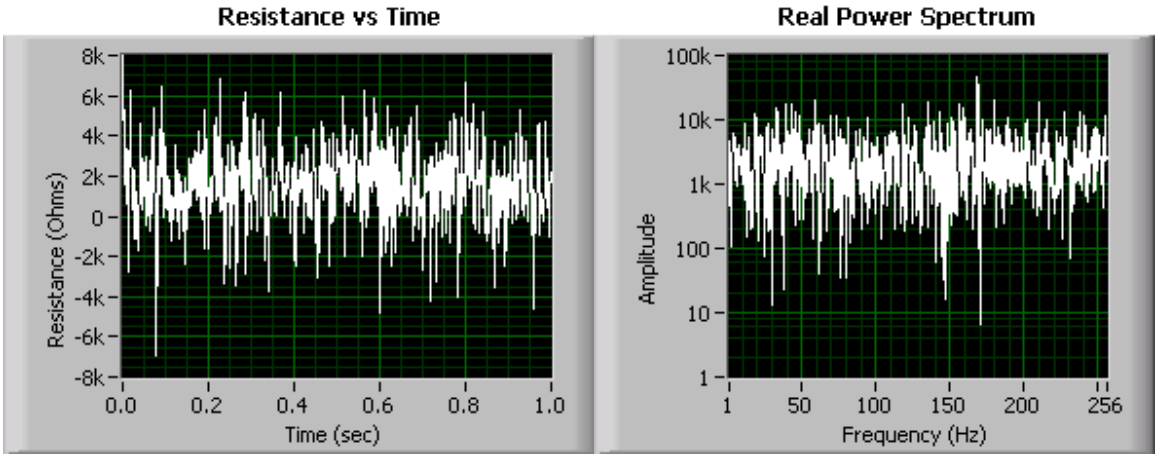


**Figure A-9. 100 kHz resistance data point time sequence and power spectrum, minimally filtered (10 µsec, 6 dB/octave), of a naked electrode. The interference can be seen in the spectral analysis and consists of many different interfering peaks, many of which are caused by the spectral folding and aliasing of higher harmonics, giving the appearance of random Gaussian noise.**

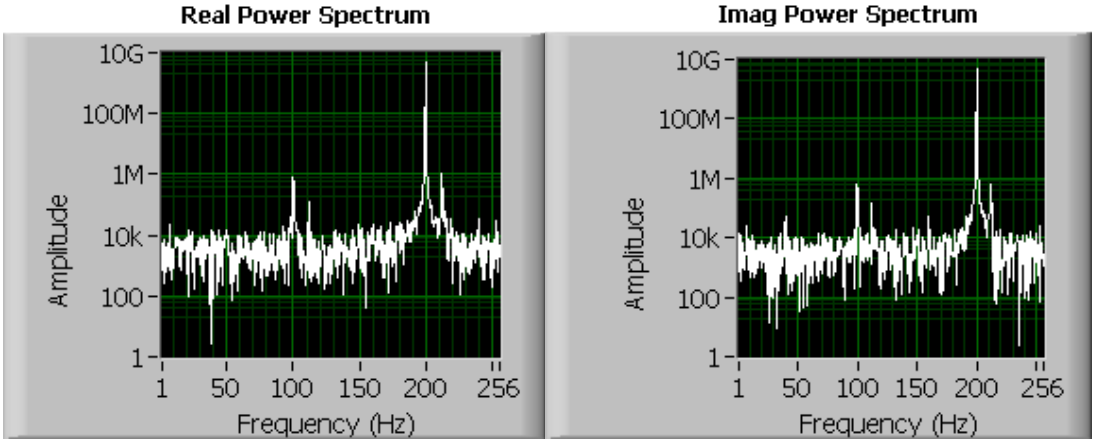


**Figure A-10. Harmonic noise represented in the power spectra of a minimally filtered (10 µsec, 6 dB/octave) 100 Hz impedance measurement of a naked gold electrode. Harmonic noise sources appear at 100 and 200 Hz.**

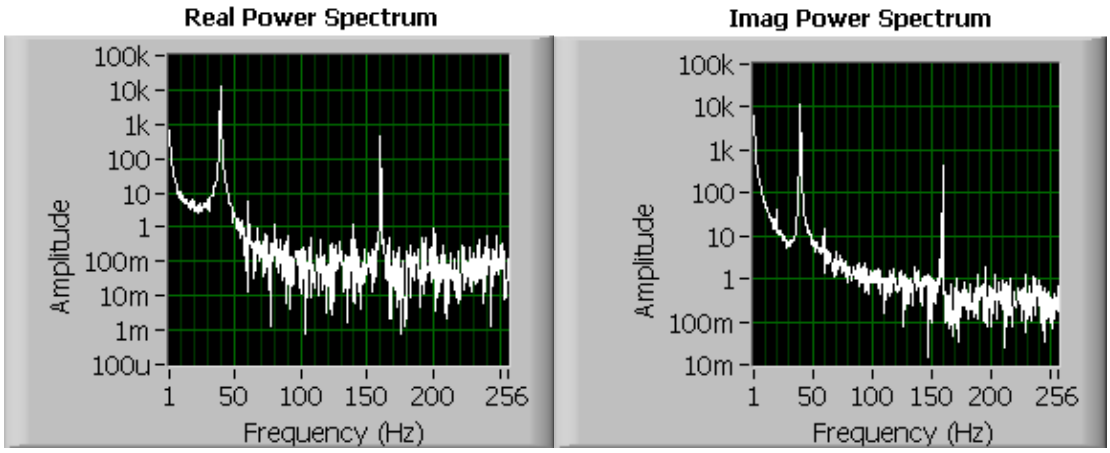


**Figure A-11. 60 Hz noise in the power spectra of a minimally filtered (10 µsec, 6 dB/octave) 100 Hz impedance measurement of a naked gold electrode following SYNC filtering. The harmonic noise peaks have been removed to reveal addition and subtraction peaks resulting from 60 Hz noise.**

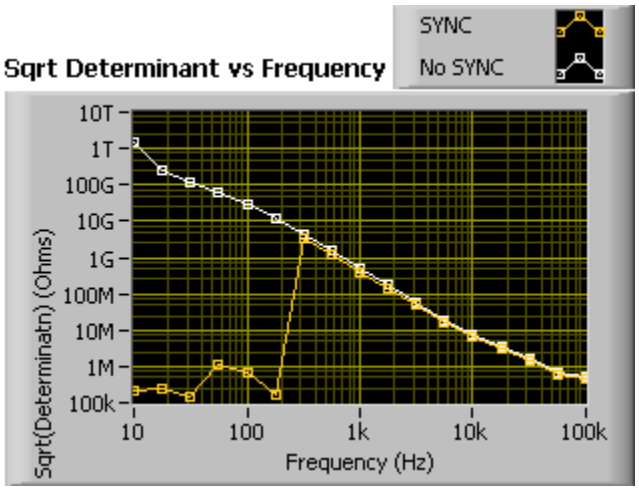


**Figure A-12. Square root determinate of the covariance of the resistive and reactive measurements, minimally filtered (10 µsec, and 6 dB/octave), of a naked electrode as a function of frequency. Using synchronous filtering (in orange) shows a much different pattern in the errors than those without SYNC filtering (in white).**

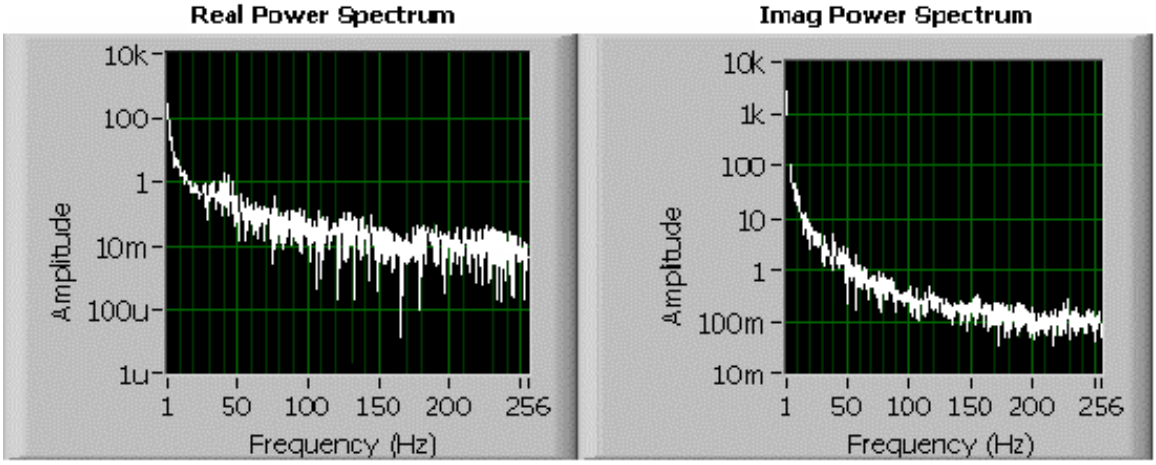


**Figure A-13. Removal of 60 Hz noise in the power spectra with a 300 ms time constant (SYNC, 6 dB/octave) in a 100 Hz reference frequency impedance measurement of a naked gold electrode.**

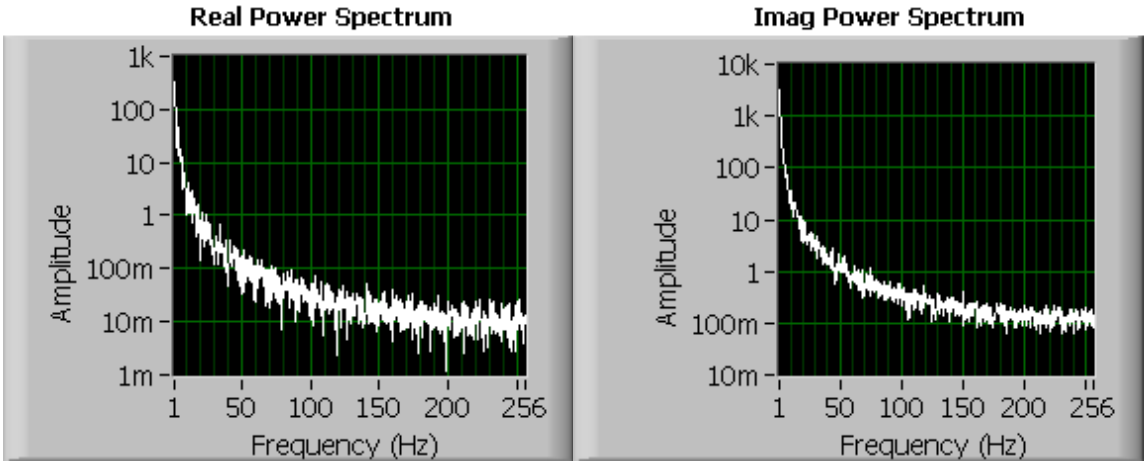


**Figure A-14. Gaussian noise minimization and aliasing of 60 Hz and Harmonic noise in the power spectra of impedance data of a naked electrode at the 100 Hz reference frequency level with SYNC, 300 ms, and 24 dB/octave filtering.[BDC23] Notice that the overall magnitude of the spectra has dramatically decreased (10k to 1k) from Figure A-11 and Figure A-13.**

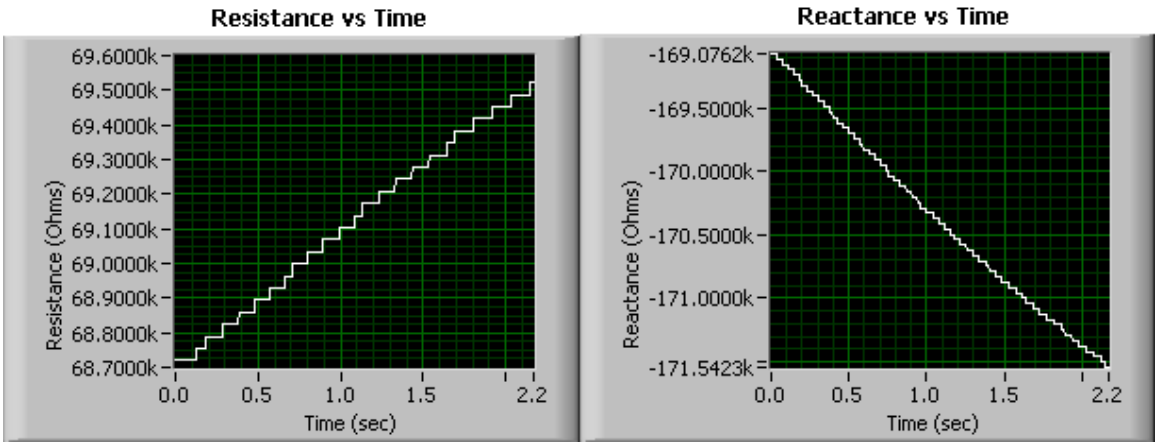


**Figure A-15. A/D Noise in real and imaginary time sequences at a reference frequency of 100 Hz using SYNC, 300 ms, and 24 dB/octave filtering. A small amount of drift is present and evidence of A/D noise can be seen in the time sequence data.**

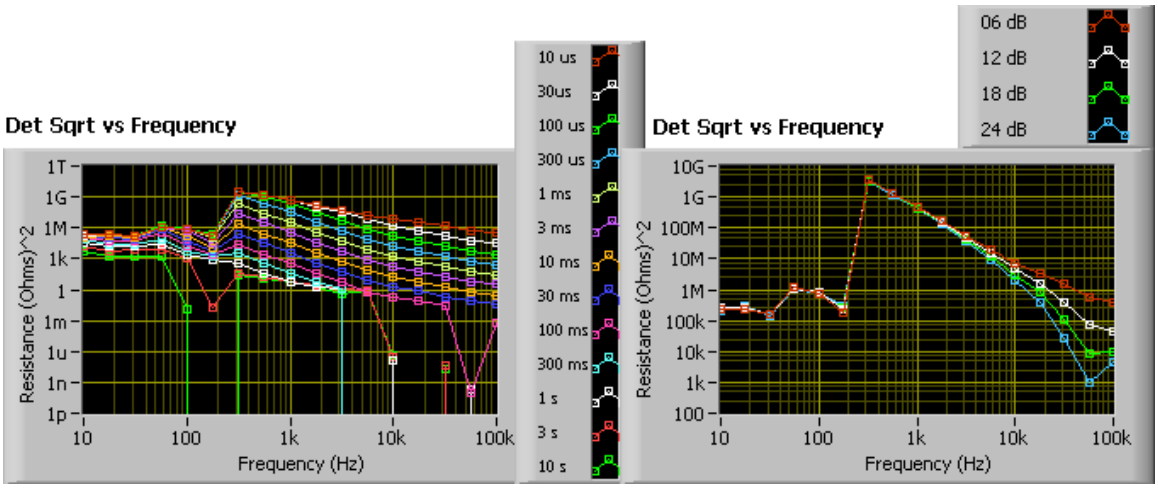


**Figure A-16. SYNC filter effect on the determinant square root of the covariance matrix for impedance averages over a full frequency scan, specifically at frequencies < 200 Hz., as a function of time constant with 6 dB roll off (LEFT) and roll off filter with a 10 µs time constant (RIGHT) that are represented by the series of colored lines. Below 200 Hz, the SYNC filter drastically reduces error. Zero values occur from A/D noise.**

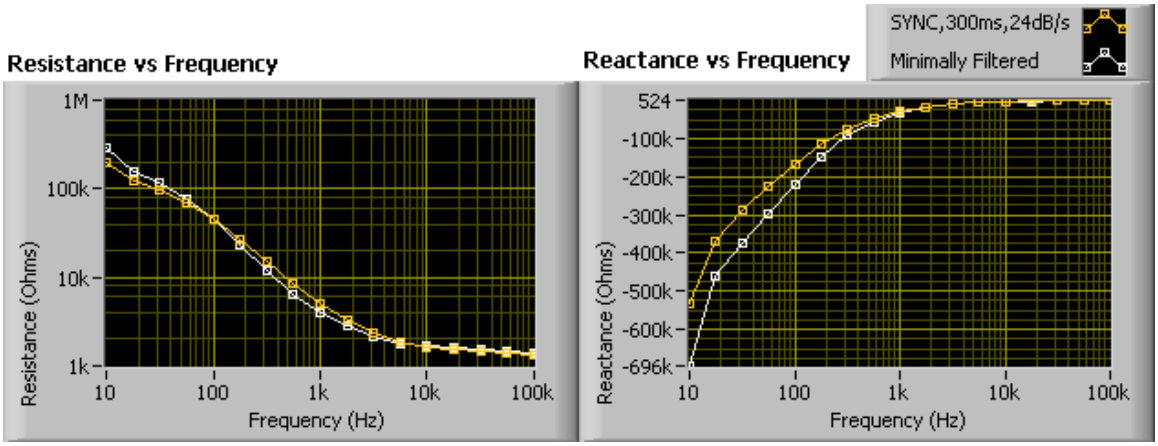


**Figure A-17. Minimally (in white) and optimally (in orange) filtered resistive and reactive average measurements of a naked gold electrode [BDC25]as a function of frequency. The optimally filtered data has dropped resistance and added impedance in the lower frequencies and gained some resistance in the mid-range frequencies, an effect of drift and minimizing the noise.**

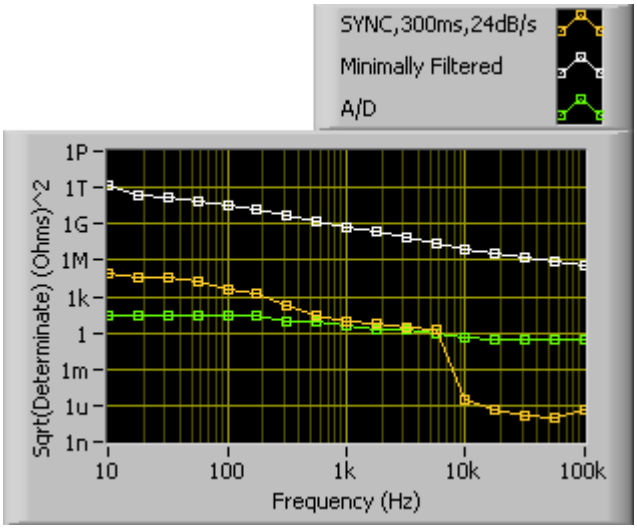


**Figure A-18. Square root determinate of minimally (in white) and optimally (in orange) filtered data. A/D levels (in green) have been included to demonstrate the area where they become important ( > 10 kHz). The square root determinate has dropped by 2 orders of magnitude, signifying a major loss of error in our measurements.**

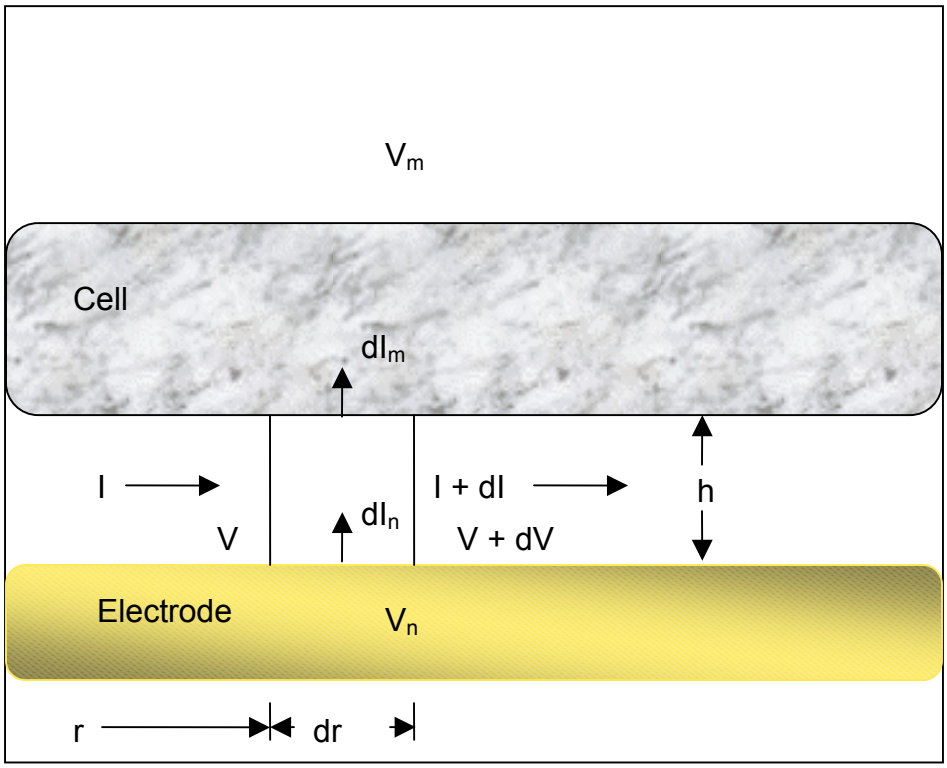


**Figure A-19. Diagram of the cell-substrate geometry, introducing spatial electrical equations. Adapted from [8]**

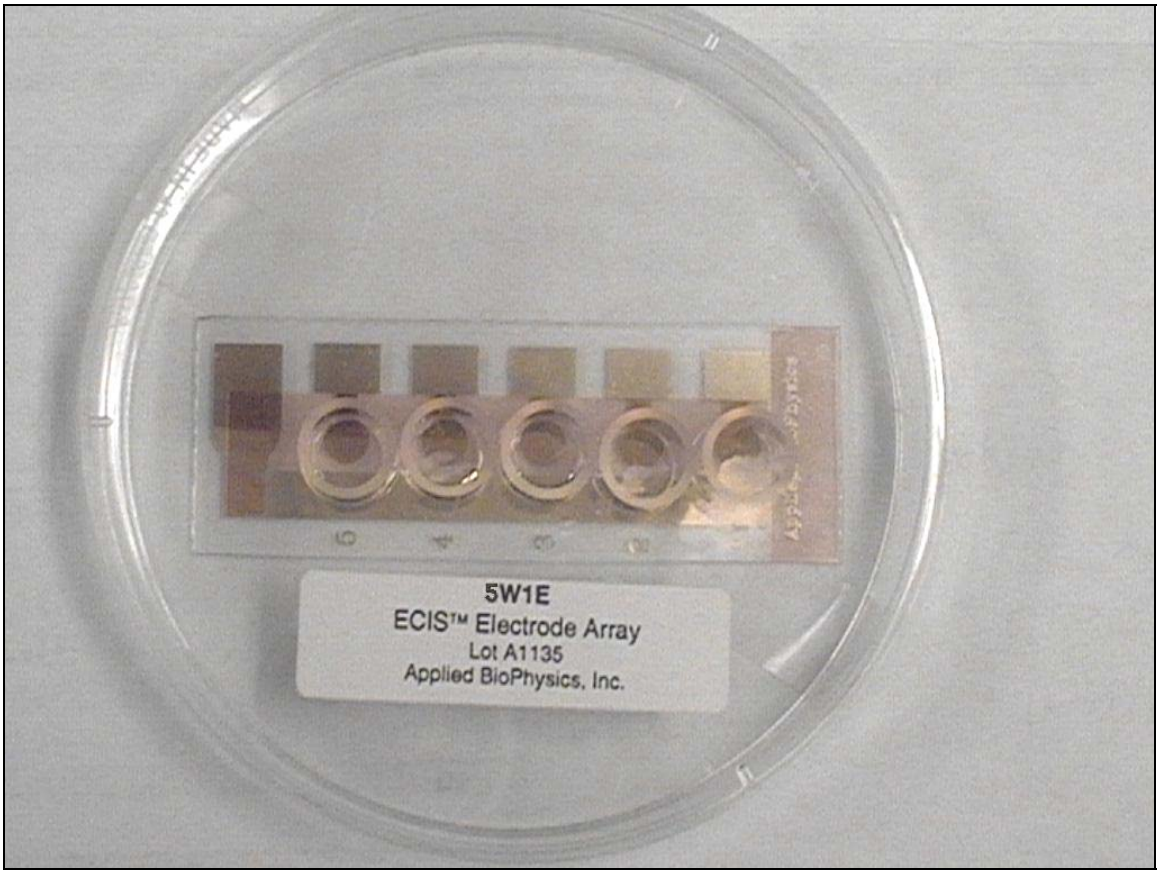


**Figure A-20. ECIS 5 well array, 5W1E, purchased from Applied Biosciences. Consisting of gold film electrodes insulated by a photoresist film and mounted on a .025 mm thick clear Lexan polycarbonate substrate that is clear enough to allow for the observation of cells using an inverted microscope. Each electrode has a 250 µm diameter exposed area and each well holds approximately 500 µL.**

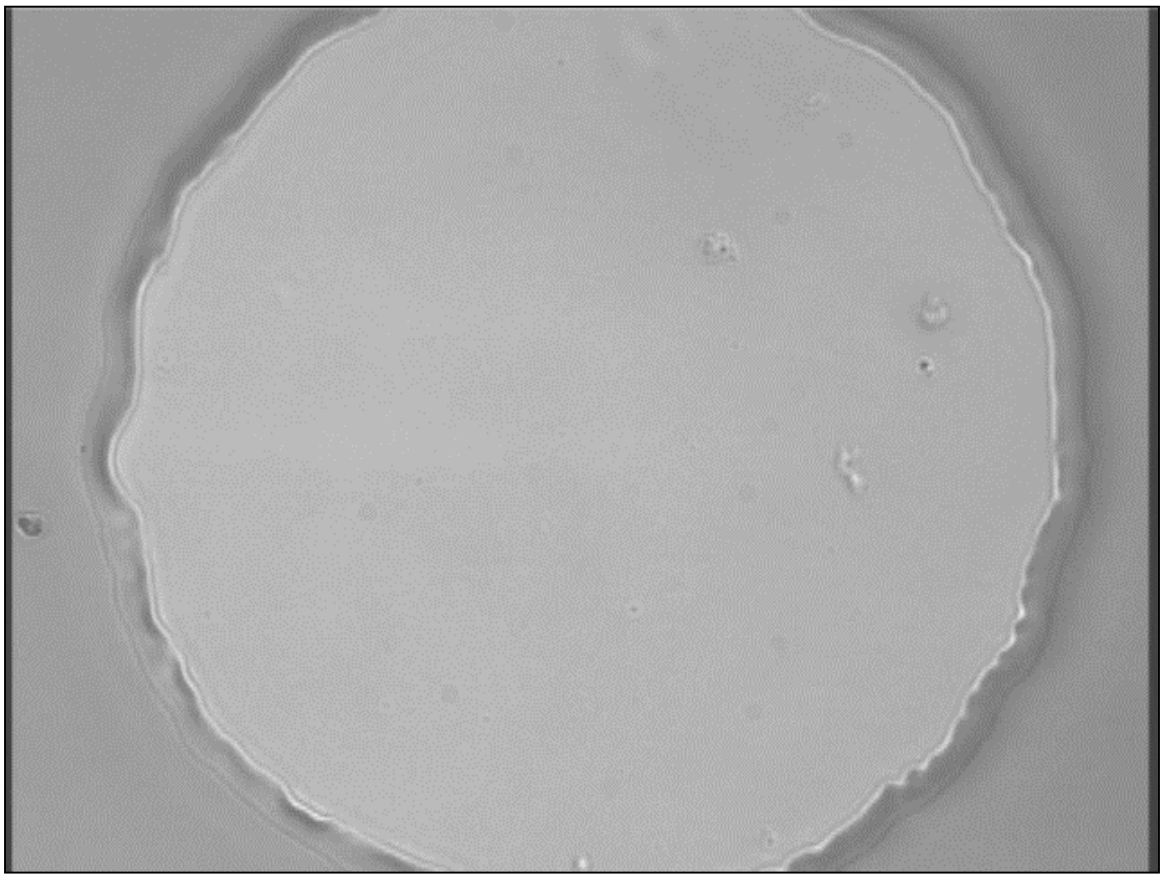

**Figure A-21. Electrode just after cell seeding, magnified 20X. The exposed electrode surface, the light area, is initially free of PPAEC. The random shaped objects out of the plane of focus are PPAEC that have not yet attached to the electrode and stretched out to form their characteristic cobblestone morphology.**

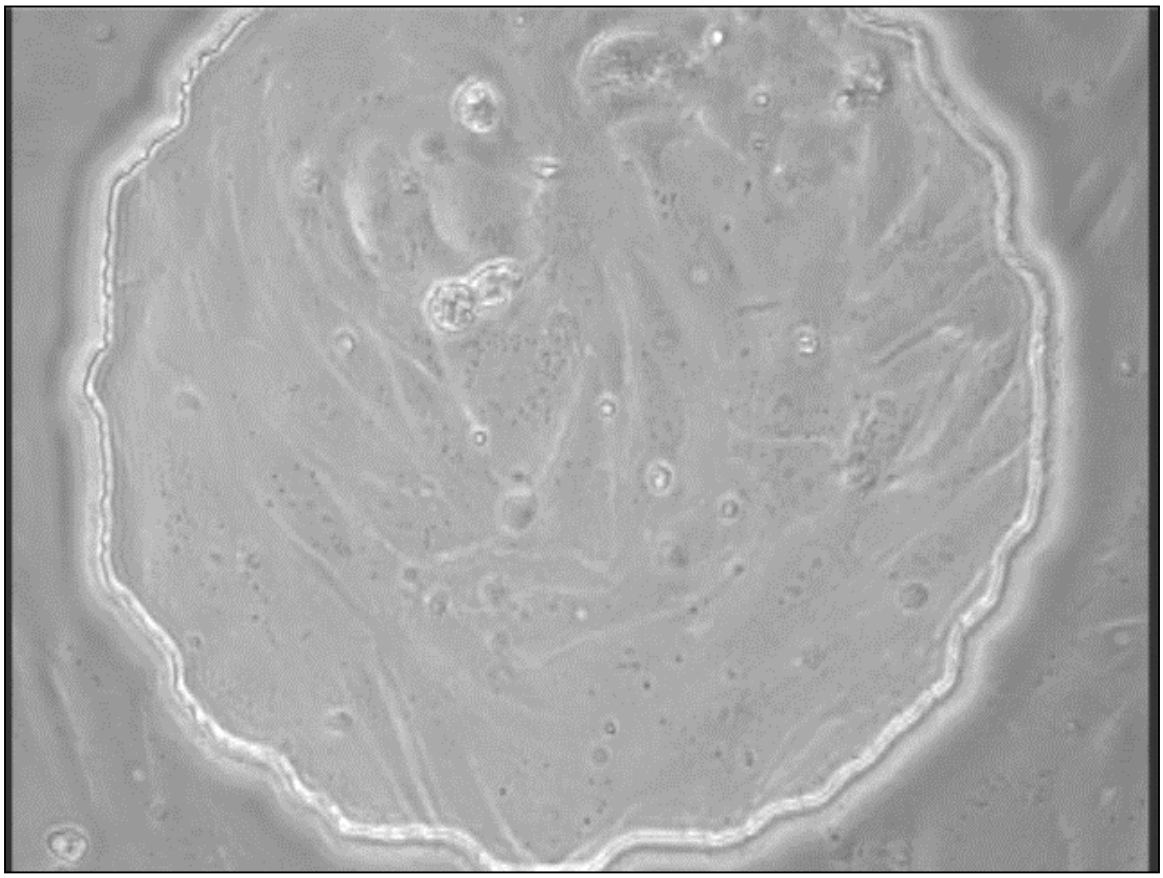

**Figure A-22. Electrode at confluence 24 hours after seeding, magnified 20X. The exposed electrode surface, the light area, is confluent with PPAEC, which now have a cobblestone appearance.**

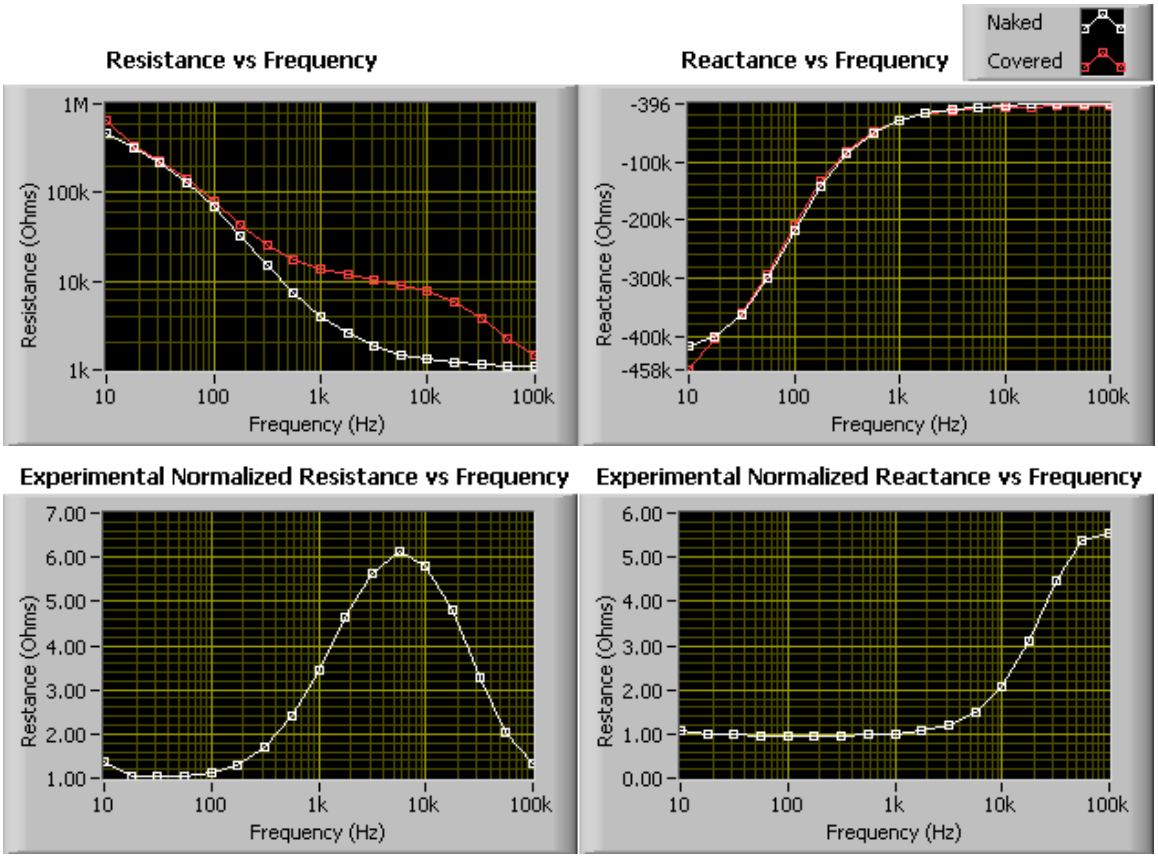


**Figure A-23. Naked and Cell Covered Real and Imaginary impedances (TOP) Normalized Real and Imaginary impedances (BOTTOM). The normalized curves demonstrate the magnitude that the PPAEC monolayer impedance has on top of that of just the naked electrode. The largest cellular effect can be seen in the resistance at the 5.62 kHz frequency level, approximately 6 times the effective impedance of the naked electrode at that level.**

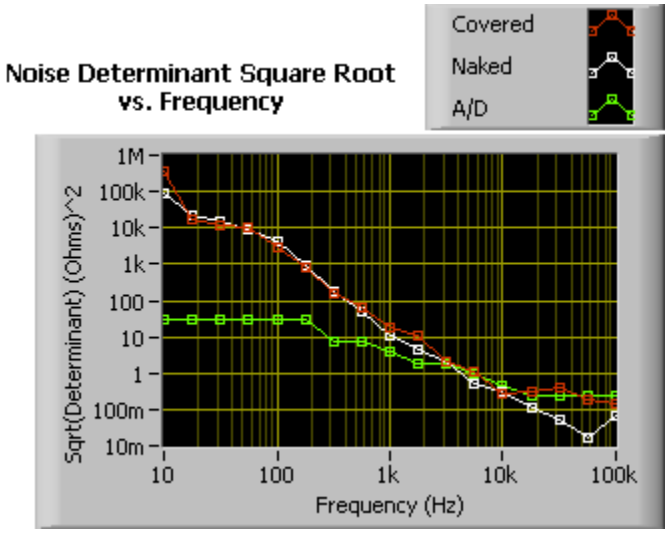


**Figure A-24. Square-root determinant vs. frequency, exemplifying the noise of the system. The A/D noise level is included as a basis for the size of the relative noise component. A/D noise becomes important at the 10 kHz level and above.**

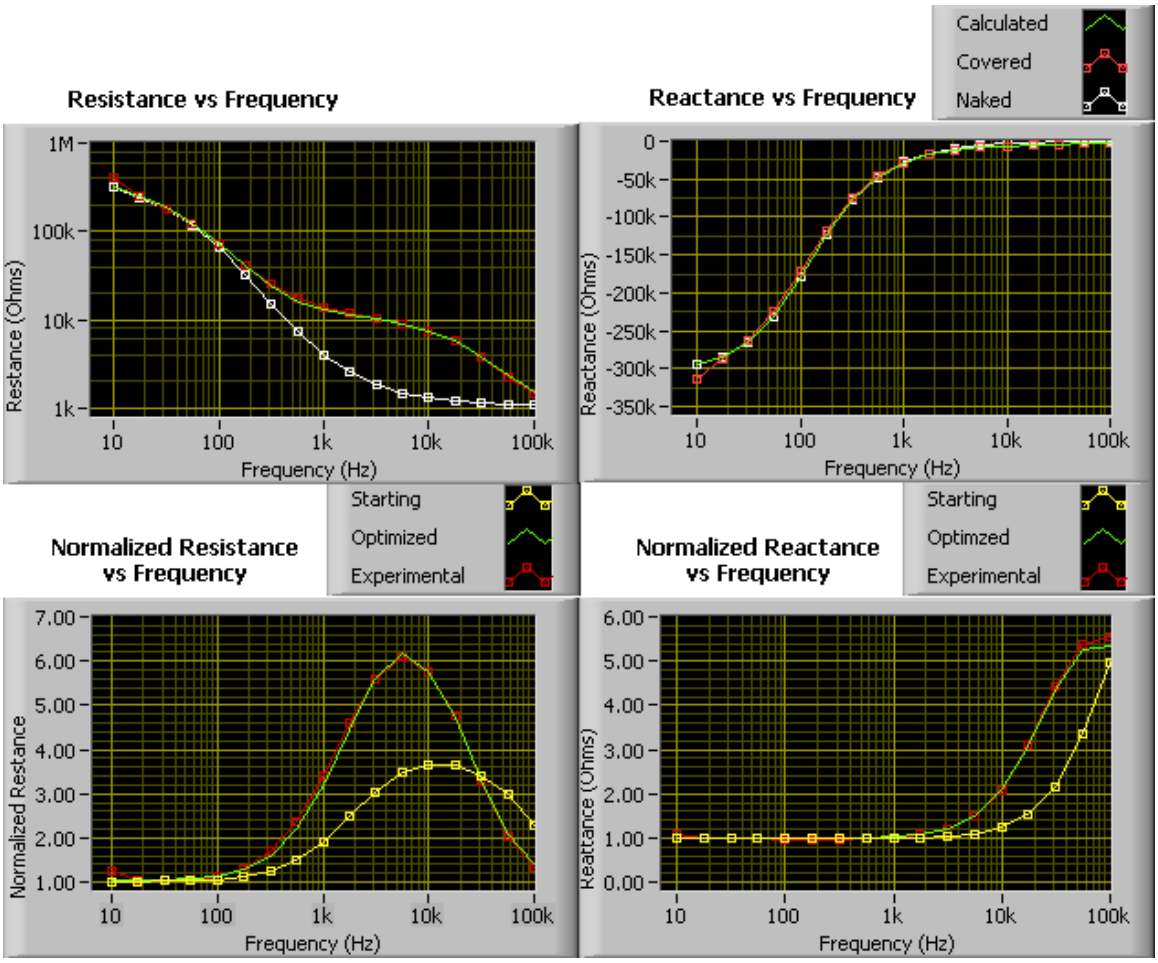


**Figure A-25. Impedance curves, raw and normalized, with interpolated curves from the calculated $\alpha$,, Rb, & Cm parameters, in green. In the normalized curves, the curve calculated from the arbitrary starting parameters input into the Marquardt analysis is also given, in yellow, showing the improvement of the interpolation with iteration.**

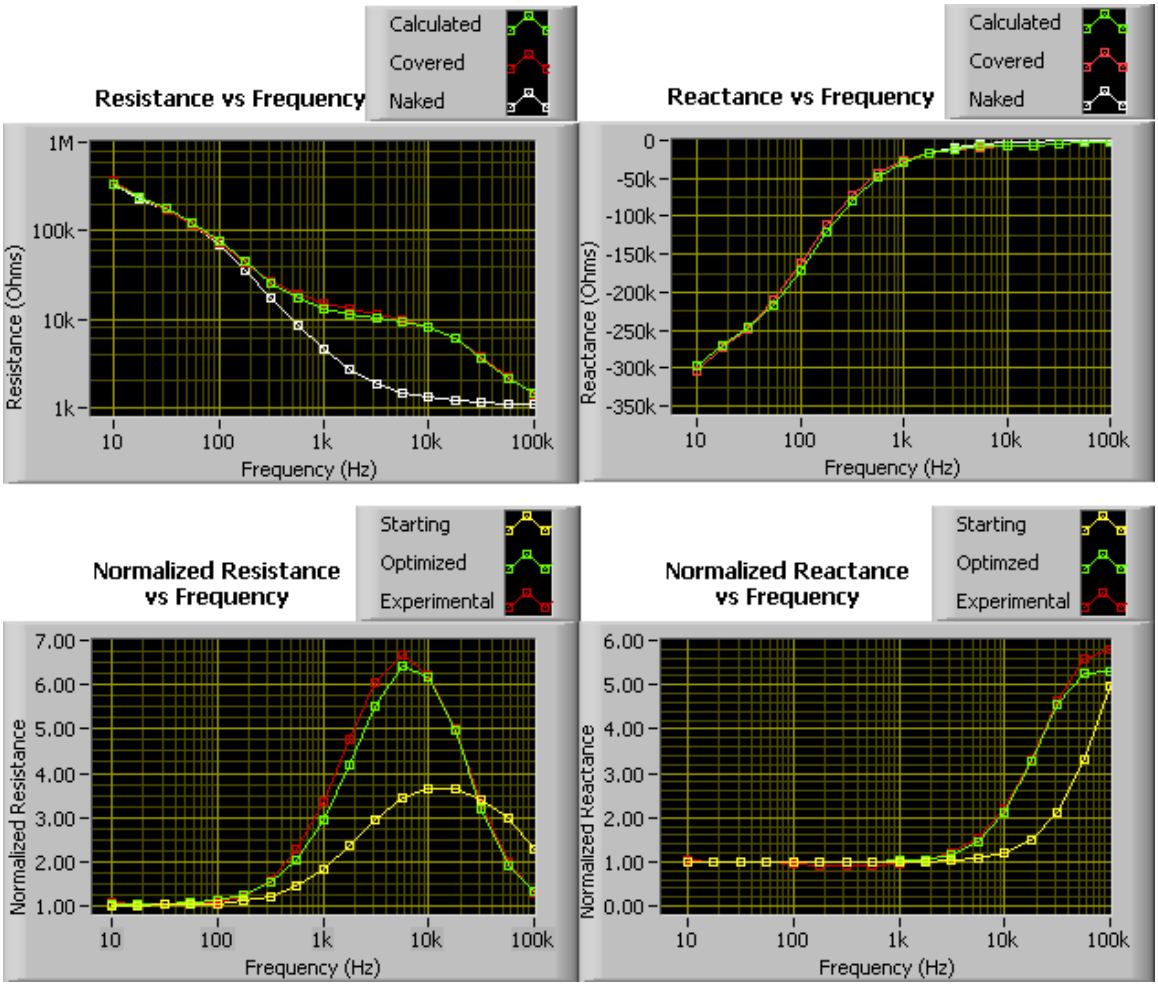


**Figure A-26. Impedance curves, raw and normalized, with interpolated curves from the calculated α,.Rb, & Cm parameters, in green for well 1, which had a large reduced chi-square value. In the normalized curves, the curve calculated from the arbitrary starting parameters input into the Marquardt analysis is also given, in yellow. The small amount of deviation of the fitted curve, in green, from the normalized resistance, in red, represents the large chi-square term. This is still a very good fit to the data.**

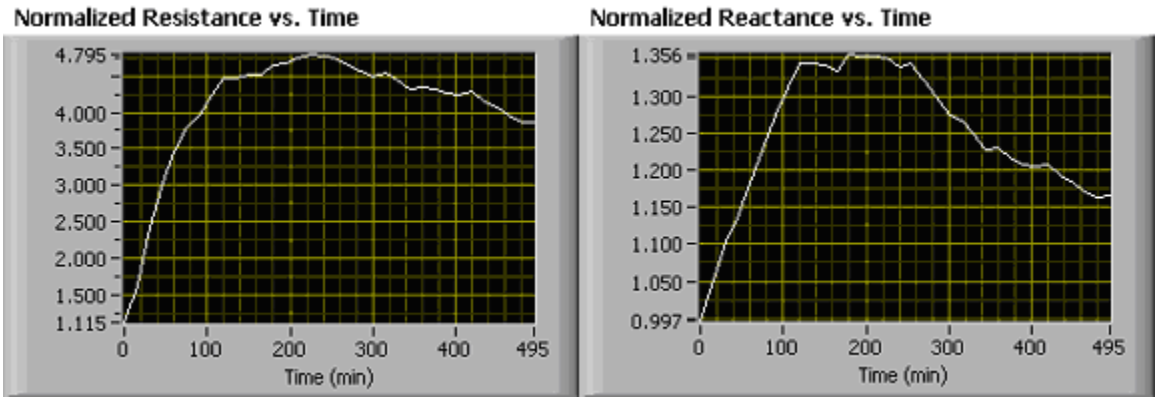


**Figure A-27. Time study of PPAEC attachment to the electrode at the 5.62 kHz level. Impedance levels increase as the cells attach and reach confluence, with the greatest level typically seen in the real channel.**

[BDC27]

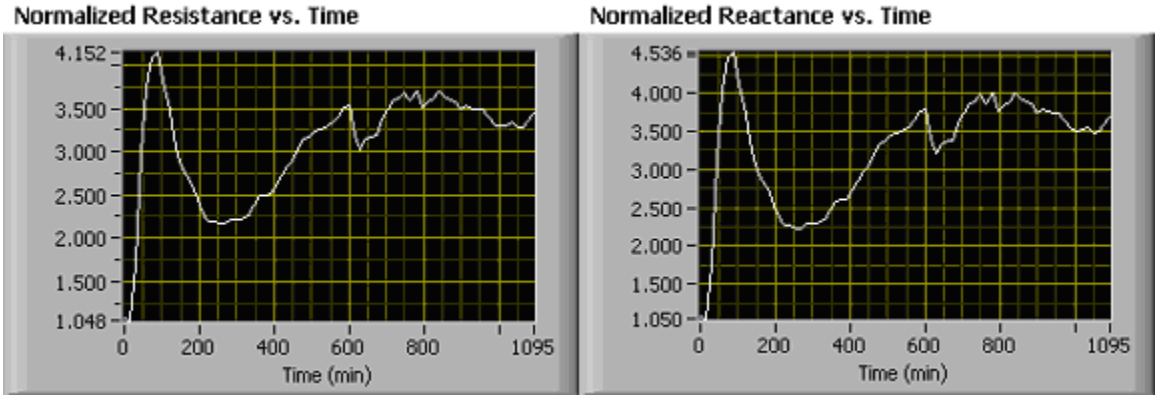


**Figure A-28. Time study of micromotion at the 5.62 kHz frequency level. Fluctuations in the impedance represent the changing shape of the PPAEC.**

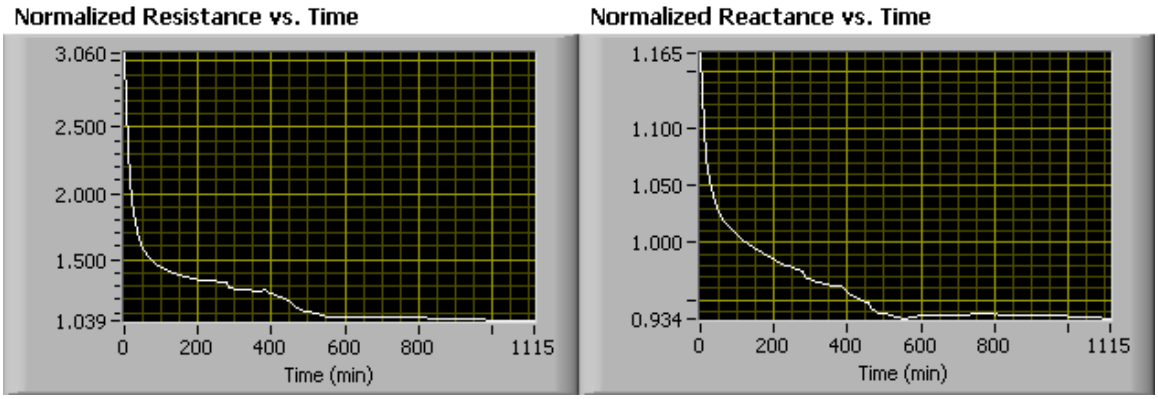


**Figure A-29. Time study of the ceasing of micromotion due to addition of cytochalasin-D, an actin and contractile microfilament inhibiting chemical. The fluctuations in the normalized impedance vs. time curve at the 5.62 kHz level move towards unity, meaning that there is no difference between the naked and cytochalasinated cell covered measurements.**

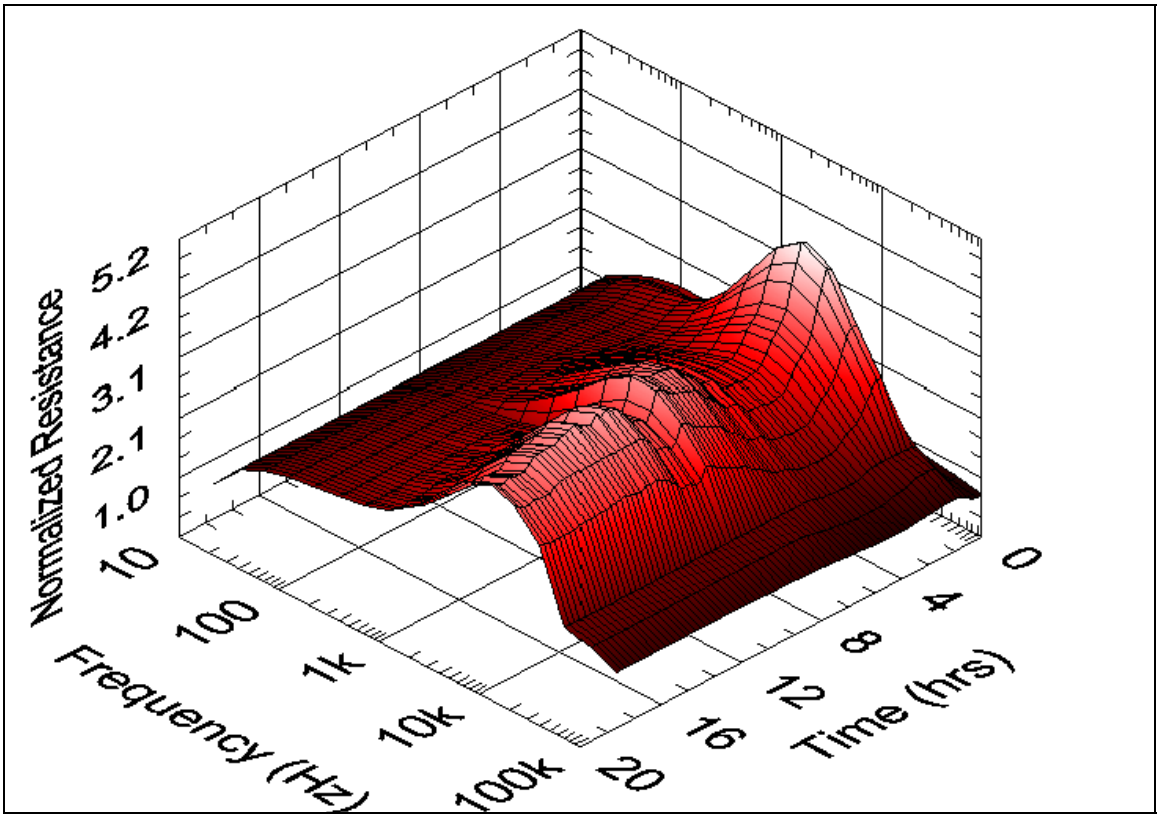


**Figure A-30. 3-D surface plot of a full frequency scan of resistance over time. This analysis allows for a better understanding of the effective time period for studying the PPAEC by the relative cellular effect, because it is relative the maximum ridge of the normalized resistance vs. frequency vs. time surface. Even after 16 hours, the relative magnitude of the PPAEC normalized impedance has noticeably dropped.**

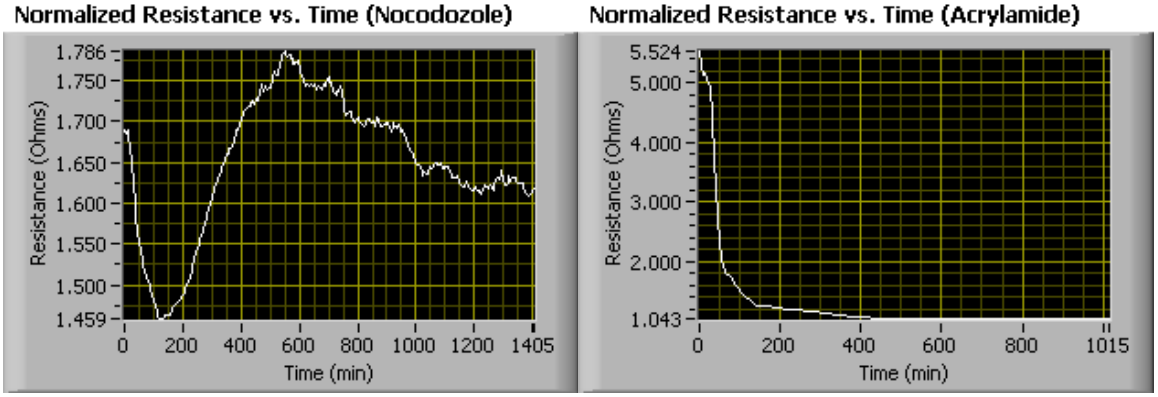


**Figure A-31. Time study of the affect of nocodozole, a microtubule disruptor, and acrylamide, an actin disruptor, on micromotion. The normalized resistance drops immediately upon the administration of nocodozole and reaches a minimum at 2 hours. However, the PPAEC return to normal after about 10 hours and retain a normal micromotion. The acrylamide seemingly has a more permanent effect. The response rate for acrylamide was also faster than that of the cytochalasin (Figure A-29), reaching unity approximately 3 hours before the cytochalasin.**

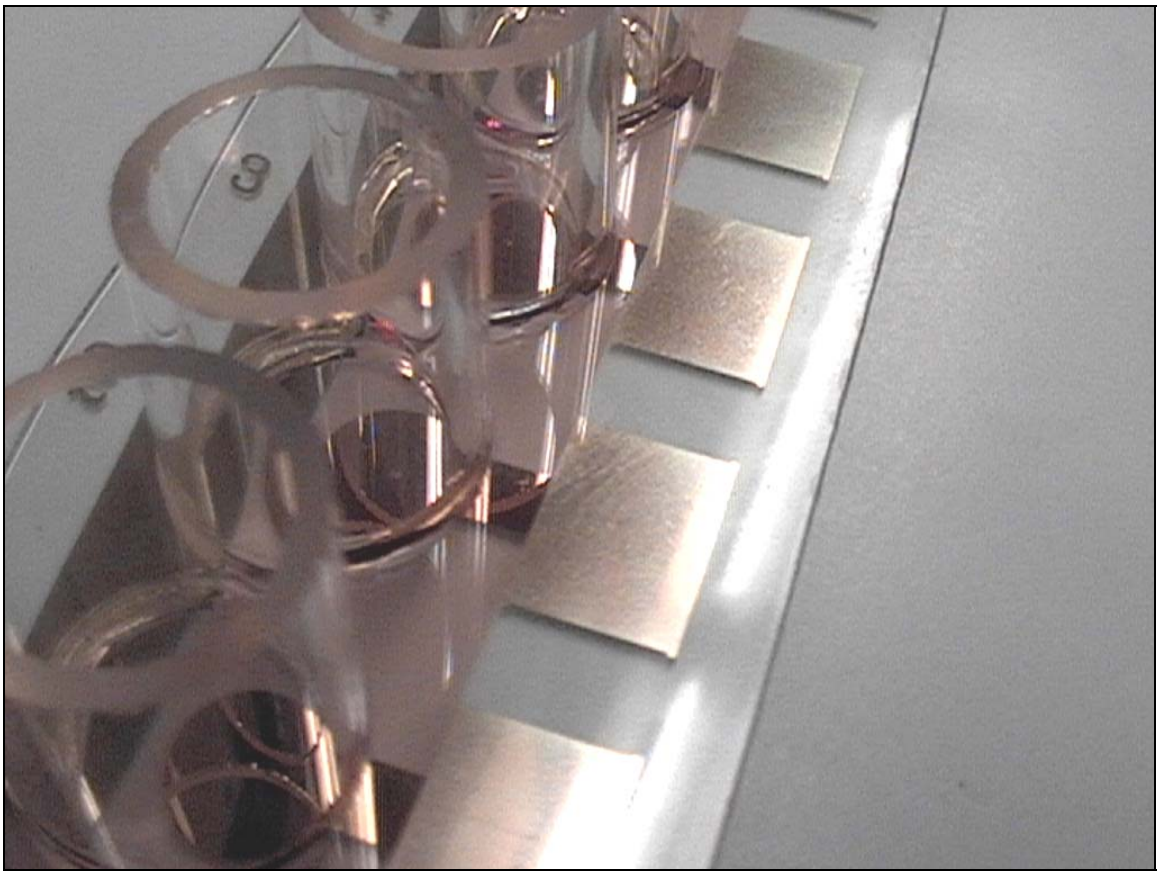

**Figure A-32. ECIS array with gold leaf contamination. Contamination of the electrode arrays from manufacturing processes and finger prints was found to introduce error into the system.**

**Figure A-33. Shaker used to induce vibration in the PPAEC monolayers contained in the 5 well ECIS array.**

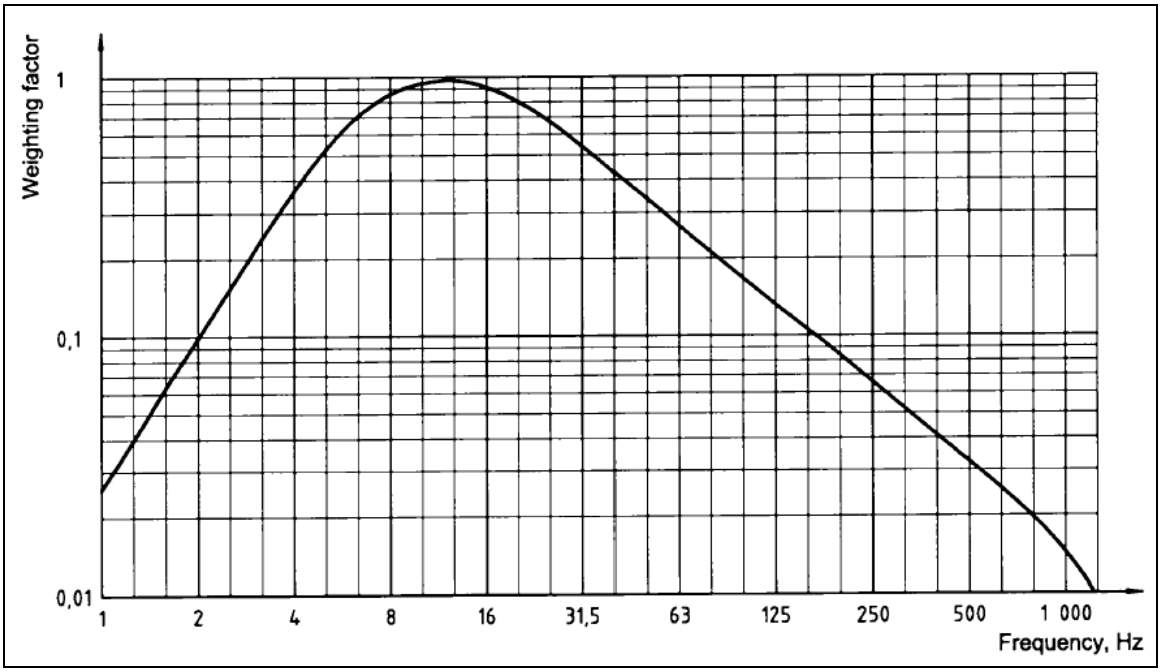


**Figure A-34. ISO 5349 frequency-weighting curve for hand-transmitted vibration. The frequency that will deliver the highest weighting factor, 1, will be around the 15 Hz level. [53]**

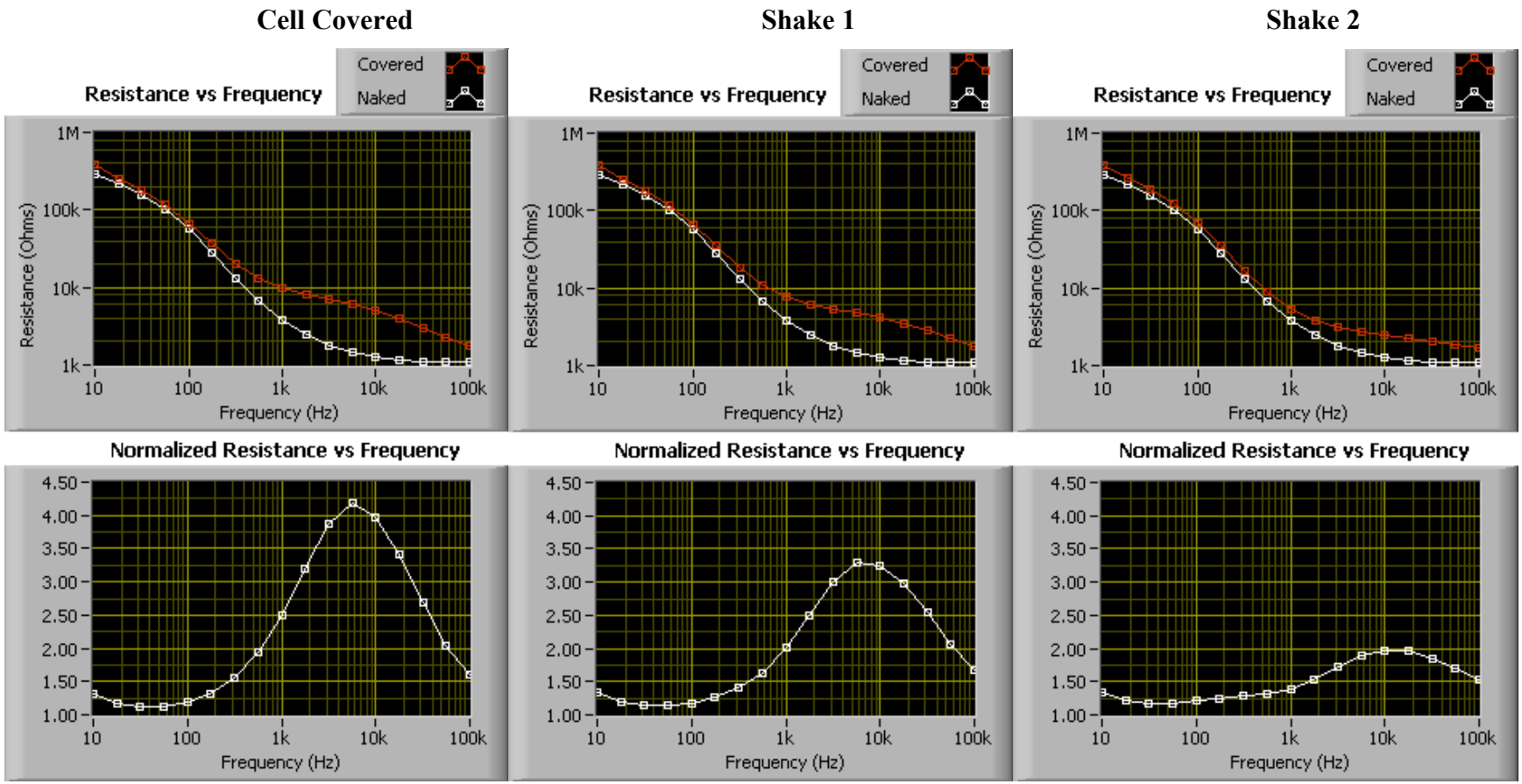


**Figure A-35. Shaken well preliminary acceleration exposure dose study normalized resistances at confluence (Cell Covered), following the first round of vibration (Shake 1), and following the second round of vibration (Shake 2). The slight drop in normalized resistance over the three scans is caused by the diminishing health of the PPAEC monolayer over time, typical of monolayer impedances over a period of a few days. There does not appear to be a response to the cells from vibration.**

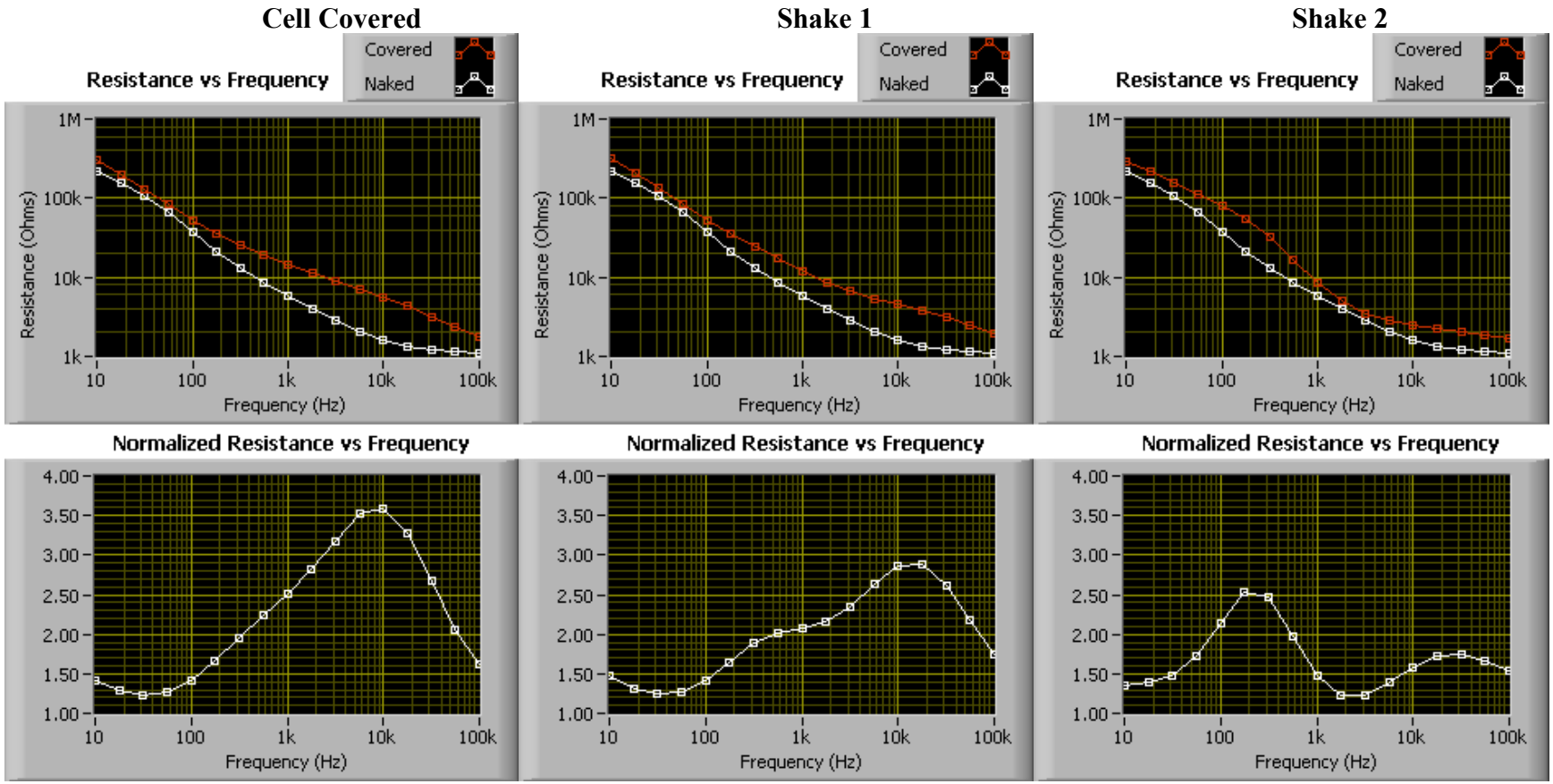


**Figure A-36. Control well preliminary acceleration exposure dose study normalized resistances at confluence (Cell Covered), following the first placement in the fume hood (Shake 1), and following the second placement in the fume hood (Shake 2). There is no apparent difference between the well that was shaken (Figure A-35) and the control. However, the control appears to be faulty and not representative of a normally functioning electrode (the large normalized resistance hump in the lower frequencies).**

**Attach** **Shake 1** **Shake 2**

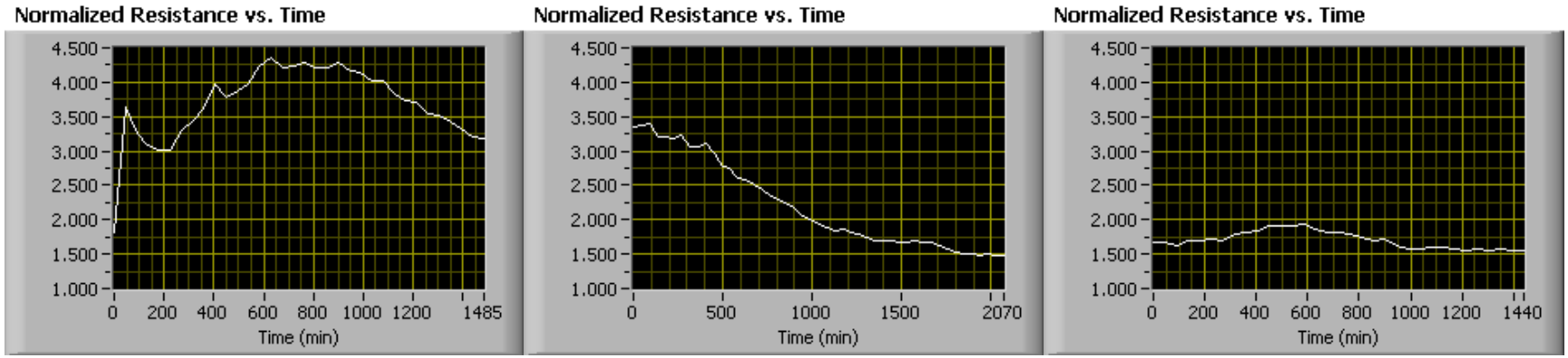


**Figure A-37. Time study of primary acceleration exposure dose to the shaken well. The plateau effect between the three scans is mostly likely indicative of the refreshing of cell media, and not a vibration induced response.**

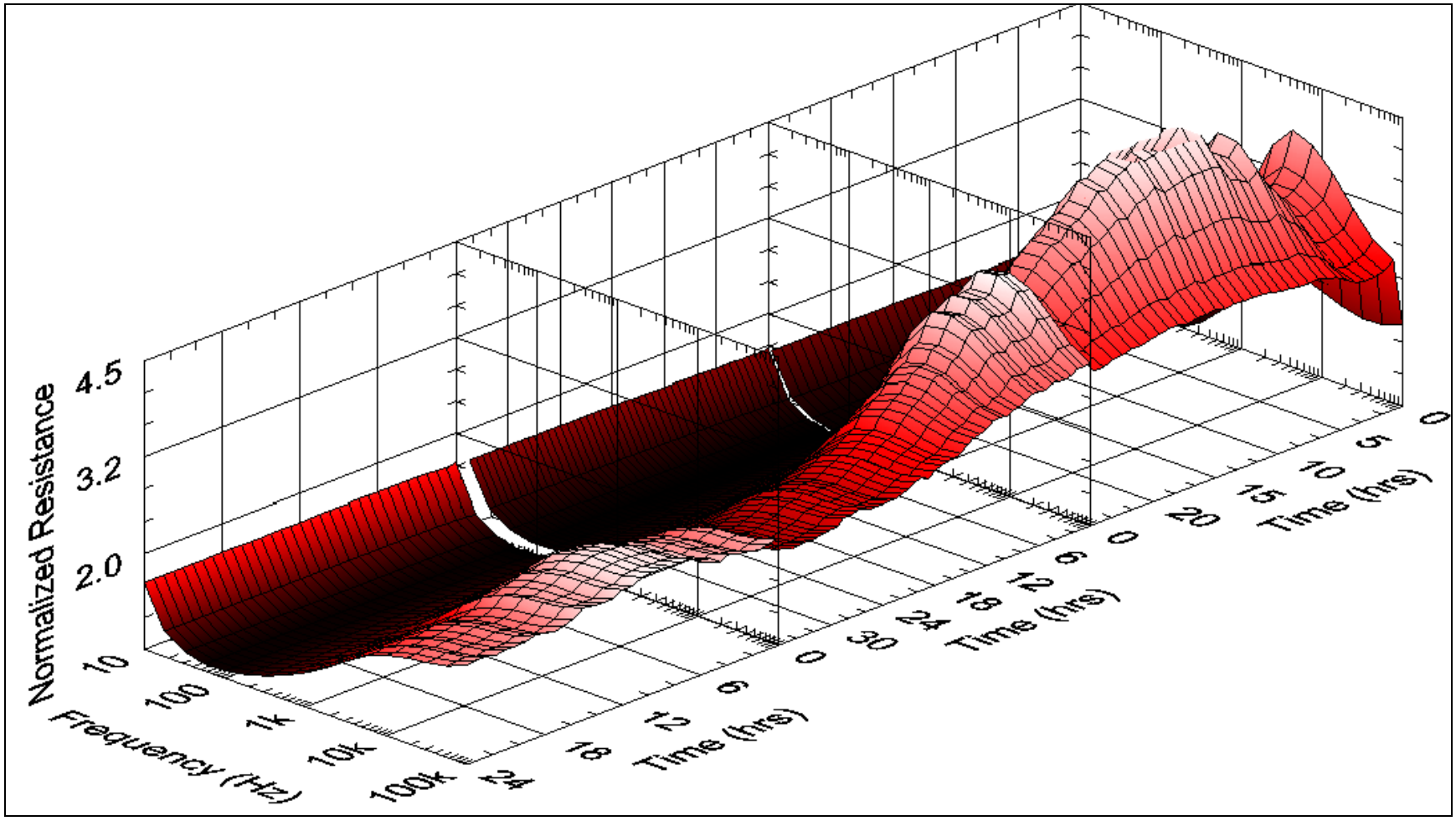


**Figure A-38. 3-D surface plot of the normalized resistance frequency scans vs. time of the primary acceleration exposure dose study shaken well. The difference between each scan indicates an increase of resistance, probably caused by the addition of cell media.**

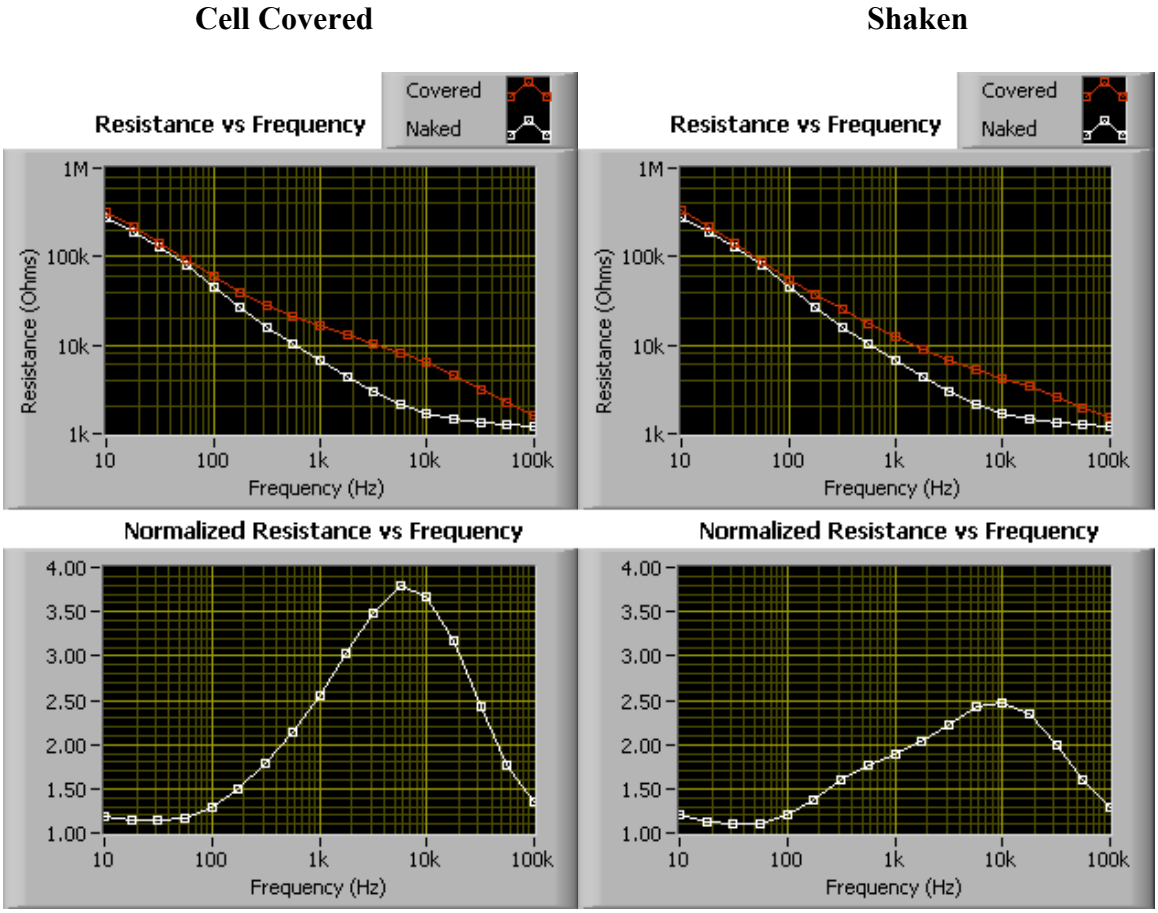


**Figure A-39. Shaken well second acceleration exposure dose study normalized resistances at confluence (Cell Covered), following a round of vibration (Shaken). Again, the slight drop in normalized resistance between the two scans is caused by the diminishing health of the PPAEC monolayer over time. This is typical of monolayer impedances over a period of a few days. There does not appear to be a response to the cells from vibration.**

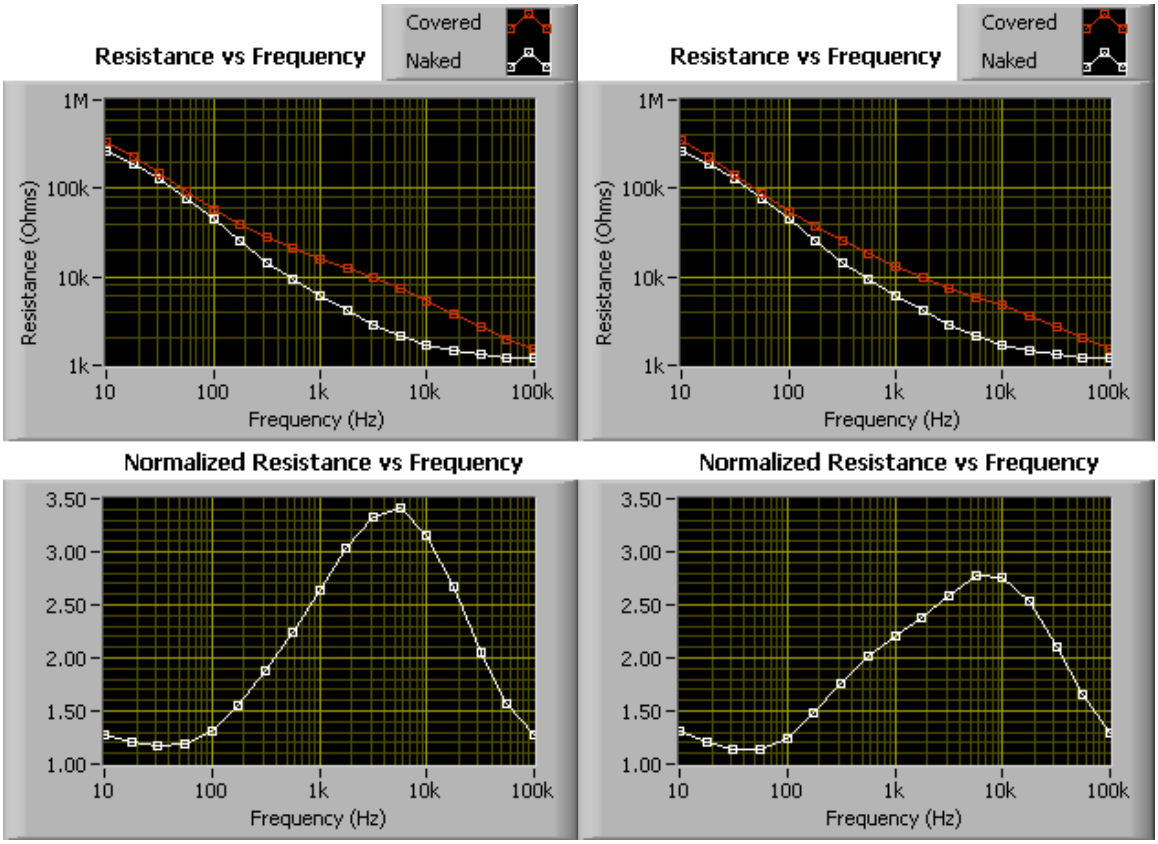


**Figure A-40. Control well second acceleration exposure dose study normalized resistances at confluence (Cell Covered), following the placement in the fume hood (Shaken). There is no apparent difference between the well that was shaken (Figure A-39) and the control. The control electrode appears to be functioning properly this time.**

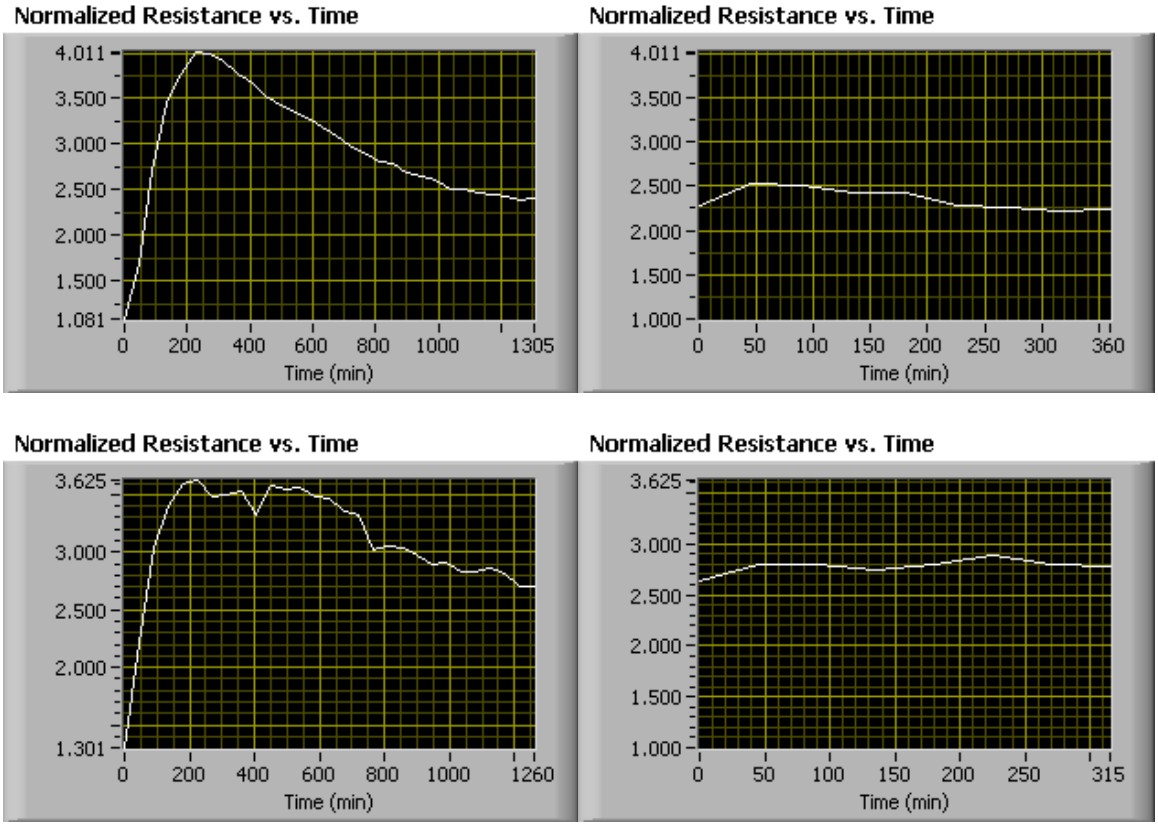


**Figure A-41. Time study of second acceleration exposure dose study for the shaken well (TOP) and unshaken control well (BOTTOM). There is no plateau effect between the two scans as in the initial experiment, indicating that there was no effect from the acceleration exposure dose to the shaken well.**

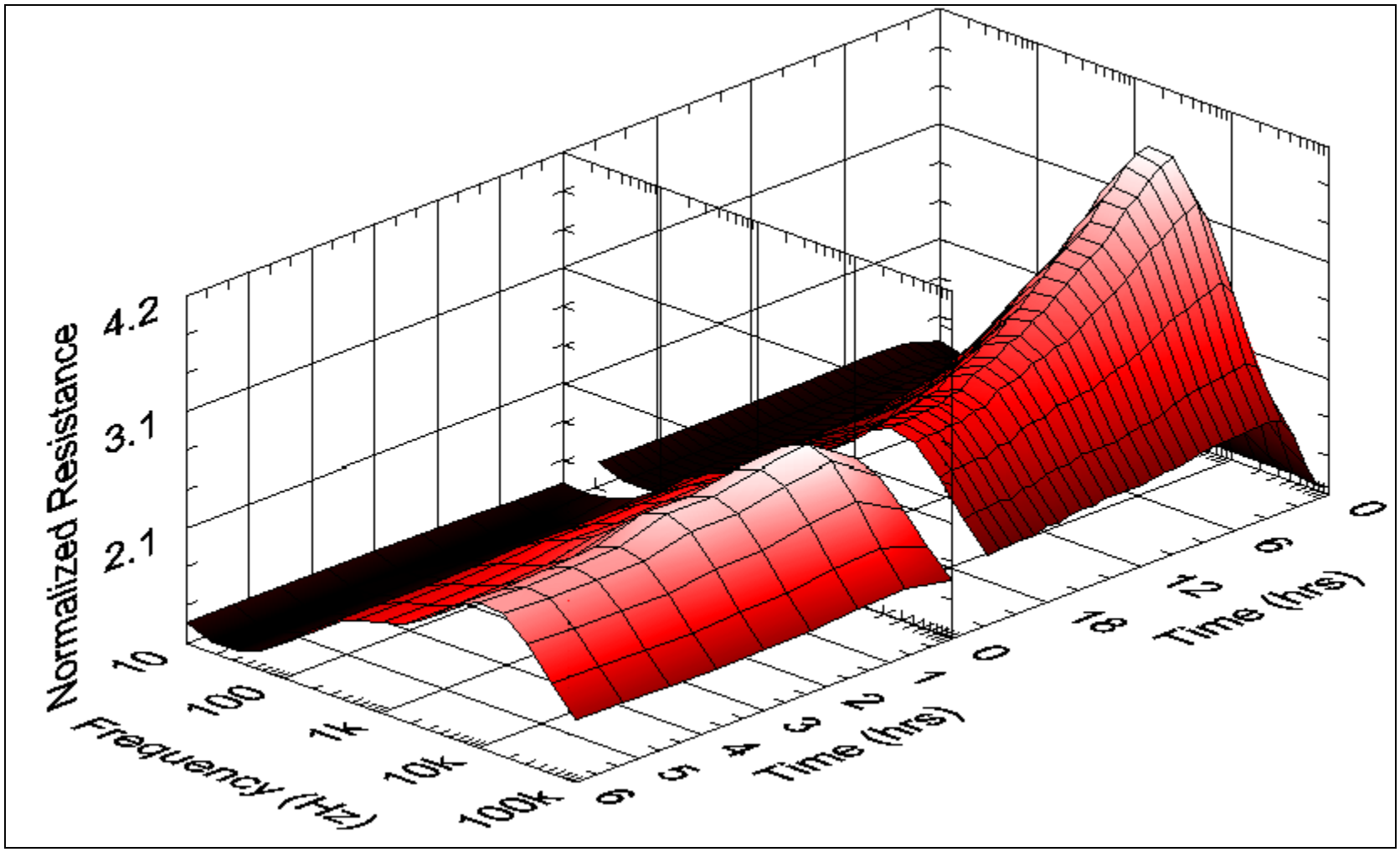


**Figure A-42. 3-D surface plot of the normalized resistance frequency scans vs. time of the second acceleration exposure dose study shaken well. There appears to be no difference between the scans, indicating no cellular response.**

# VITA:

Benjamin David Cowan was born May the 7th, 1979 in Chattanooga, Tennessee. He graduated from Hixson High School in 1997. He came to the University of Tennessee, Knoxville to purse a B.S. in Biomedical Engineering and the Latin language, which he received in May of 2001. He decided to stay on at the University of Tennessee for his M.S. in Engineering Science with a Biomedical emphasis. Benjamin is currently looking for a position in Biomedical Engineering.